

## Self-consistent formulations for stochastic nonlinear neuronal dynamics

Jonas Stapmanns,<sup>1,2,\*</sup> Tobias Kühn<sup>1,2,\*†</sup>, David Dahmen,<sup>1</sup> Thomas Luu,<sup>3</sup> Carsten Honerkamp,<sup>2,4</sup> and Moritz Helias<sup>1,2</sup>

<sup>1</sup>*Institute of Neuroscience and Medicine (INM-6) and Institute for Advanced Simulation (IAS-6) and JARA BRAIN Institute I, Jülich Research Centre, Jülich, Germany*

<sup>2</sup>*Institute for Theoretical Solid State Physics, RWTH Aachen University, 52074 Aachen, Germany*

<sup>3</sup>*Institut für Kernphysik (IKP-3), Institute for Advanced Simulation (IAS-4) and Jülich Center for Hadron Physics, Jülich Research Centre, Jülich, Germany*

<sup>4</sup>*JARA-FIT, Jülich Aachen Research Alliance–Fundamentals of Future Information Technology, Germany*



(Received 16 January 2019; revised manuscript received 18 December 2019; accepted 18 December 2019; published 21 April 2020)

Neural dynamics is often investigated with tools from bifurcation theory. However, many neuron models are stochastic, mimicking fluctuations in the input from unknown parts of the brain or the spiking nature of signals. Noise changes the dynamics with respect to the deterministic model; in particular classical bifurcation theory cannot be applied. We formulate the stochastic neuron dynamics in the Martin-Siggia-Rose de Dominicis-Janssen (MSRDJ) formalism and present the fluctuation expansion of the effective action and the functional renormalization group (fRG) as two systematic ways to incorporate corrections to the mean dynamics and time-dependent statistics due to fluctuations in the presence of nonlinear neuronal gain. To formulate self-consistency equations, we derive a fundamental link between the effective action in the Onsager-Machlup (OM) formalism, which allows the study of phase transitions, and the MSRDJ effective action, which is computationally advantageous. These results in particular allow the derivation of an OM effective action for systems with non-Gaussian noise. This approach naturally leads to effective deterministic equations for the first moment of the stochastic system; they explain how nonlinearities and noise cooperate to produce memory effects. Moreover, the MSRDJ formulation yields an effective linear system that has identical power spectra and linear response. Starting from the better known loopwise approximation, we then discuss the use of the fRG as a method to obtain self-consistency beyond the mean. We present a new efficient truncation scheme for the hierarchy of flow equations for the vertex functions by adapting the Blaizot, Méndez, and Wschebor approximation from the derivative expansion to the vertex expansion. The methods are presented by means of the simplest possible example of a stochastic differential equation that has generic features of neuronal dynamics.

DOI: [10.1103/PhysRevE.101.042124](https://doi.org/10.1103/PhysRevE.101.042124)

### I. INTRODUCTION

Neuronal networks are interesting physical systems in various respects: they operate outside thermodynamic equilibrium [1], a consequence of directed synaptic connections that prohibit detailed balance [2]; they show relaxational dynamics and hence do not conserve but rather constantly dissipate energy; and they show collective behavior that self-organizes as a result of exposure to structured, correlated inputs and the interaction among their constituents. But their analysis is complicated by three fundamental properties: Neuronal activity is stochastic, the input-output transfer function of single neurons is nonlinear, and networks show massive recurrence [3] that gives rise to strong interaction effects. They hence bear similarity with systems that are investigated in the field of (quantum) many particle systems. Here, as well, (quantum) fluctuations need to be taken into account and the challenge is to understand collective phenomena that arise from the

nonlinear interaction of their constituents. Not surprisingly, similar methods can in principle be used to study these two *a priori* distinct system classes [4–8].

But so far the techniques employed within theoretical neuroscience just begin to harvest this potential. Here we adapt methods from statistical field theory and functional renormalization group techniques to the study of neuronal dynamics.

A reader may wonder in which cases functional methods that we review and extend here are needed to study neuronal network dynamics. In fact, in many cases, simpler techniques could be sufficient: as long one is sure that the dominant behavior of a network is not affected by fluctuations, a mean-field approximation is enough [9,10]. For example, if one wants to know the stationary firing rates of neurons in typical network settings (but see Ref. [11] for an exception). Or if one seeks to understand first-order phase transitions, where the mean activity suddenly changes: The transition from a quiescent to a highly active state in a bistable neuronal network is a prime example [10]; the activation of attractors embedded into the connectivity of a Hopfield network is a second [12].

An inherent danger of the mean-field approximation, though, is that by construction it is “too self-consistent”; this

\*These authors contributed equally to this work.

†Present address: Laboratoire de Physique Théorique de l’ENS 24, Rue Lhomond 75231, Paris Cedex 05 - France.

means that there is no way of determining its limit of validity as long as it is not embedded into a wider framework that assesses the importance of fluctuations. The loop expansion, briefly reviewed here, is this wider framework (see also Ref. [13], Sec. 6.4, for a discussion of this point in the context of Landau theory).

Even if fluctuations are important, it may be sufficient to use linear response theory around the mean-field approximation. This approach has indeed been pursued quite successfully [10,14–21], for example, to explain why correlations are weak in inhibition-dominated networks [20,22].

So why bother about methods that go beyond this widely established, simple, and successful methodology?

If it was clear that the considerable variability observed in the brain was meaningless noise, one should not invest any work in going beyond linear response theory. But there is surely no neuroscientist who would sign this statement. On the contrary, experiments have clearly shown that fluctuations of neuronal activity are indeed linked in a meaningful way to the animal's behavior (see, e.g., Refs. [23–25]). Treating fluctuations in linear response theory means that they follow linear equations: Fluctuating signals that are simultaneously injected at various places of the brain then travel through it without mutual interference. The function the brain performs at this level of approximation is thus that of a linear filter; clearly a too limited view to explain most of its functions.

The diagrammatic techniques considered here were developed over decades within the physics community to capture the interaction of fluctuations in nonlinear systems and they are widely used in many fields [26]. In the neuronal context, they thus enable the investigation of potential functional roles of the variability observed in neuronal systems.

The finding of signatures of criticality in neuronal activity is an example of a network state that is dominated by fluctuations, a scenario where mean-field and linear response theory clearly break down. Parallel recordings in cell cultures [27] and *in vivo* [28] show power law distributions in the numbers of coactive neurons, suggestive of scale-free dynamics, which typically indicates a continuous phase transition. Critical states also have consequences for information processing: reservoir computing [29,30] with random networks close to criticality indeed shows the highest computational performance [31], maximizing the wealth of transformations.

The renormalization group was one of the major achievements of theoretical physics of the past century to understand collective phenomena close to continuous phase transitions [32]. So far, however, these methods have rarely been employed to neuronal networks. The need for a formalism of dynamical critical phenomena of neuronal networks has explicitly been articulated by Mora and Bialek [33]: “Except in a few cases, the mathematical language that we use to describe criticality in statistical systems is quite different from the language that we use in dynamical systems. Efforts to understand, for example, current data on networks of neurons will force us to address the relations between statistical and dynamical criticality more clearly” (p. 288).

The current work presents such a formalism. The functional renormalization group [34–36] allows the study of critical fluctuations in networks that operate outside thermodynamic equilibrium: dynamical critical phenomena [6].

This method has witnessed successes in condensed matter physics in problems ranging from classical and quantum critical phenomena over the explorations of the ground states of interacting many-body systems to the improved determination of effective model parameters from *ab initio* theories. It systematically improves the physical description beyond mean-field theory by including fluctuations and by removing ambiguities.

To showcase the importance of continuous phase transitions we here demonstrate that networks with connectivity close to the point of balance between excitation and inhibition exhibit critical fluctuations. We reduce the network model to a spatially homogeneous version of “model A” of the seminal characterization of dynamical critical phenomena by Hohenberg and Halperin [5].

Techniques similar to the ones reviewed and extended in the current article have already been used in computational neuroscience. One technical motivation comes from the need to study disordered systems, for example, networks with randomly drawn connections. The formulation with help of a generating functional is useful to investigate the impact of connectivity structure on dynamics. For example, Martí *et al.* [37] study the slowdown of fluctuations in networks with an overrepresentation of symmetric connections, as they are observed in cortex [38]. Their analysis rests on the Martin-Siggia-Rose-de Dominicis-Janssen (MSRDJ) formalism [39–41] presented here (see also Refs. [7,8] for concise reviews). Crisanti and Sompolinsky [42] compute the transition to chaos and the stability of mean-field solutions in deterministic random networks. Schuecker *et al.* [43] find a novel dynamical state, between the breakdown of linear stability and the onset of chaos that has optimal sequential memory. Dahmen *et al.* [44] describe a state of critical dynamics in neuronal networks that is hidden within the high-dimensional space of all neurons.

Another motivation comes from the study of correlated activity between pairs of cells. The loopwise expansion as a systematic extension of the commonly performed mean-field approximation has been applied to understand fluctuations in recurrent networks of neurons with discrete activation states [45,46], to obtain fluctuation corrections to the mean activity and higher order correlations, structure-dynamics relationships in stochastic spiking networks [11], and to study spiking networks of quadratic integrate-and-fire models [47]. The recent work by Brinkman *et al.* [48] addresses the pertinent question whether and how hidden units bias the estimation of connectivity from correlations. These works use different variants of the systematic fluctuation expansion discussed here on minimal examples.

In the context of critical phenomena, the study by Di Santo *et al.* [49] is worth mentioning. The authors propose a field theory of neuronal activity on a two-dimensional sheet, reminiscent of a Ginzburg-Landau theory (Ref. [5], model A). So far, this model has been investigated by help of the mean-field approximation and a first-order transition has been found. An investigation of critical phenomena of a continuous phase transition in this model would require renormalization group methods that we discuss here. Formally, their model resembles the Kardar-Parisi-Zhang equation [50], one of the most prominent models of dynamical criticality which

requires the functional renormalization group [51,52] or mode coupling theory [53].

The aim of the current paper is thus to review a sequence of formulations for the statistics in neuronal-inspired stochastic dynamics, coherently presented in the order of increasing self-consistency: mean-field approximation, loop expansion, and functional renormalization group. To our knowledge, advanced methods such as the functional renormalization group have so far not been applied to neuronal systems. We feel that a work explaining this method in the context of neuronal dynamics with help of minimal examples and in relation to the simpler approaches, the mean-field approximation and the loop expansion, may be helpful for researchers who are interested in neuronal variability.

The presentation together with more widely used approaches also allows us to address some of the more subtle points that we could not find documented in the literature. In particular, we discuss issues of convexity of the cumulant-generating functional, the need for the Legendre-Fenchel transform in systems with dynamic symmetry breaking, the different definitions of the effective potential in equilibrium and nonequilibrium systems and its use to investigate phase transitions. We also point out particularities of the MSRDJ formalism compared to the field theories more commonly covered in textbooks.

## II. RESULTS

### A. Outline of the paper

The outline of the paper is as follows: in Sec. II A we define the class of stochastic differential equations that have been used in the literature to describe neuronal dynamics and we define the simplest nontrivial example that will serve us throughout the paper to illustrate the essence of the respective methods. We briefly review the simplest approximation, the mean-field solution of a stochastic differential equation. The following sections then develop self-consistent schemes of increasing complexity.

These more elaborate schemes rely on a representation of the stochastic system in terms of a cumulant-generating functional and its Legendre transform, the effective action. We therefore introduce in Sec. II B the Onsager-Machlup (OM) field theory, which has a rigorous basis for stochastic differential equations with Gaussian noise. Section II C explains the central role of Legendre transforms for the construction of self-consistency equations.

We proceed to the MSRDJ-field theory in Sec. II D, which has computational advantages compared to OM. We show in Sec. II E that the resulting self-consistency equation takes the form of an effective, deterministic, integro-differential equation for the mean value of the stochastic process. The concept of vertex functions is introduced as a set of time nonlocal coupling kernels that appear in this equation. Our first main result is the relation of the effective actions in the OM and the MSRDJ formulation; thus we extend the definition of the OM effective action for non-Gaussian noise.

These formal prerequisites allow us in Sec. III to briefly review the loop expansion as a systematic extension of the mean-field approximation; it enables practical and systematic

calculations of vertex functions and of probabilistic quantities, which, by construction, are self-consistent on the level of the first moments. In Sec. II J we present the effective self-consistency equation for the mean value of the exemplary stochastic process in one loop approximation; it shows how fluctuations influence the relaxation back to baseline after a small perturbation and provides an intuition for the meaning of vertex functions. A stochastic linear convolution equation is presented that has the same second-order statistics as the full nonlinear system; it explains the meaning of self-energy corrections for stochastic dynamics.

The most advanced method of self-consistency covered here is the functional renormalization group, shown in Sec. II K. It extends the self-consistency up to arbitrary orders of the vertex functions. In particular, in Sec. II K 1, we present a new interpretation of the BMW approximation [54] within the vertex expansion. We show that all terms of the bare action flowing in this altered BMW-fRG scheme lead to an improvement over the one-loop result.

Finally, Sec. II L visits the problem of self-consistency from the perspective of bifurcations. On the example of a neuronal population dynamics close to the loss of balance, we show that a bifurcation point in the deterministic model corresponds to a continuous phase transition in the stochastic dynamics, illustrating the use of the OM effective action for nonequilibrium dynamics.

In Sec. III we discuss the presented concepts in comparison to other approaches and provide an outlook towards applications within theoretical neuroscience.

### B. Stochastic rate equations inspired by neuronal dynamics

The study of rate equations has a long history in theoretical neuroscience [55,56]. Initially these equations described the time evolution of the average number of active neurons in a given time interval: a set of deterministic, coupled differential equations. To cater for fluctuations of neuronal activity [57], stochastic models are needed. Markov models, for example, describe the stochastic evolution of the active number of neurons [9,45,58]. Such Markov jump processes may be approximated by stochastic differential equations using a Kramers-Moyal expansion [59].

But also the dynamics of deterministic spiking network models [60] has been shown heuristically to be approximated by effective stochastic differential equations [21,61–64]. Typically the resulting equations describe population averages, and thus comprise only a single or a few components. Stochastic spiking network models, moreover, can be treated within a variant of the field theoretical formalism [65,66] used in the current work [48,67].

Last, stochastic differential equations may be regarded as a direct generalization of their deterministic counterparts in their own right. For example, the classical model by Sompolinsky, Crisanti, and Sommers [68] has been extended to stochastic dynamics [43].

A typical network dynamics is of the form

$$dx_i(t) + x_i(t) dt = \sum_j J_{ij} \phi(x_j(t)) dt + dW_i(t), \quad (1)$$

with a stochastic increment  $dW(t)$  as a centered Gaussian with first and second moments given by

$$\langle dW_i(t) \rangle = 0, \quad \langle dW_i(t) dW_j(s) \rangle = D \delta_{i,j} \delta_{t,s} dt.$$

Here  $\phi$  is the gain function which is thought to transfer the internal state variable  $x$  (e.g., the membrane potential) into the output (the firing rate). The term  $x dt$  shall describe the leaky dynamics of neurons.

The aim of this article is to survey methods to construct self-consistent solutions to such stochastic nonlinear differential equations. The  $N$  components in (1) do not qualitatively increase the difficulty—rather, the interplay of fluctuations and the nonlinearity is the cause of complications. To illustrate the concepts in the simplest but nontrivial setting, in the remainder of this article we therefore mostly concentrate on the scalar equation

$$dx(t) = f(x(t)) dt + dW(t). \quad (2)$$

This is, moreover, identical to (1) for the case of a fully connected network  $J_{ij} = N^{-1}J$  and perfectly correlated stochastic increments  $dW_i$  across neurons, if one defines  $f(x) = -x + J\phi(x)$ . For the function  $\phi$  we assume an expansive nonlinearity of convex down shape. This is a typical result of neurons firing in the fluctuation-driven regime with low firing rates [[69], Eq. (2.6) and Fig. 2]. For specific calculations in minimal examples, we consider a quadratic form for the gain function that is thus the simplest approximation of this qualitative shape. Similar approximations have recently been used to study critical avalanche dynamics in neuronal networks [[49], Eq. (1)].

Of course, besides the interpretation as the firing rate or activity of a neuron or of a population of neurons, here  $x$  could as well denote a magnetization, the concentration of some chemical substance, the number of animals that reproduce and die, or the value of a stock [70–72].

### 1. Mean-field approximation

This article investigates a sequence of approximation techniques to compute the statistics of the system self-consistently. We present methods in order of increasing complexity and accuracy, starting with the simplest possible self-consistent approximation: the neglect of fluctuations altogether, which leads to a self-consistency equation for the mean  $\langle x \rangle$ . Throughout the text we use  $\langle x^n \rangle$  to denote the  $n$ th moment of  $x$  and  $\langle\langle x^n \rangle\rangle$  to denote the  $n$ th cumulant [70].

This simplest self-consistent approximation to the stochastic differential equation (2) consists in neglecting the noise and instead solving the ordinary differential equation

$$\frac{d}{dt}x(t) = f(x(t)). \quad (3)$$

Finding the stationary solution to this differential equation amounts to a fixed point problem, that is,  $f(x_0) = 0$ . Small fluctuations around that solution can, to first approximation, be accounted for by linearizing (2) around  $x_0$ . By writing  $x(t) = x_0 + \delta x(t)$ , we obtain

$$\frac{d}{dt} \delta x(t) = f'(x_0) \delta x(t) + \xi(t) + O(\delta^2 x(t)), \quad (4)$$

where  $\xi$  is a centered Gaussian white noise with variance  $D$  (formally the derivative of  $dW$ ). Denoting the Fourier transform of  $x$  as  $X$ , we describe the first- and second-order statistics of these small fluctuations as

$$\begin{aligned} 0 &= \langle \delta X(\omega) \rangle = \frac{\langle \xi(\omega) \rangle}{i\omega - f'(x_0)}, \\ \langle \delta X(\omega) \delta X(\omega') \rangle &= \frac{2\pi D \delta(\omega + \omega')}{(i\omega - f'(x_0))(i\omega' - f'(x_0))}. \end{aligned} \quad (5)$$

This approach is, however, restricted to small noise amplitudes and cannot be straight-forwardly generalized. From a conceptual point of view, this approximation is furthermore not self-consistent, because we solve the deterministic equation (3) to determine the first moment  $x_0$  and then study fluctuations around it to determine the second-order statistics as (5). Such fluctuations would, in turn, affect the mean value, due to the nonlinear parts of  $f$ . Continuing the Taylor expansion of  $f$  in (4) to second order, this *ad hoc* approach would then yield a correction to the mean given by

$$\langle x \rangle \simeq x_0 + \frac{1}{2} f''(x_0) \frac{D}{-2f'(x_0)}, \quad (6)$$

because the variance of the process, by (5), is  $\langle \delta x^2 \rangle = \frac{D}{-2f'(x_0)}$ . Thus we get an approximation for the mean that is inconsistent with the value  $x_0$  that we assumed to perform the approximation in the first place. The common thrust of the methods surveyed in the remainder of this article is to strive for self-consistency of the statistics and to systematically compute such fluctuation corrections that are self-consistent also on the level of higher moments.

## C. Generating functionals for stochastic differential equations

### 1. Onsager-Machlup path integral

To study the system more systematically, we introduce the path-integral formalism, starting with its Onsager-Machlup (OM) formulation [73,74]. We assign a probability  $p[x] \mathcal{D}x$  to every path  $x(t)$ , where we define the integral measure  $\mathcal{D}x$  as

$$\int \mathcal{D}x \cdots := \lim_{M \rightarrow \infty} \int dx_{t_0} \cdots \int dx_{t_{M-1}} \cdots,$$

where  $t_0, \dots, t_{M-1}$  is a uniform discretization of the time axis into segments of length  $\Delta t$  that scales inversely with  $M$ . We here stick to the Itô convention, which means that we evaluate the integrand at the beginning  $t_i$  of every subinterval  $[t_i, t_{i+1})$ . For additive noise, as it appears in (2), all choices for a discretization converge to the same limit (see Ref. [70], chap. 4.3.6). Furthermore, we define  $p[x] = \frac{1}{Z} \exp(S_{\text{OM}}[x])$  via

$$\begin{aligned} S_{\text{OM}}[x] &= -\frac{1}{2} \lim_{M \rightarrow \infty} \sum_{i=0}^{M-1} \left[ \left( \frac{x_{i+1} - x_i}{\Delta t} - f(x_i) \right) D^{-1} \right. \\ &\quad \times \left. \left( \frac{x_{i+1} - x_i}{\Delta t} - f(x_i) \right) \right] \Delta t \\ &= -\frac{1}{2} \int dt \{ \partial_t x - f(x(t)) \} D^{-1} \{ \partial_t x - f(x(t)) \} \end{aligned} \quad (7)$$



[59,73–76],<sup>1</sup> and

$$\mathcal{Z}^{-1} := \int \mathcal{D}x \exp(S_{\text{OM}}[x])$$

is chosen such that the probability  $p[x]$  is properly normalized. The probability of the occurrence of deviations from the solution fulfilling  $\partial_t x = f(x)$  are suppressed exponentially. Allowing for arbitrary time-dependent solutions  $x(t)$ , for example, by fixing the initial point  $x(0) = x_0$  and the final point  $x(T) = x_T$ ,  $p[x]$  determines the probability for any path between these points; applied to the dynamics of the membrane potential of a neuron, it can be used to determine the probability to exceed the firing threshold. The rate of escape is, to leading exponential order, given by  $p[x^*]$ , where  $x^*$  minimizes  $S_{\text{OM}}$ . A thorough discussion of this kind of setting is beyond the scope of this work; good introductions can be found, e.g., in Ref. [77], Sec. 10.5, or Ref. [78], Sec. 5.

The moments of the ensemble of paths

$$\langle x(t_1) \cdots x(t_n) \rangle := \int \mathcal{D}x p[x] x(t_1) \cdots x(t_n) \quad (8)$$

can be expressed as functional derivatives with respect to  $j(t)$  of the moment-generating functional<sup>2</sup>

$$Z[j] := \int \mathcal{D}x p[x] \exp\left(\int dt j(t)x(t)\right), \quad (9)$$

evaluated at  $j(t) = 0$ . The cumulant-generating function (or Helmholtz free energy)

$$W = \ln Z \quad (10)$$

encodes the statistics in terms of cumulants, the derivatives of  $W$ . This is more efficient than encoding with moments, because higher order cumulants do not contain information already contained in lower orders.

#### D. Stochastic dynamics as a variational problem

With the expressions for the actions  $S_{\text{OM}}$  one can calculate moments and cumulants of activity as derivatives of the respective functionals  $Z$  and  $W$ . For a self-consistent determination of the mean activity, it is, however, beneficial to consider the variational problem of some functional  $\Gamma_{\text{OM}}[x^*]$  that assumes stationary points at the true mean value  $\bar{x}(t) \equiv \langle x(t) \rangle$ . To calculate it, we then have to solve the so-called equation of state  $\frac{\delta}{\delta x^*} \Gamma_{\text{OM}} = 0$  self-consistently, where  $\frac{\delta}{\delta x^*}$  denotes a functional derivative.

Indeed, such a functional is readily defined via the Legendre-Fenchel transform

$$\Gamma_{\text{OM}}[x^*] := \sup_j j^T x^* - W[j], \quad (11)$$

where  $x^T y = \int_{-\infty}^{\infty} x(t)y(t) dt$  denotes the inner product with respect to time. The so-defined  $\Gamma_{\text{OM}}$  is the effective action (or Gibbs free energy) [4].<sup>3</sup> It is central to the study of phase transitions, which reduces to finding the stationary points or regions of  $\Gamma_{\text{OM}}$  (see Ref. [79], i.p. chap. 6).<sup>4</sup> The variational formulation naturally solves the problem that derivatives of  $W$  become multivalued at first-order phase transitions; when  $W$  has a cusp and thus the system has multiple states with different values for the mean  $\langle x(t) \rangle$  at the same set of parameters. We study an example where spontaneous symmetry breaking causes such a cusp in Sec. II H.

Since  $W[j]$  is convex down in  $j$ , the Legendre-Fenchel transform in (11) is well defined. Note that the Legendre-Fenchel transform is a generalization of the Legendre transform for cases where  $W$  has a nondifferentiable point  $j_c$  (see also Appendix A 3 for a proof of convexity of  $W$ ). In such a case the mean of the field  $\langle x \rangle$  takes different values if  $j$  approaches  $j_c$  from the left or from the right; such systems show an abrupt change of the solution as a function of some control parameter, such as  $j$ ; an example is multistability in an attractor network. At the corresponding points  $\langle x \rangle$ ,  $\Gamma_{\text{OM}}$  has a flat segment, but is continuously differentiable everywhere<sup>5</sup> and is thus analytically simpler than the nonanalytical  $W$  (for a more detailed discussion on convexity, spontaneous symmetry breaking, and the necessity of the Legendre-Fenchel transform, see Appendix A 3). Another favorable property of the effective action is that symmetries of  $S_{\text{OM}}$  are also symmetries of  $\Gamma_{\text{OM}}$ , giving rise to Ward-Takahashi identities [13] and the study of Goldstone fluctuations in symmetry-broken states of systems that admit a continuous symmetry.

The simplest approximation to the effective action is the tree-level approximation. In correspondence to (3) we replace the integral over all configurations  $x$  in the definition of  $Z$  in (9) by its supremum, which yields  $W[j] \simeq \ln \sup_x \exp(S_{\text{OM}}[x] + j^T x) - \ln Z[0]$ . The monotonicity of  $\exp$  and the involution property of the Legendre transform (11) then yield

$$\Gamma_{\text{OM}}[x^*] \simeq -S_{\text{OM}}[x^*] + \text{const.} \quad (12)$$

The name “tree level” comes from the fact that if expanded in  $x^*$ , only diagrams of tree shape contribute (see, e.g., Ref. [4], p. 128, or Ref. [80], the Appendix “Equivalence of loopwise expansion and infinite resummation”). In the evaluation of the integral, one therefore neglects all fluctuations. Practically computing corrections in the OM formalism is complicated by the action involving a second-order differential operator. In the following section we review a formalism that circumvents this difficulty.

<sup>1</sup>Note that the notation as an integral is meant symbolically: For concrete calculations of the path integral, one always has to use the discrete version with a finite sum, perform the integrations, and draw the limit afterwards.

<sup>2</sup>Note the sign convention of the action in Eq. (9), which is defined without a minus sign in front. We will stick to this convention throughout this paper.

<sup>3</sup>Generalizing this approach, we could also allow for a nonvanishing source  $j$ , then minimizing  $\Phi[x^*; j] := \Gamma_{\text{OM}}[x^*] - j^T x^*$ .

<sup>4</sup>Throughout this paper, “i.p.” stands for “in particular.”

<sup>5</sup>At least in physically reasonable settings: A discontinuity in the derivative in  $\Gamma$  means that  $W$ , in turn, would have a flat segment. In such systems, changing the source field would not affect the mean; also fluctuations would vanish completely.

### E. Martin-Siggia-Rose-de Dominicis-Janssen path integral

It has been realized by Martin *et al.* [39] that computing response functions simultaneously together with correlation functions (8), simplifies practical computations. This is achieved by introducing a second field, the response field  $\tilde{x}$  by expressing the OM action with Gaussian noise (7) as

$$S_{\text{OM}}[x] = \text{extremize}_{\tilde{x}} S_{\text{MSRDJ}}[x, \tilde{x}]. \quad (13)$$

$S_{\text{MSRDJ}}$  is the Martin-Siggia-Rose-de Dominicis-Janssen (MSRDJ) action [39–41,81], defined on the  $2M$ -dimensional phase space as

$$S_{\text{MSRDJ}}[x, \tilde{x}] := \tilde{x}^T (\partial_t x - f(x)) + \tilde{x}^T \frac{D}{2} \tilde{x}. \quad (14)$$

Alternatively, one may obtain this result by performing a Hubbard-Stratonovitch transform, that is, by using the identity  $e^{-\frac{x^2}{2}} = \frac{1}{\sqrt{2\pi}} \int_{-\infty}^{\infty} e^{\frac{x^2}{2} + \tilde{x}x} d\tilde{x}$  with the response field as an additional auxiliary variable  $\tilde{x}$ . The MSRDJ formulation has the advantage that only a single first-order differential operator in time appears.

As for the OM form, we define the cumulant-generating functional in the MSRDJ formalism as

$$W[j, \tilde{j}] = \ln \int \mathcal{D}x \int \mathcal{D}\tilde{x} \exp(S_{\text{MSRDJ}}[x, \tilde{x}] + j^T x + \tilde{j}^T \tilde{x}). \quad (15)$$

Compared to its OM form,  $W[j, \tilde{j}]$  in addition incorporates the response properties of the system as differentiating once with respect to  $\tilde{j}$  and  $j$  each, respectively, yields the response function, the deviation of the mean of the process caused by a  $\delta$ -shaped inhomogeneity. This follows from comparing (14) with (15) to see that  $\tilde{j}$  can as well be regarded as an inhomogeneity in the stochastic differential equation (2) of the form

$$dx(t) = [f(x(t)) - \tilde{j}(t)] dt + dW(t). \quad (16)$$

This form also allows the extension of the MSRDJ formalism to non-Gaussian noise: If the stochastic increments  $W$  have a cumulant-generating functional  $W_\xi(j)$ , the last term  $\tilde{x}^T \frac{D}{2} \tilde{x}$  in the action (14) becomes  $W_\xi(-\tilde{x})$  [7]. The form (16) also shows that  $W[j, \tilde{j}]$  is real for real-valued  $j$  and  $\tilde{j}$ ; this is because (15), once  $\tilde{x}$  is integrated, is identical to the OM form (10),  $W[j] = \langle e^{j^T x} \rangle \in \mathbb{R}$ , for  $j \in \mathbb{R}$ , where  $x$  solves the SDE (16) and thus  $x \in \mathbb{R}$ .

The effective action in the MSRDJ formalism  $\Gamma[x, \tilde{x}]$  is defined in analogy to (11) as

$$\Gamma[x^*, \tilde{x}^*] = \tilde{j}^T \tilde{x}^* + \sup_j j^T x^* - W[j, \tilde{j}], \quad (17)$$

where  $\tilde{j}$  is chosen such that the right-hand side is stationary. Since  $W$  is convex down in  $j$ , taking the Legendre-Fenchel transform with regard to  $j$  is involutive; this even holds for  $W[j, \tilde{j}]$  that are nondifferentiable in  $j$ . We show in Appendix A 4 that the transform from  $j$  to  $x^*$  renders the resulting functional differentiable in  $\tilde{j}$ , given the system is in thermodynamic equilibrium or given that linear response functions of cumulants of arbitrary order exist.

Like  $Z$  and  $W$ ,  $\Gamma$  contains the full information of the system, including effects from noise-driven fluctuations. The

definition of  $\Gamma$  as the Legendre transform of  $W$  implies the identities

$$\begin{aligned} \Gamma_x^{(1)}[x^*, \tilde{x}^*] &:= \frac{\delta}{\delta x^*} \Gamma[x^*, \tilde{x}^*] = j, \\ \Gamma_{\tilde{x}}^{(1)}[x^*, \tilde{x}^*] &:= \frac{\delta}{\delta \tilde{x}^*} \Gamma[x^*, \tilde{x}^*] = \tilde{j}, \end{aligned} \quad (18)$$

which are implicit equations for  $x^*$  and  $\tilde{x}^*$ , the equations of state. For the physically relevant value  $j = 0$  of the source field, normalization in systems with conserved probability implies that the first equation (18) always admits a solution  $\tilde{x}^* \equiv 0$  (Appendix). We further show in Appendix A 1 that the second equation is then equivalent to the requirement that the fluctuations around the true mean value average to zero within the OM formalism; the additional Legendre transform from  $\tilde{j}$  to  $\tilde{x}$ , which is not always well defined [82], can therefore be regarded a formal step only that does not require convexity of  $W[j, \tilde{j}]$  in  $\tilde{j}$ .

Approximating  $\Gamma \simeq -S$  up to the tree level, reduces (18) to the naive mean-field approximation (3) showing their tight relation. The resulting path maximizes the probability. Because it ignores fluctuations, we also refer to it as the saddle point approximation, or the mean-field approximation.

The use of the MSRDJ formalism simplifies the calculations of the effective action with respect to the OM formalism. As a consequence of the response fields being only auxiliary variables, their expectation values vanish, i.e.,  $\langle \tilde{x}^n \rangle = 0 \forall n$  for solutions with stationary statistics (for a proof see Coolen [83] or Appendix A 5 here).

To see why the Legendre transform is closely linked with the construction of self-consistent solutions for the mean values of the fields  $x^*$  and  $\tilde{x}^*$ , it is instructive to rewrite (17) analogously with  $y = (x, \tilde{x})$  and  $k = (j, \tilde{j})$  as<sup>6</sup>

$$\begin{aligned} \Gamma[y^*] &= -\ln \int_y \exp(S[y] + k^T(y - y^*)) \\ \text{with } \frac{\delta \Gamma}{\delta k} &\stackrel{!}{=} 0. \end{aligned} \quad (19)$$

The latter condition enforces that  $\langle y - y^* \rangle \stackrel{!}{=} 0$ , so we integrate over ensembles of configurations that obey this constraint; in other words, the mean values for both fields  $x$  and  $\tilde{x}$  take the values given by the argument of  $\Gamma$ . The right-hand side of (19) will hence depend via  $y^*$  on the self-consistently determined value. In Sec. III L we will show that this step is crucial to study systems at bifurcations.

### F. Effective equation of motion, vertex functions

To see how the equations of state (18) lead to self-consistency equations, we expand  $\Gamma$  around a reference point  $(\bar{x}, \bar{\tilde{x}})$

$$\Gamma[x^*, \tilde{x}^*] = \sum_{n=0}^{\infty} \sum_{m=0}^{\infty} \frac{1}{n!m!} \frac{\delta^{n+m} \Gamma}{(\delta x^*)^n (\delta \tilde{x}^*)^m} [\bar{x}, \bar{\tilde{x}}] \delta x^n \delta \tilde{x}^m, \quad (20)$$

<sup>6</sup>In the following equation the symbol “ $\stackrel{!}{=}$ ” denotes “is supposed to equal”; that is, the argument of the function is to be determined such that equality holds.

where we introduced the derivatives  $\frac{\delta^{n+m}\Gamma}{(\delta x^*)^n(\delta \tilde{x}^*)^m}$ , the vertex functions, as covectors and the deflections  $\delta x(t) := x^*(t) - \bar{x}$  and  $\delta \tilde{x}(t) := \tilde{x}^*(t) - \bar{\tilde{x}}$  together with the notation

$$\begin{aligned} & \frac{\delta^{n+m}\Gamma}{(\delta x^*)^n(\delta \tilde{x}^*)^m}[\bar{x}, \bar{\tilde{x}}] \delta x^n \delta \tilde{x}^m \\ &:= \Pi_{i=1}^n \int dt_i \Pi_{j=1}^m \int ds_j \\ & \times \frac{\delta^{n+m}\Gamma[x^*, \tilde{x}^*]}{\delta x^*(t_1) \cdots \delta x^*(t_n) \delta \tilde{x}^*(s_1) \cdots \delta \tilde{x}^*(s_m)} \Big|_{x^*=\bar{x}, \tilde{x}^*=\bar{\tilde{x}}} \\ & \times \delta x(t_1) \cdots \delta x(t_n) \delta \tilde{x}(s_1) \cdots \delta \tilde{x}(s_m) \\ &:= \Gamma_{\underbrace{x \dots x}_{n\text{-times}} \underbrace{\tilde{x} \dots \tilde{x}}_{m\text{-times}}}^{(n+m)} \delta x^n \delta \tilde{x}^m. \end{aligned} \quad (21)$$

We determine the true mean values  $\bar{x}$  and  $\bar{\tilde{x}}$  of the two fields by solving the two implicit equations  $\Gamma^{(1)}[x^*, \tilde{x}^*] \stackrel{!}{=} 0$  [compare (18)]. All further Taylor coefficients (or Volterra kernels) in (20) have physical meanings.  $\Gamma_{\tilde{x}\tilde{x}}^{(2)}$  includes all corrections to the Gaussian component of the noise and the mixed second-order derivatives are the inverse of the response functions. Consequently,  $\Gamma^{(2)}$  contains the corrections to the second cumulant since it is the inverse of  $W^{(2)}$ . The Taylor coefficients of order  $n$  describe the interdependence of measurements at  $n$  points in time. We make this more explicit by considering  $\Gamma_{\tilde{x}xx}^{(3)}$  in the second equation of state  $\Gamma_{\tilde{x}}^{(1)}[x^*, \tilde{x}^*] = \tilde{j}(t)$  [see second line in (18)]. We use the decomposition of the effective action into the action and the fluctuation correction  $\Gamma = -S + \Gamma_{\text{fl}}$  and expand  $\Gamma_{\tilde{x}}^{(1)}$  in a Volterra series as shown for  $\Gamma$  in (20). Then the second equation of state takes the form

$$\begin{aligned} \tilde{j}(t) = & - \left[ \frac{\partial}{\partial t} - f'(\bar{x}) \right] \delta x(t) - D \delta \tilde{x}(t) \\ & + \frac{1}{2} f''(\bar{x}) \delta x(t) \delta x(t) + \cdots + \int ds \Gamma_{\tilde{x}x, \text{fl}}^{(2)}(t, s) \delta x(s) \\ & + \frac{1}{2} \int ds \int du \Gamma_{\tilde{x}xx, \text{fl}}^{(3)}(t, s, u) \delta x(s) \delta x(u) + \cdots \end{aligned} \quad (22)$$

The first equation of state (18)  $\Gamma_x^{(1)} = j \equiv 0$  admits the solution  $\tilde{x}^* = 0$  if probability is conserved (see, e.g., Appendix A 1). Thus,  $\Gamma_{\text{fl}}$  accounts for the corrections due to the noise. Additionally, we neglect all higher order terms as well as the remaining components of  $\Gamma^{(3)}$ , which are subleading, as we discuss in Sec. II K after (43). Looking at the fluctuation corrections in (22), we notice that in general the noisy system exhibits interactions that are nonlocal in time [cf. (21)] even if the deterministic system does not contain such terms. As a consequence, it is not possible to define a potential for which  $\partial_t x(t) = -\partial_x V(x)$  even if we set  $\tilde{x} = 0$ , in contrast to the tree-level approximation. The first occurrence of an effective equation of motion as (22) in the context of neuronal networks has been presented in Ref. [[84], Eqs. (42) and (43)] using the Doi-Peliti formalism [85,86] applied to Markovian systems with discrete state spaces.

We call the derivatives appearing in (20) “full vertices” or “full vertex functions” as opposed to those of the action  $S$ , which we refer to as “bare vertices.” The vertex functions

not only serve as means to calculate cumulants, as we show next, but can also be interpreted directly. For example, those with only one derivative with respect to  $\tilde{x}$  (and at least one with respect to  $x$ ) can be seen as temporal kernels in an effective differential equation for the mean (22). Vertices with more derivatives with respect to  $\tilde{x}$  represent effective noise terms. Henceforth, we will therefore focus our attention on vertices to obtain effective descriptions of nonlinear stochastic systems.

### G. Extracting statistical dependencies from vertex functions

The computation of the effective action  $\Gamma$  or its Taylor coefficients, the vertex functions  $\Gamma^{(n)}$ , ultimately serves the goal to compute observables, the statistics of  $x$ .

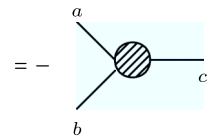
The second cumulant, the covariance  $W^{(2)}$ , obeys the relation

$$\begin{aligned} \Gamma^{(2)}[x^*, \tilde{x}^*] &= \begin{pmatrix} \frac{\delta^2 \Gamma[x^*, \tilde{x}^*]}{\delta x^{*2}} & \frac{\delta^2 \Gamma[x^*, \tilde{x}^*]}{\delta x^* \delta \tilde{x}^*} \\ \frac{\delta^2 \Gamma[x^*, \tilde{x}^*]}{\delta \tilde{x}^* \delta x^*} & \frac{\delta^2 \Gamma[x^*, \tilde{x}^*]}{\delta \tilde{x}^{*2}} \end{pmatrix} \\ &= \begin{pmatrix} \frac{\delta^2 W[j, \tilde{j}]}{\delta j^2} & \frac{\delta^2 W[j, \tilde{j}]}{\delta j \delta \tilde{j}} \\ \frac{\delta^2 W[j, \tilde{j}]}{\delta \tilde{j} \delta j} & \frac{\delta^2 W[j, \tilde{j}]}{\delta \tilde{j}^2} \end{pmatrix}^{-1} = [W^{(2)}]^{-1}, \end{aligned} \quad (23)$$

which follows by differentiating (18). Differentiating the latter relation  $n-1$  times with respect to  $j$ , using  $\frac{\partial}{\partial j} = \frac{\partial x^*}{\partial j} \frac{\partial}{\partial x^*} = (\Gamma^{(2)})^{-1} \frac{\partial}{\partial x^*}$ , and repeated application of (23) yields expressions for the  $n$ th cumulant, expressed in terms of derivatives of  $\Gamma$  (see also Ref. [87], p. 115ff.).

The resulting expressions have the form of tree graphs, with vertex functions forming the nodes and edges formed by the full propagators  $(\Gamma^{(2)})^{-1}$  (see, e.g., Ref. [4], Sec. 6.3, or [80], Sec. XIII). The third-order cumulants, for example, follow as

$$W_{abc}^{(3)} = - \sum_{a'b'c'} \Gamma_{a'b'c'}^{(3)} (\Gamma^{(2)})_{a'a}^{-1} (\Gamma^{(2)})_{b'b}^{-1} (\Gamma^{(2)})_{c'c}^{-1}$$



Depending on the choice of the sources  $a, b, c$ , we either get the third-order cumulant of the variable  $x$  [for  $a = j(s)$ ,  $b = j(t)$ ,  $c = j(u)$ ] or the second-order response kernel of the mean to a perturbation of the system [for  $a = j(s)$ ,  $b = \tilde{j}(t)$ ,  $c = \tilde{j}(u)$ ], or the change of the autocorrelation due to a perturbation at linear order [for  $a = j(s)$ ,  $b = j(t)$ ,  $c = \tilde{j}(u)$ ]. The combination with  $a, b, c$  each equal to a  $\tilde{j}$  vanishes identically in stationary states, because the moments of  $\tilde{x}$  all vanish (see Appendix A 2).

Even though we here consider the dynamics of a single neuron, the formalism transparently extends to compute higher order statistics of neuronal activity also across different neurons, the only difference being that the source fields and original field will obtain an additional index that identifies the

respective neuron. Computing such correlations is a topic of considerable interest in neuroscience [88].

### H. Relation between the effective actions $\Gamma_{\text{OM}}$ and $\Gamma_{\text{MSRDJ}}$

A notable advantage of the MSRDJ formalism is that it can be easily generalized to arbitrary noise statistics. By integrating out the response field  $\tilde{x}$  we can define the corresponding OM action by

$$S_{\text{OM}}[x] = \ln \int \mathcal{D}\tilde{x} \exp(S_{\text{MSRDJ}}[x, \tilde{x}]).$$

We show in Appendix A 5 that if the effective actions exist in both formalisms, they are related by

$$\Gamma_{\text{OM}}[x^*] = \text{extremize}_{\tilde{x}^*} \Gamma_{\text{MSRDJ}}[x^*, \tilde{x}^*]. \quad (24)$$

Choosing  $\tilde{x}^*$  in (24) so that it extremizes  $\Gamma_{\text{MSRDJ}}$ , conserves the full information on the fluctuations. The more convenient MSRDJ formalism can therefore be used to perform the actual computation and only subsequently one obtains the physically and probabilistically interpretable OM form.

The definition (24) hence makes the physically interpretable OM effective action available even if an OM action  $S_{\text{OM}}$  cannot be formulated in the non-Gaussian case. Therefore, relating approximations of the respective effective actions can be nontrivial: Cooper *et al.* derived that  $\Gamma_{\text{MSRDJ}}$  and  $\Gamma_{\text{OM}}$  of the KPZ model yield the same effective equations if one performs a saddle-point approximation in the auxiliary fields of the Hubbard-Stratonovitch transform of the non-Gaussian parts of the respective actions [89]. We here provide a general relation between the two effective actions, that is valid in full generality beyond specific approximations. It may therefore be used to check whether a pair of approximations, each formulated for one of the two effective actions, is equivalent. The finding by Cooper *et al.* [89] is one such pair of equivalent approximations.

As a minimal non-Gaussian example, we study the influence of a nonvanishing third-order cumulant of the noise defined by its cumulant-generating function

$$W_\xi(y) = \frac{D}{2}y^2 + \frac{\alpha}{3!}y^3 + O(y^4) \quad (25)$$

on the generalized OM action, where we assume that  $\frac{\alpha}{D^2} \ll 1$  and that we can neglect all higher order terms  $O(y^4)$ . A straightforward perturbation calculation in  $\alpha$ , shown in Appendix A 6, demonstrates that

$$S_{\text{OM}}[x] = \frac{1}{2} \ln \left( \frac{2\pi}{D} \right) - \underbrace{\frac{[\dot{x} - f(x)]^2}{2D} - \frac{\alpha}{3!} \frac{[\dot{x} - f(x)]^3}{D^3}}_{=\text{extremize}_{\tilde{x}} S_{\text{MSRDJ}}[x, \tilde{x}] + O(\alpha^2)} + \frac{\alpha}{2D^2} [\dot{x} - f(x)] + O(\alpha^2). \quad (26)$$

So, while (24) holds for arbitrary statistics of the noise, the analogous relation for the respective actions (13) does not in this case. Therefore, we encounter the interesting case that the effective action in the OM formalism might be easier to determine than the corresponding action. An example

where the noise is non-Gaussian is the stochastic dynamics of pulse-coupled (spiking) network models. Here typically the statistics of the noise is close to the Poisson process [11,48].

A simple special case arises if the noise, including all fluctuation corrections, remains Gaussian. The field  $\tilde{x}$  then still appears quadratically in the effective action. Extremizing with respect to  $\tilde{x}$  in (24) is then identical to performing the integral over  $\tilde{x}$ . A corollary is that under these conditions, the OM effective action has the same form as its tree-level approximation (7), only with vertices  $S^{(n)}$  replaced by effective vertices  $-\Gamma^{(n)}$ . For example, the noise matrix  $D = S_{\tilde{x}\tilde{x}}^{(2)}$  is replaced by  $-\Gamma_{\tilde{x}\tilde{x}}^{(2)}$ , an approximation that is valid if corrections of order  $O(\tilde{x}^3)$  are small.

### I. Loop expansion


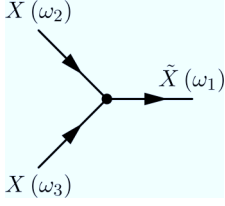
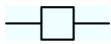
The effective action characterizes the state of a stochastic system. Fluctuations provide corrections to the effective action that are commonly defined as  $\Gamma = -S + \Gamma_{\text{fl}}$ . A standard approach in statistical physics and quantum field theory to obtain these corrections is the loop expansion. For an introduction, consult for example the books by Kleinert [[72], chap. 3.23.] or Zinn-Justin [[4], chap. 7.7.ff]. This technique has first been applied in the context of neuronal networks by Buice and Chow [45]; see, e.g., Refs. [8,80] for recent reviews.

We here briefly outline the loop expansion on the concrete example for four reasons. First, all terms in the action are at least of linear order in the response field  $\tilde{x}$ ; its equation of state therefore always admits a trivial solution  $\tilde{x} \equiv 0$  and the  $\tilde{x}\tilde{x}$ -propagator vanishes. These are features specific to the MSRDJ formalism that deserve some comments. Second, to illustrate that the Feynman diagrams (sometimes referred to as Mayer graphs [79,90]) in the one-loop approximation are essentially the same as those that appear in the less standard functional renormalization group method. Third, the loop expansion gives us the leading order fluctuation corrections beyond tree level,  $\Gamma = -S$ . It will allow us in subsequent sections to derive an effective deterministic equation for the mean and a linear convolution equation for the variance of the process. One-loop corrections also show which new vertices are generated along the renormalization group flow. And, fourth, the loop expansion provides a systematic way to derive self-consistency equations for the mean of a process, an idea that is conceptually continued in the functional renormalization group approach to arbitrary orders of the statistics.

In contrast to mean-field theory, the loopwise expansion can be improved systematically because it is an expansion in a parameter that measures the fluctuation strength, often related to the system size. Here we consider a one-dimensional system, but it also depends on a small parameter that organizes the loop expansion. In Appendix A 7 we demonstrate that adding a loop to a given diagram introduces an additional factor which equals the product of the strength of the nonlinearity  $\beta$  squared [see (27)] and the variance of the noise  $D$ . Thus, in our case the loop expansion amounts to an expansion in terms of powers of  $\beta^2 D$ .



TABLE I. Translation between graphical elements of Feynman diagrams and corresponding algebraic terms. Amputated legs do not introduce an additional factor in the algebraic expression but indicate the value of the field  $X$  (ingoing leg) or  $\tilde{X}$  (outgoing leg) at which we evaluate the expression. A diagram contributing to an  $n$ -point interaction  $\frac{\delta^n}{\delta \tilde{X}(\sigma_1) \cdots \delta X(\sigma_n)} \Gamma_{\text{fl}}$  has  $n$  external amputated legs where the number of ingoing and outgoing legs corresponds to the number of functional derivatives with respect to  $X$  and  $\tilde{X}$ . The generalization of the interaction vertex to higher order interactions is straightforward (see Appendix A 12 for an example). The prefactor is that of a usual Taylor expansion.

Graphical representation	Algebraic term (loop expansion)	Algebraic term (fRG)	Meaning
$X(\omega) \longleftrightarrow X(\omega')$	$\Delta_{XX}^0(\omega, \omega') = \frac{2\pi D}{\omega^2 + m^2} \delta(\omega + \omega')$	$\Delta_{XX,\lambda}(\omega, \omega') = [\Gamma_\lambda^{(2)}]_{XX}^{-1}(\omega, \omega')$	$xx$ -component of the bare/full propagator
$\tilde{X}(\omega) \longrightarrow X(\omega')$	$\Delta_{\tilde{X}X}^0(\omega, \omega') = \frac{2\pi}{i\omega + m} \delta(\omega + \omega')$	$\Delta_{\tilde{X}X,\lambda}(\omega, \omega') = [\Gamma_\lambda^{(2)}]_{\tilde{X}X}^{-1}(\omega, \omega')$	$\tilde{x}x$ -component of the bare/full propagator
 $\tilde{X}(\sigma)$	—	—	External (amputated) leg
	$\frac{1}{12!} S_{XXX}^{(3)}(\omega_1, \omega_2, \omega_3) = -\frac{\beta}{(2\pi)^2} \delta(\omega_1 + \omega_2 + \omega_3)$	$\frac{1}{12!} \Gamma_{\tilde{X}XX,\lambda}^{(3)}(\omega_1, \omega_2, \omega_3)$	Bare/full three-point interaction vertex
	—	$\frac{\partial R_\lambda}{\partial \lambda}$	Derivative of the regulator term

Because the solvable part of our theory is Gaussian, we express cumulants of higher order by cumulants of order two in  $x$  and  $\tilde{x}$ . We call

$$\Delta(t-s) = \begin{pmatrix} \langle x(t) x(s) \rangle & \langle x(t) \tilde{x}(s) \rangle \\ \langle \tilde{x}(t) x(s) \rangle & \langle \tilde{x}(t) \tilde{x}(s) \rangle \end{pmatrix} = \begin{pmatrix} x(t) \longleftrightarrow x(s) & x(t) \longrightarrow \tilde{x}(s) \\ \tilde{x}(t) \longrightarrow x(s) & 0 \end{pmatrix}$$

the propagators of the theory, where we have chosen a representation in time, but we will often switch to frequency space (and back). Further ingredients are the bare interaction vertices which, in general, are given by the nonquadratic components of the action, in our case the Taylor coefficients of the term  $\tilde{x} f(x)$ . We provide the translation between diagrammatic expressions and their algebraic counterparts in Table I.

Henceforth, we consider the corrections to the mean value, the variance and one of the three-point vertices in the neuroscientific case, where  $f(x) = -x + J g(x)$ . For small activities we can expand the gain function and keep only its linear and quadratic terms. This is in line with the observation that activation functions are typically convex in the vicinity of the working point [91]. We define

$$g(x) = x + \alpha x^2.$$

Therefore, the only bare vertex is  $S_{\tilde{x}xx}^{(3)}$ . We choose this quadratic nonlinearity also for pedagogical reasons, as it constitutes the simplest nontrivial example which is suitable to demonstrate the methods. For practical calculations it is convenient to switch the parametrization to

$$f(x) = -lx + \beta x^2, \quad (27)$$

where  $l = 1 - J > 0$  and  $\beta = \alpha J > 0$ . Then in frequency domain the bare propagator reads

$$\Delta^0(\omega, \omega') = [-S^{(2)}]^{-1} = \left[ \begin{pmatrix} 0 & -i\omega + m \\ i\omega + m & -D \end{pmatrix} \frac{\delta(\omega + \omega')}{2\pi} \right]^{-1} = \begin{pmatrix} \frac{D}{\omega^2 + m^2} & \frac{1}{-i\omega + m} \\ \frac{1}{i\omega + m} & 0 \end{pmatrix} 2\pi \delta(\omega + \omega'), \quad (28)$$

where  $m = -l + 2\beta x^*$  plays the role of a masslike term in the theory. For the definition of the Fourier transform, as we use it throughout this paper; see Appendix A 13. Similarly, for the interaction vertex we obtain

$$\begin{array}{c} X(\omega_2) \\ \searrow \\ \bullet \\ \nearrow X(\omega_1) \end{array} \begin{array}{c} \tilde{X}(\omega_3) \\ \longrightarrow \end{array} = \frac{1}{2} S_{\tilde{X}XX}^{(3)} = -\frac{\beta}{(2\pi)^2} \delta(\omega_1 + \omega_2 + \omega_3).$$

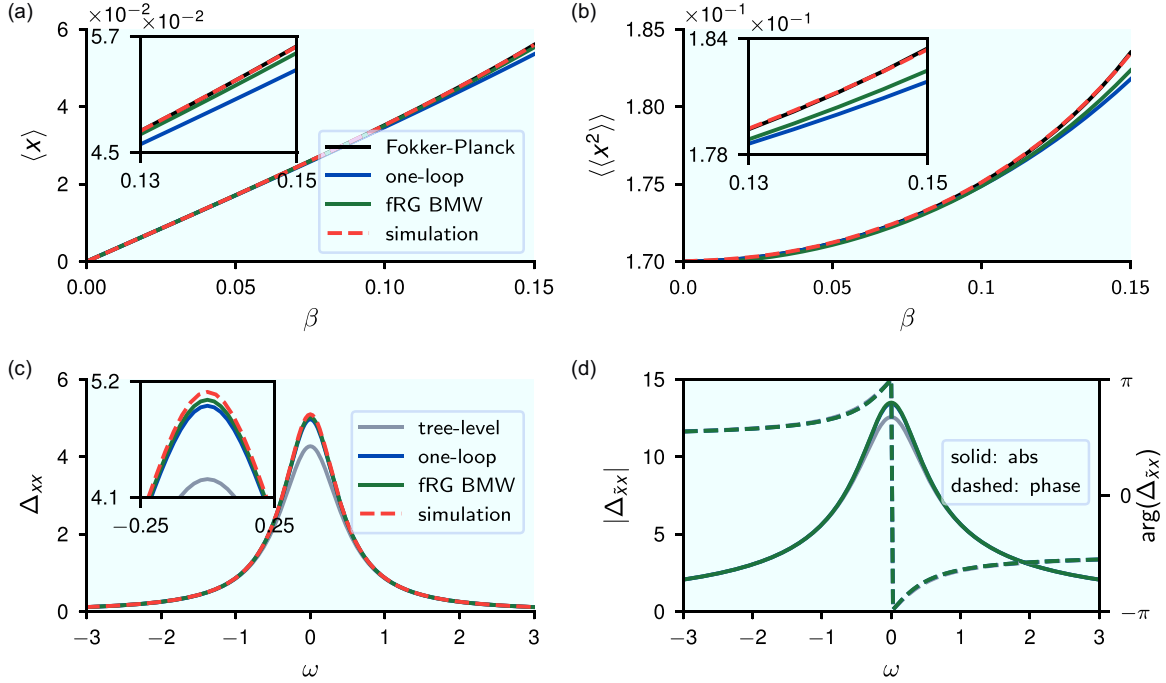


FIG. 1. Mean (a) and variance (b) as functions of the strength  $\beta$  of the nonlinearity for different methods. Parameters:  $l = 0.5$ ,  $D = 0.17$ . (c) Power spectrum of the system from simulations compared to different approximations. (d) Absolute value (solid lines) and phase (dashed lines) of the response function. Its zero mode corresponds to the integrated response of a neural network to a delta-shaped perturbation; for other frequencies the response is weighted according to the respective mode. The results of the one-loop and the fRG BMW approximation coincide at this resolution. For comparison between simulations and theory results of the response of the system was subject to small (but not infinitesimally small) perturbations; see Sec. II J, Fig. 2. Parameters for (c) and (d):  $l = 0.5$ ,  $D = 0.17$ , and  $\beta = 0.15$ .

The frequencies are conserved at each vertex and each propagator. Since in the action  $S[x, \tilde{x}]$  the function  $f(x)$  is multiplied with one  $\tilde{x}$  [see (14)], we conclude that the  $n$ th Taylor coefficient of  $f(x)$  leads to an interaction vertex with  $n$  incoming  $x$ -legs and one outgoing  $\tilde{x}$ -leg.

### 1. One-loop correction to the mean value

The first correction to the mean value is given by the contribution known as the tadpole diagram that consists of one interaction vertex whose two incoming legs are connected by an undirected propagator ( $\Delta_{xx}$ ):

$$\Gamma_{\tilde{x}, \text{fl.}}^{(1)}(\sigma) = (-1) \text{ (tadpole diagram) } = \frac{2\pi\beta}{(2\pi)^2} \int d\omega \frac{D}{\omega^2 + m^2} \delta(\sigma) = \frac{\beta D}{2|m|} \delta(\sigma). \quad (29)$$

Henceforth, the  $\sigma_i$  denote the external frequencies of the derivatives of the effective action, which are represented by wiggly lines. In Appendix A 7 we provide a brief summary of how to evaluate the Feynman diagrams that we use in this paper. Intuitively, the above diagram represents the naïve estimation for the correction to the mean (6) that is obtained by taking the expectation value of the quadratic nonlinearity (vertex with two incoming legs) over the Gaussian fluctuations around the stationary mean (propagator connecting these two legs). A conceptual difference is, though, that the mean value

$\tilde{x}$  here affects the point about which we perform the linear response approximation, thus it appears on the right-hand side through the value of the mass term  $m(\tilde{x})$  in the propagators: The approximation is hence self-consistent in the mean, defining  $\tilde{x}$  as the solution of the equation of state (18) as

$$0 = \tilde{j} = -S_{\tilde{x}}^{(1)} + \Gamma_{\text{fl.}, \tilde{x}}^{(1)} = f(\tilde{x}) + \frac{\beta D}{2|m(\tilde{x})|} \quad (30)$$

$$= -l\tilde{x} + \beta\tilde{x}^2 + \frac{\beta D}{2|-l + 2\beta\tilde{x}|}. \quad (31)$$

But here, too, we take into account the nonlinearity only by considering its effect of shifting the mean value and therefore the linear order ( $-l \rightarrow m(\tilde{x})$ ), as in our naïve approximation in linear response in (4), and then calculate the expectation value of the nonlinearity using this approximation. This contribution is indeed the only one to consider at this loop order as we demonstrate in Appendix A 7. The result for the corrected mean value as a function of the strength of the nonlinearity is shown in Fig. 1. Due to conservation of frequencies at the vertex, there are only corrections for the zero frequency mode of the mean value.

### 2. One-loop correction to the variance and higher order statistics

To compute the one-loop corrections to the variance, we determine the corrections to the propagator by using the relation  $\Delta = (\Gamma^{(2)})^{-1}$  (23). The first-order correction to  $\Gamma^{(2)}$

is given by the sum of all one-loop diagrams with two external legs. The diagrams and the corresponding expressions can be found in Appendix A 7 and finally yield

$$\Delta_{xx}(t) = - \left[ \frac{D[m_1^2 - (2m)^2 + A]}{2(m_1^2 - m_2^2)m_1} e^{m_1|t|} + \frac{D[(2m)^2 - m_2^2 - A]}{2(m_1^2 - m_2^2)m_2} e^{m_2|t|} \right],$$

for the correlation function, where

$$\begin{aligned} A &= 2\beta^2 D/m \\ m &= -l + 2\beta\tilde{x} \\ m_{1/2} &= 3m/2 \pm \sqrt{m^2/4 - A}. \end{aligned}$$

The value at  $t = 0$  equals the variance  $\langle\langle x \rangle\rangle$ , which is plotted in Fig. 1(b). In this figure we compare the mean value and the variance computed using various methods, where we use the solution by the Fokker-Planck equation [92] as the ground truth, which indeed agrees very well with the simulated results. In particular, we observe that the one-loop approximation is markedly better than the tree-level approximation, which predicts  $\langle x \rangle = 0$  and  $\langle\langle x^2 \rangle\rangle = 0.17$  for all  $\beta$ . Figures 1(c) and 1(d) show the power spectrum  $[\Delta_{xx}(\sigma)]$  and the response function  $[\Delta_{\tilde{x}x}(\sigma)]$  of the system. Like the correction to the three-point vertex (compare Appendix A 7), the corrections to the propagator are largest for  $\sigma_i = 0$  and decay algebraically with increasing frequency. In particular the fluctuation corrections to  $\Delta_{\tilde{x}x}(\sigma)$  lead to an elevation of the power at low frequencies. This qualitative effect depends only on coarse features of the system, such as the convexity of the nonlinearity. One may therefore expect qualitatively similar features in networks which operate in regimes in which the neuronal transfer function is expansive, as typical for the low rate regimes of the cortex [91].

In principle we could try to find a more accurate approximation of the effective action by going to higher loop orders. However, this already becomes unwieldy at the next order because the number of diagrams quickly increases and the integration of the loop momenta becomes numerically expensive. Instead, we will use renormalization group techniques to obtain self-consistency at arbitrary levels of the statistics.

Even though the one-loop calculations are not confined to a certain parameter range, we may not disregard the fact that strictly speaking there is no stationary solution for our particular choice for  $g(x)$ , because  $x$  escapes towards infinity almost surely for  $t \rightarrow \infty$ . However, for finite times and  $l/\beta \gg \sqrt{D}$ , the second unstable fixed point  $x_1 = l/\beta$  is far away from the stable fixed point  $x_0 = 0$  measured in units of the fluctuations. Therefore, the escape probability is negligible and we confine our analysis to this case by effectively setting the escape probability to zero, in particular for the otherwise exact Fokker-Planck solution to which we compare the results of the loop expansion. As we show in Appendix A 7 d, the position  $x_1$  of the second unstable fixed point and the strength of the nonlinearity are controlled by the same effective parameter. In the presented example one therefore cannot increase the magnitude of fluctuation corrections without also increasing the escape rate. Figure 6 shows a different

system that has notable fluctuation corrections. A rigorous analysis of the complete setting including escape is a problem on its own requiring the introduction of a probability for a path conditioned on the requirement that it has not escaped to infinity. For a leak term equal to zero, this analysis has recently been performed [93]. Another possibility is to consider the time-dependent problem, as is done, for example, in the context of laser physics [94].

The stochastic differential equation considered here is similar to a typical differential equation describing the evolution of the membrane potential of a neuron fed by fluctuating input from the network. Examples are the quadratic integrate-and-fire neuron [95] or the exponential integrate-and-fire neuron [96]. The escape of the dynamical variable across the second, unstable fixed point here denotes the firing of the cell. The biophysical mechanism of the repolarization subsequently resets the membrane potential to a low value after the escape. The firing rate of a model can in principle be computed by determining this probability of escape. One-loop corrections to the escape probability, however, require the computation of Gaussian fluctuations around the most likely escape path; the path itself is here a function of time. Thus it is more complicated than determining the stationary statistics considered here (see, e.g., Ref. [97] for more details on rare events in metastable systems).

We will demonstrate in the next chapter by comparing to simulations that neglecting the possibility of escaping is justified in the presence of a leak term for sufficiently low noise and nonlinearity.

## J. Time dependence of statistics

Applications often also require the study of the time-dependent response of a system. In the context of neuronal networks, for example, we would like to quantify the response of the system to an applied stimulus. It is *a priori* not clear what the effect of noise is for a response that is driven by a transient stimulus. The simplest approximation (4) that neglects the effect of the noise also provides us with the lowest order approximation of such a response. A special “input” is the noise-mediated influence of the past of the mean value of  $x$  on itself. The following example illustrates how the effective equation of motion (22) with vertex functions computed in one-loop approximation explains the nontrivial interplay of noise and nonlinearities.

### 1. Relaxation of a small departure from the mean

As an example, we consider the response of the system to a stimulus, represented by the deflection of the system from its mean value at time  $t_0 = 0$  by setting  $\tilde{j}(t) = -\delta x(0)\delta(t)$  in (22) and examine the equation of motion that describes its relaxation back to the baseline. We derive the equation of motion by solving the second equation of state, for example, in the form of (22), for  $\partial_t \delta x(t)$ . We ensure that we consider only nonescaping trajectories by setting  $\tilde{x} \equiv 0$  (see Appendix A 1). By inserting the tree-level approximation  $\Gamma_{\tilde{x}} = 0$  into (22), we obtain

$$\partial_t \delta x(t) = -l\delta x(t) + \beta\delta x(t)^2,$$

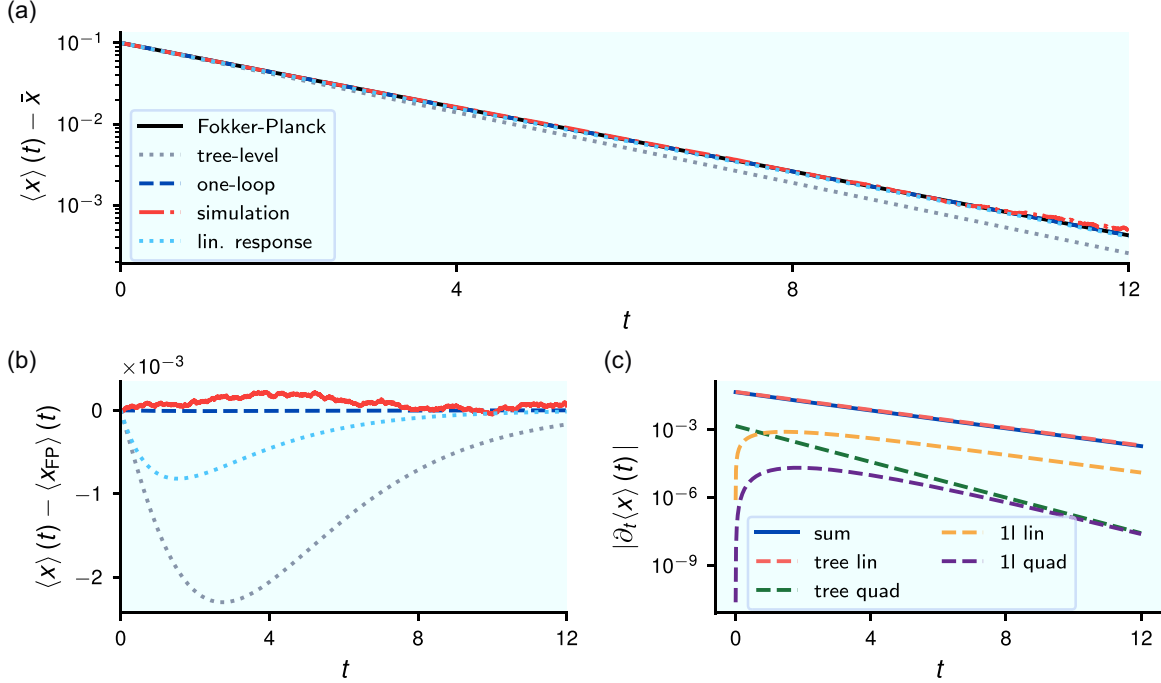


FIG. 2. Relaxation after deflection described by effective equation of motion. The one-loop result is given by (32) and the Fokker-Planck result by the coupled differential equations (A35) and (A36). For the simulations, we let the activity of the system decay to its baseline and then stimulate it by a small perturbation  $\delta x_0$  applied to the current value of  $x$ . Subsequently, the activity relaxes back to its stationary state. (a) Mean activity averaged over  $2.9 \times 10^9$  trials of the relaxation process. (b) Difference between the various approximations and the simulation to the Fokker-Planck result. The linear response (dotted light blue) contains solely the terms in (32) that are linear in  $\delta x$ . (c) Different contributions to the right-hand side of (32). Sum shows the full right-hand side (blue); linear part in  $\delta x$  of the tree-level term (dashed salmon pink); quadratic part in  $\delta x$  of the tree-level terms (dashed green); linear term of one-loop correction (dashed yellow); quadratic term of one-loop corrections (dashed violet).

which we can integrate analytically

$$\begin{aligned} \delta x(t) &= \frac{c}{e^{lt} + \frac{c\beta}{l}(1 - e^{lt})} \\ &= ce^{-(l-c\beta)t + O((lt)^2)} + O\left(\left(\frac{\beta c}{l}\right)^2\right), \quad \text{where } c = \delta x(0). \end{aligned}$$

We notice that the second term in the denominator is due to the nonlinearity and leads to a slower relaxation of the system back to its mean value compared to the time constant  $l^{-1}$  of the linear part of the dynamics. In the previous section, Sec. III, we computed the one-loop corrections to  $\Gamma_{fl}$ , which we can insert into (22) to obtain a one-loop approximation of the equation of motion

$$\begin{aligned} \partial_t \delta x(t) &= m \delta x(t) + \beta \delta x(t)^2 - \frac{2\beta^2 D}{m} \int_{t_0}^t dt' \underbrace{e^{2m(t-t')} \delta x(t')}_{\propto \Gamma_{xx,fl}^{(2)}(t,t')} \\ &\quad - \frac{8\beta^3 D}{m} \int_{t_0}^t dt' \int_{t_0}^t dt'' \underbrace{H(t' - t'') e^{2m(t-t')}}_{\propto \Gamma_{xxx,fl}^{(3)}(t,t',t'')} \\ &\quad \times \delta x(t') \delta x(t''), \end{aligned} \quad (32)$$

where  $H(t)$  denotes the Heaviside step function. Let us inspect the single terms in (32) in more detail: The first line is the tree-level contribution.  $\Gamma_{fl}^{(2)}$  mediates a linear self-feedback for the departure  $\delta x$  of the process from its stationary value. One of the interpretations of  $\Gamma_{xxx}^{(3)}$ , writing it as  $\Gamma_{xxx}^{(3)}(t, t', t'') =$

$\frac{\delta}{\delta x(t'')} \Gamma_{xx}^{(2)}(t, t')$ , is that it quantifies the change of the linear response kernel of the self-energy at times  $t, t'$  due to a change of the activity at time  $t''$ . This shows that only the interplay between an interaction and noise, as apparent by the prefactors composed of both  $\beta$  and  $D$ , creates a self-interaction of the mean that is nonlocal in time. This phenomenon is also generally observed if certain degrees of freedom are implicitly taken into account to describe the quantity of interest (see Ref. [98], e.g., chap. 1.6).

An alternative way to arrive at (32) is to derive ODEs for the first two moments from the Fokker-Planck equation [92] and to use a Gaussian closure. The loop expansion then amounts to a Taylor expansion of the Fokker-Planck solution in  $\delta x$  and assuming that  $\langle x^3 \rangle \ll \langle x^2 \rangle$ ,  $\langle x \rangle$  (known as Gaussian closure), as we show in detail in Appendix A8. In Fig. 2 we compare the full Fokker-Planck solution with Gaussian closure to the one-loop result. Indeed, the semilogarithmic plot of the relaxation as a function of time shows an elevated time constant due to fluctuations compared to the tree-level approximation. Analyzing the origin of the elevated time constant, Fig. 2(c) compares the different contributions to the right-hand side of (32). The linear part of the tree-level approximation yields the largest contribution. For sufficiently long times, we find that the linear part of the one-loop correction comes next with opposite sign compared to the term stemming from the bare interaction: this shows that only the cooperation of the nonlinearity with the fluctuations in



the system causes this correction and is more important than the nonlinearity itself, the quadratic tree-level contribution. Furthermore, the three-point interaction gets enhanced by the fluctuation corrections, so that in total, the relaxation is slower than in the deterministic system.

In the context of neuronal dynamics this example shows how the response of a system to a stimulus is shaped by the presence of nonlinearities and noise. An increase of the timescale of the response may be employed by such systems to implement increased memory for past stimuli. In heterogeneous networks, where the linear part of the dynamics is given by a matrix that couples different neurons as  $dx(t) = -x(t) + Jx(t)dt + \dots$ , the effective leak term  $m = J - 1$  correspondingly becomes a matrix. The  $i$ th eigendirection of the matrix then evolves with timescale  $(\lambda_i - 1)^{-1}$ . For random connectivity, the eigenvalues are typically circularly distributed in the complex plane [99]; thus a quasicontinuum of timescales appears already in tree-level approximation [1], Fig. 6]. The one-loop corrections to the self-energy generate additional timescales, as shown in Eq. (32) and also Eq. (A32) and Eq. (A33) for the one-dimensional case. The emergence of multiple timescales has been discussed previously in the literature. Some works proposed multiple adaptation mechanisms as the origin [100]. Others have shown that timescales of responses to stimuli may change systematically within the hierarchy of a complex neuronal network, from fast timescales in early areas, to long ones in higher levels of the hierarchy [101]. Loop corrections obtain an important meaning when considering the influence of nonrecorded neurons on the correlation structure of the observed ones [48]: A one-loop correction to the self-energy in this context contains the reverberation of activity within the network, thus including the indirect effect due to the presence of nonrecorded neurons. Such reverberations generate additional timescales in the mutual coupling kernel between individual neurons, mediated via the nonrecorded intermediate cells.

## 2. Power spectrum

So far we have discussed an effective equation of motion for the mean value of the process that also allowed us to obtain an interpretation for the various vertex functions. We can ask a corresponding question for the second-order statistics, namely, whether there is a linear system that possesses the same second-order statistics as the full nonlinear system. Such a reduction may be useful to obtain insights into the structure of network fluctuations and also to reduce the complexity of stochastic nonlinear systems to simpler, linear ones.

Indeed, we can use the expression for the Hessian (23) of the effective action to obtain the action of a linear system that, up to second order, reproduces the stationary statistics of the full system. To this end, we define

$$S_{\text{lin}} := -(\delta\tilde{x}^T \Gamma_{\tilde{x}\tilde{x}}^{(2)} \delta\tilde{x} + \frac{1}{2} \delta\tilde{x}^T \Gamma_{\tilde{x}\tilde{x}}^{(2)} \delta\tilde{x}). \quad (33)$$

The corresponding equation of motion reads

$$\begin{aligned} \frac{d}{dt} \delta x(t) &= -I \delta x(t) + \int dt' \Gamma_{\tilde{x}\tilde{x}, \text{fl.}}^{(2)}(t, t') \delta x(t') + \xi(t), \\ \text{where } \langle \xi(t) \rangle &= 0 \\ \text{and } \langle \langle \xi(t) \xi(t') \rangle \rangle &= D \delta(t - t') + \Gamma_{\tilde{x}\tilde{x}, \text{fl.}}^{(2)}(t, t'). \end{aligned} \quad (34)$$

By construction this stochastic integro-differential equation (34) reproduces the stationary variance  $\Delta_{xx}(t, s) = W_{xx}^{(2)}(t, s) = \langle \delta x(t) \delta x(s) \rangle$  as well as the linear response  $\Delta_{x\tilde{x}}(t, s) = W_{x\tilde{x}}^{(2)}(t, s) = \langle \delta x(t) \delta \tilde{x}(s) \rangle$  of the full system, because the solution of the Gaussian system (33) implicitly inverts the kernel  $\Gamma^{(2)}$ , which, by (23), yields the covariance matrix  $W^{(2)}$ . We could also take into account the effect of transient values of  $x(t)$  on the variance to obtain a corresponding reduction that is valid in the nonstationary case. For this, however, we would need to know  $\Gamma_{\tilde{x}\tilde{x}, \text{fl.}}^{(2)}$  evaluated at arbitrary  $x(t)$ . In this case, it is therefore more convenient to use the second Legendre transform that treats the variance as given, just like  $x^*$  in the case of the first Legendre transform, as shown by Bravi and co-workers [102].

The construction of a linear system leads to a new perspective of the effect of the nonlinearity: Up to the second cumulant, the nonlinear system is equivalent to a linear one with a specific causal memory kernel and a corresponding nonwhite Gaussian noise term, caused by the self-energy correction  $\Gamma_{\tilde{x}\tilde{x}}^{(2)}$ .

## K. Functional renormalization group

The loopwise expansion, by virtue of approximating the effective action, yields self-consistent equations for the mean. But we saw above that also the second-order statistics and the higher order vertex functions experience fluctuation corrections. One would therefore like to have a scheme that is self-consistent with regard to these higher order vertex functions, too.

One possible approach that has lead to reasonable results, is to correct the mean, the propagator and the interaction vertex by the one-loop results and therein replace the bare quantities by the corrected ones to gain an even better approximation. This procedure is repeated until the result eventually converges. This approach corresponds to taking into account only specific diagrams with infinitely many loops and is called self-consistent one-loop approximation. It typically corrects the mean value and the self-energy while keeping the interaction vertices at their bare values; it is then known as the ‘‘Hartree-Fock approximation’’ [8,79]. But of course this scheme can be extended to arbitrary order of the vertex functions. A formal way to derive such approximations systematically is by multiple Legendre transforms, an idea going back to the seminal work by De Dominicis and Martin [103]: One reexpresses interaction potentials in terms of connected correlation functions. Parquet equations are, for example, obtained by the fourth Legendre transform of an even theory (see, e.g., Ref. [79] for a review, especially chap. 6.2.10).

We here want to follow a different scheme that is inherently self-consistent to arbitrary desired orders, the functional renormalization group (fRG). The fRG scheme naturally takes into account fluctuation corrections by renormalizing the mean value, the propagators, and all interaction vertices simultaneously.

Technically, the functional renormalization group (fRG) [35] is an alternative way to calculate  $\Gamma$ . It is one of the exact renormalization group (eRG) schemes [36,104,105], in essence going back to the seminal work by Wegner and Houghton [34]. It does not rely on an expansion in a small

parameter, in contrast to the loopwise expansion, but it is nevertheless represented by diagrams with a one-loop structure. The technique induces an infinite hierarchy of coupled differential equations for  $\Gamma^{(n)}$ , so that in practice, we have to apply approximations, typically by truncating the hierarchy. Yet this technique is, as all exact renormalization group schemes, exact only on the level of the full functional  $\Gamma[x, \tilde{x}]$  and not for a particular truncation in terms of a subset of  $\Gamma^{(n)}$ .

The essential technical trick of the fRG is to simplify the theory by adding an initially large quadratic term  $-\frac{1}{2}y^T R_\lambda y$  in the fields  $y$ , parametrized by the regulator  $R_\lambda$ , to the action. It is a differentiable function of a so-called flow parameter  $\lambda$  and can be chosen arbitrarily up to the following properties:

$$\lim_{\lambda \rightarrow \Lambda} |R_\lambda| = \infty \quad \text{and} \quad \lim_{\lambda \rightarrow 0} R_\lambda = 0. \quad (35)$$

The first property ensures that the theory for  $\lambda = \Lambda$  has no fluctuations, and its vertices correspond to the ones of the bare action, while for  $\lambda = 0$ , the original system is recovered. For systems that exhibit symmetries it is often necessary that the regulator is consistent with these symmetries of the effective action, so that they are conserved during the flow. To interpolate between the two limits of the noninteracting and the full system, a functional differential equation for the effective action is derived by differentiating with respect to  $\lambda$ . This is the Wetterich equation [35], whose derivation for our setting, in particular for the presence of the response field, we will sketch in the following adhering to the conventions of Berges *et al.* [36]. We will derive it for the effective action evaluated at stationary  $X^*$  and  $\tilde{X}^*$  so that the resulting equation boils down to an ODE.

Since the regulator  $R_\lambda$  is intended to suppress fluctuations, it is sufficient for our case to add it to the off-diagonal terms of the free part of the action, defining

$$\begin{aligned} S_\lambda[X, \tilde{X}] &= S_0[X, \tilde{X}] + \Delta S_\lambda[X, \tilde{X}] + S_{\text{int}}[X, \tilde{X}], \quad \text{where} \\ \Delta S_\lambda[X, \tilde{X}] &= -\frac{1}{2} \int \frac{d\omega}{2\pi} \begin{pmatrix} X(-\omega) \\ \tilde{X}(-\omega) \end{pmatrix} \begin{pmatrix} 0 & \frac{1}{2}R_\lambda \\ \frac{1}{2}R_\lambda & 0 \end{pmatrix} \begin{pmatrix} X(\omega) \\ \tilde{X}(\omega) \end{pmatrix} \\ S_{\text{int}}[X, \tilde{X}] &= -\beta \int \frac{d\omega}{2\pi} \int \frac{d\omega'}{2\pi} \tilde{X}(\omega) X(\omega') X(-\omega - \omega'). \end{aligned} \quad (36)$$

By (28), the regulator modifies the leak term  $m$ , thus controlling the variance of the fluctuations. A general discussion on the choice of frequency-dependent regulators can be found in Ref. [106]: The  $XX$ -diagonal element must always be zero to maintain normalization (see also Appendix A 1). A regulator on the  $\tilde{X}\tilde{X}$  element corresponds to a modification of the second cumulant of the driving noise. For systems in equilibrium, the fluctuation-dissipation theorem constrains the choice of the regulator further.

For the choice in (36), the bare propagator reads

$$\Delta_\lambda^0(\omega, \omega') = \begin{pmatrix} \frac{D}{\omega^2 + (m + \frac{1}{2}R_\lambda)^2} & \frac{1}{-i\omega + m + \frac{1}{2}R_\lambda} \\ \frac{1}{i\omega + m + \frac{1}{2}R_\lambda} & 0 \end{pmatrix} 2\pi \delta(\omega + \omega').$$

We notice that  $R_\lambda$  has to be negative to avoid a vanishing leak term (since  $m < 0$ ) and thus a fluctuation singularity at  $\omega = 0$  along the RG trajectory. We define  $\tilde{\Gamma}_\lambda[X^*, \tilde{X}^*]$  as the Legendre transform of the cumulant-generating functional, given by

$$\begin{aligned} W_\lambda[J, \tilde{J}] &= \ln \int \mathcal{D}X \int \mathcal{D}\tilde{X} \\ &\times \exp(S_\lambda[X, \tilde{X}] + J^T X + \tilde{J}^T \tilde{X}), \end{aligned}$$

where we used the abbreviation  $J^T X = \int d\omega J(\omega) X(\omega)$ . Defining  $\Gamma_\lambda$ , we remove the “direct” effect of the regulator

$$\Gamma_\lambda[X^*, \tilde{X}^*] := \tilde{\Gamma}_\lambda[X^*, \tilde{X}^*] + \Delta S_\lambda[X^*, \tilde{X}^*], \quad (37)$$

so that  $\lim_{\lambda \rightarrow 0} \Gamma_\lambda = \Gamma$  and  $\lim_{\lambda \rightarrow \Lambda} \Gamma_\lambda = -S$ . The latter limit follows, because at  $\lambda = \Lambda$  the regulator suppresses all fluctuations, so that the mean-field approximation  $\tilde{\Gamma}_\Lambda \simeq -S_\Lambda = -(S + \Delta S_\Lambda)$  becomes exact. Consequently, by definition (37), one then obtains the stated limit [see also Eqs. (2.9) to (2.12) in Ref. [36]]. To derive the flow equation for the effective action of the theory defined in (36), we take the partial derivative of  $W_\lambda$  with respect to the flow parameter and deduce from this the respective derivatives of  $\tilde{\Gamma}_\lambda$  and  $\Gamma_\lambda$  (for details consult Appendix A 9), which results in the Wetterich equation

$$\begin{aligned} \frac{\partial \Gamma_\lambda[X^*, \tilde{X}^*]}{\partial \lambda} &= \frac{1}{2} \text{Tr} \left\{ \Delta_{\tilde{X}X, \lambda} \frac{\partial R_\lambda}{\partial \lambda} \right\} \\ &= \frac{1}{2} \text{Tr} \left\{ \left[ \Gamma_\lambda^{(2)}[X^*, \tilde{X}^*] + \begin{pmatrix} 0 & \frac{1}{2}R_\lambda \\ \frac{1}{2}R_\lambda & 0 \end{pmatrix} \right]_{\tilde{X}X}^{-1} \frac{\partial R_\lambda}{\partial \lambda} \right\} = \frac{1}{2} \text{Tr} \left[ \text{Diagram} \right], \end{aligned} \quad (38)$$

where in this section, lines denote full propagators

$$\Delta_\lambda := (\tilde{\Gamma}_\lambda^{(2)})^{-1} = \left[ \Gamma_\lambda^{(2)} + \begin{pmatrix} 0 & \frac{1}{2}R_\lambda \\ \frac{1}{2}R_\lambda & 0 \end{pmatrix} \right]^{-1} \quad (39)$$

and open squares represent  $\frac{\partial R_\lambda}{\partial \lambda}$ . The translation between graphical representations and algebraic expressions is also shown in Table I. For the final result ( $\lambda = 0$ ), the choice of the concrete form of  $R_\lambda$  is arbitrary as long as it fulfills (35) and does not lead to acausal terms in the action. The interpretation of  $\Gamma_\lambda$  along the trajectory of the flow equations, however, depends on the regulator.

The simplest choice is the uniform regulator, for example  $R_\lambda = -\lambda$ . In this case all frequencies get damped equally. Its equivalence to an additional leak term [compare (14) and (39)] bears a second interpretation: We may as well interpret each

point along the solution of the flow equation as one system with a different value for the leak term. In this context, a vanishing value and hence a pole in the propagator at vanishing frequency becomes meaningful again: it corresponds to a critical point where fluctuations dominate the system behavior.

The simplest measure to extract from  $\Gamma_\lambda$  is the mean value  $\check{x}_\lambda$  defined by the equation of state  $\tilde{\Gamma}_{\check{x}, \lambda}^{(1)}[x_\lambda^*, \check{x}_\lambda^*] = 0$ .<sup>7</sup> Differentiating this equation with respect to  $\lambda$  leads to

$$\begin{aligned} 0 &= \frac{d}{d\lambda} \tilde{\Gamma}_\lambda^{(1)}(\omega) = \frac{\partial \tilde{\Gamma}_\lambda^{(1)}(\omega)}{\partial \lambda} + \int d\omega' \tilde{\Gamma}_\lambda^{(2)}(\omega, \omega') \frac{\partial}{\partial \lambda} \left( \frac{\check{X}_\lambda(\omega')}{\check{X}_\lambda(\omega)} \right) \\ \Leftrightarrow \frac{\partial}{\partial \lambda} \left( \frac{\check{X}_\lambda(\sigma)}{\check{X}_\lambda(\sigma)} \right) &= -\Delta_\lambda(\sigma) \left[ \frac{\partial \Gamma_\lambda^{(1)}(-\sigma)}{\partial \lambda} + \frac{1}{4\pi} \frac{\partial R_\lambda}{\partial \lambda} \left( \frac{\check{X}_\lambda(\sigma)}{\check{X}_\lambda(\sigma)} \right) \right]. \end{aligned} \quad (40)$$

To obtain (40), we have multiplied the line above by the propagator  $\Delta_\lambda$  and used  $\Delta_\lambda \tilde{\Gamma}_\lambda^{(2)} = 1$ . We observe that we now need a flow equation for  $\tilde{\Gamma}^{(1)}$ , which we obtain by differentiating (38) with respect to  $(x, \tilde{x})$  leading to

$$\begin{aligned} \frac{\partial \Gamma_{X,\lambda}^{(1)}(\sigma)}{\partial \lambda} &= -\frac{1}{2} \text{ (diagram: a wavy line labeled } \sigma \text{ connected to a vertex, which is part of a loop with a square box)} \\ &= -\frac{1}{2} \int \frac{d\omega}{2\pi} \Gamma_{\tilde{X}XX,\lambda}^{(3)}(\sigma, -\omega, \omega) \Delta_{\tilde{X}X,\lambda}(\omega) \frac{\partial R_\lambda}{\partial \lambda} \Delta_{\tilde{X}X,\lambda}(\omega) \end{aligned} \quad (41)$$

$$\begin{aligned} \frac{\partial \Gamma_{\tilde{X},\lambda}^{(1)}(\sigma)}{\partial \lambda} &= -\frac{1}{2} \text{ (diagram: a wavy line labeled } \sigma \text{ enters a vertex, which is connected to a loop with a square box)} \\ &= -\frac{1}{2} \int \frac{d\omega}{2\pi} \Gamma_{\tilde{X}XX,\lambda}^{(3)}(\sigma, -\omega, \omega) \Delta_{XX,\lambda}(\omega) \frac{\partial R_\lambda}{\partial \lambda} \Delta_{\tilde{X}X,\lambda}(\omega). \end{aligned} \quad (42)$$

In the last step for both diagrams we defined  $\Delta_\lambda(\omega, \omega') =: \Delta_\lambda(\omega)\delta(\omega + \omega')$  and  $R_\lambda(\omega, \omega') =: R_\lambda\delta(\omega + \omega')/(2\pi)$ . Since the three-point vertex conserves momentum  $\Gamma_{\lambda\lambda\lambda}^{(3)}(\omega, \omega', \omega'') \propto \delta(\omega + \omega' + \omega'')$ , the external momentum is fixed at  $\sigma = 0$ . Inserting these equations into (40) yields the final results, which are equivalent to Ref. [107], Eq. (210), and Ref. [108], Eq. (7.94), Fig. 7.7. Because of the closed response loop in (41), the right-hand side of this equation is always identically zero leading to  $\check{X}_\lambda = 0 \forall \lambda$ . The same applies to all other diagrams with one loop and one external leg different from (41) or (42), because they also contain either  $\Delta_{\bar{\chi}\bar{\chi}} = 0$ , response loops, or a vertex  $\Gamma_{\chi\chi\lambda}^{(3)}$ . The last is always identically zero as shown in Appendix A 2. So only (42) contains information on the flow of  $\check{X}_\lambda$ , finally yielding

$$\frac{\partial}{\partial \lambda} \check{X}_\lambda(\sigma) = -\Delta_{X\check{X},\lambda}(\sigma) \left[ \frac{\partial \Gamma_{\check{X},\lambda}^{(1)}(-\sigma)}{\partial \lambda} + \frac{1}{4\pi} \frac{\partial R_\lambda}{\partial \lambda} \check{X}_\lambda(\sigma) \right]. \quad (43)$$

The right-hand side of this equation depends on  $\Delta_\lambda$  and  $\Gamma_{\check{X}XX,\lambda}^{(3)}$  via (42) which in turn are also defined by flow equations containing vertices of the respective next two orders. This induces an infinite hierarchy. A first approximation of the mean value  $\check{X}_\lambda$  is gained by truncating the hierarchy after  $\Gamma_\lambda^{(1)}$ , that is using the bare quantities for  $\Delta_\lambda$  and  $\Gamma_{\check{X}XX,\lambda}^{(3)}$  and integrating the flow (43). We then also get a corrected value for the variance by inserting  $\check{X}_\lambda$  into  $\Delta_{XX}^0$ . The flow equations at this level of approximation can be integrated exactly: They recover the one-loop approximation.

We can improve the accuracy by taking into account the flow of higher derivatives of  $\Gamma$ . In this work we included the flow of the self-energy and the interaction vertex  $\Gamma_{\bar{x}xx}^{(3)}$ , but neither the one of  $\Gamma_{\bar{x}\bar{x}x}^{(3)}$  and  $\Gamma_{\bar{x}\bar{x}\bar{x}}^{(3)}$  nor that of all higher order vertices. The one loop correction of  $\Gamma_{\bar{x}xx}^{(3)}$  ( $\Gamma_{\bar{x}\bar{x}\bar{x}}^{(3)}$ ) involves two (three)  $xx$ -propagators, so that, in systems with small fluctuations, which scale with  $D$ , this diagram is less important than the others. Compared to the one-loop correction of  $\Gamma_{\bar{x}\bar{x},\text{fl.}}^{(2)}$ ,  $\Gamma_{\bar{x}\bar{x}xx}^{(3)}$  bears the same number of  $xx$ -propagators, but one additional interaction, which scales with the other small factor  $\beta$ . Therefore we neglect the corrections to  $\Gamma_{\bar{x}\bar{x}xx}^{(3)}$  and  $\Gamma_{\bar{x}\bar{x}\bar{x}}^{(3)}$  but not to  $\Gamma_{\bar{x}xx,x}^{(3)}$ . In conclusion, we renormalize exactly those terms that also appear in the bare

<sup>7</sup>The condition  $\Gamma_{\tilde{x},\lambda}^{(1)}[x_\lambda^*, \tilde{x}_\lambda^*] = 0$  would of course lead to the same result because we are eventually interested in  $\lambda = 0$ , where both quantities agree, but using  $\tilde{\Gamma}$  leads to the occurrence of the propagator including the regulator term in (40), which is more convenient.

action. Under these constraints, the nonvanishing and non-negligible diagrams for the self-energy are given by

$$\begin{aligned} \frac{\partial \Gamma_{\tilde{X}X,\lambda}^{(2)}(\sigma_1, \sigma_2)}{\partial \lambda} &= \frac{1}{2} \text{diagram 1} + \frac{1}{2} \text{diagram 2} \\ &+ \frac{1}{2} \text{diagram 3} \\ \frac{\partial \Gamma_{\tilde{X}\tilde{X},\lambda}^{(2)}(\sigma_1, \sigma_2)}{\partial \lambda} &= \frac{1}{2} \text{diagram 4} + \sigma_1 \leftrightarrow \sigma_2. \end{aligned}$$

The translation of these diagrams is shown in Appendix A 10 together with the respective diagrams for the interaction vertex.

In general, the diagrams have the same form as those that appear in the fluctuation expansion, except for the presence of a single regulator in one of the propagator lines. The combination of two propagators “sandwiching” a regulator  $\Delta_\lambda(\omega, -\omega) \frac{\partial R_\lambda}{\partial \lambda}(\omega, -\omega) \Delta_\lambda(\omega, -\omega)$  is called “single scale propagator” because the regulator is often chosen in a way such that its derivative is peaked around frequencies with  $|\omega| = \lambda$ , thus contributing at a single scale. Due to the one-loop structure of the diagrams and the conservation of frequencies at the vertices, we have to perform one integral over an internal frequency for every possible combination of fixed external frequencies. Therefore, the numerical evaluation of  $\Gamma^{(n)}$  becomes increasingly computationally expensive for higher orders because at  $n$ th order we have  $n - 1$  independent external frequencies. For practical computations we thus have to truncate the hierarchy after  $n = 3$  if we want to keep the full frequency dependence of  $\Gamma^{(n)}$ . Even at this order, the integration takes many hours on a usual desktop PC when we choose the external frequencies to range from  $-25$  to  $25$  with a resolution of  $0.1$ . Therefore, it is legitimate to ask if one can reduce the number of required frequency integrals by assuming a simplified frequency dependence of higher order vertices.

### 1. The BMW scheme

A scheme that assumes a simplified momentum dependence of higher order vertices has been suggested by Blaizot, Méndez, and Wschebor (BMW) [54,109]. It has been successfully applied for example to the Kardar-Parisi-Zhang model [51]. The principal idea is to neglect the frequency dependence of the effective action as much as possible. The most radical choice in this respect would be to assume it to be constant, which is known as the local potential approximation (LPA). BMW refined this scheme by including the exact frequency dependence of all vertices up to a certain order  $s$ , which are functions of  $s - 1$  external frequencies, and to approximate vertices of the next two orders by evaluating the additional derivatives at their zero frequency components

obtaining a partial differential equation [110]. We will pursue a different route by deriving approximate flow equations for  $\Gamma^{(s+1)}$  and  $\Gamma^{(s+2)}$  with the simplified frequency dependence.

More precisely, we consider a typical contribution of a vertex within the Wetterich flow equation for the vertex  $\Gamma^{(s)}$  containing

$$\begin{aligned} \Gamma_\lambda^{(s+1)}(\sigma_1, \dots, \sigma_s + \omega, -\omega), \\ \Gamma_\lambda^{(s+2)}(\sigma_1, \dots, \sigma_s, \omega, -\omega), \end{aligned} \quad (44)$$

where  $\omega$  is the loop frequency, that represents the frequency at the regulator. For simplicity we do not specify different components of the field. For the approximation we assume the vertices to depend only weakly on  $\omega$  and therefore set  $\omega = 0$  in (44), replacing the vertices by

$$\begin{aligned} \Gamma_\lambda^{(s+1)}(\sigma_1, \dots, \sigma_s, 0), \\ \Gamma_\lambda^{(s+2)}(\sigma_1, \dots, \sigma_s, 0, 0). \end{aligned} \quad (45)$$

The frequency dependence on  $\omega$  in the propagators and the regulator is, however, kept.

The second step of the BMW scheme allows the closure of the system: Due to the vanishing momentum on one or two legs of the vertices (45), the vertex functions with  $s + 1$  and  $s + 2$  legs can be expressed as the derivative of  $\Gamma_\lambda^{(s)}$  with respect to a uniform (background) field  $X_0^* := X^*(\sigma = 0)$ :

$$\Gamma_\lambda^{(s+1)}(\sigma_1, \dots, \sigma_s, 0) = \frac{\delta}{\delta X_0^*} \Gamma_\lambda^{(s)}(\sigma_1, \dots, \sigma_s) \quad (46)$$

$$\Gamma_\lambda^{(s+2)}(\sigma_1, \dots, \sigma_s, 0, 0) = \frac{\delta^2}{\delta X_0^{*2}} \Gamma_\lambda^{(s)}(\sigma_1, \dots, \sigma_s). \quad (47)$$

If we now use (46) and (47) to replace  $\Gamma_\lambda^{(s+1)}$  and  $\Gamma_\lambda^{(s+2)}$  by the ordinary derivatives of  $\Gamma_\lambda^{(s)}$  with respect to the zero modes of  $X, \tilde{X}$ , we close the set of flow equations and additionally we take into account the flow of order  $s + 1$  and  $s + 2$ , at least approximately. Since we reduced the number of independent frequencies by one (or two, respectively), the computation time decreases significantly.

But the resulting equation is a partial differential equation in  $\lambda$  and  $X_0^*$  [see Ref. [110], Eq. (19)]; we hence have to evaluate the derivatives with respect to  $X_0^*$  for every step at



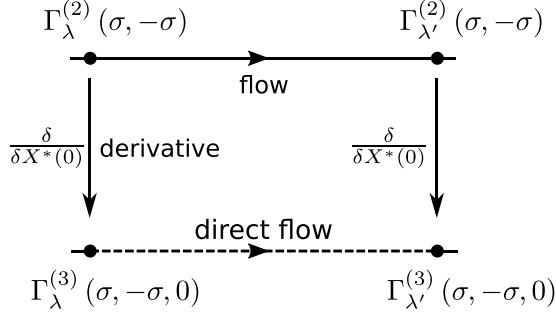


FIG. 3. Implementation of the BMW scheme within the vertex expansion. In the original formulation (top) we have to evaluate the derivatives  $\delta/\delta X^*(0)$  numerically at each  $\lambda$ . In the new interpretation (bottom) we derive an additional flow equation for  $\Gamma^{(3)}(\sigma, -\sigma, 0)$  (dashed line).

which we compute  $\partial_\lambda \Gamma^{(s)}$ . Below we develop an alternative scheme that circumvents this complication and entirely stays within the realm of a vertex expansion.

## 2. Removing the PDE

We aim to apply the BMW approximation at order  $s = 2$ , thus keeping the full frequency dependence of the self-energy.

$$\frac{\delta}{\delta X(0)} \frac{\partial \Gamma_\lambda^{(2)}(\sigma_1, -\sigma_1)}{\partial \lambda} = \frac{\delta}{\delta X(0)} \frac{1}{2} \text{diagram (1)} - \frac{1}{2} \text{diagram (2)} - \frac{1}{4} \text{diagram (3)} - \frac{1}{2} \text{diagram (4)} + \sigma_1 \leftrightarrow -\sigma_1$$

The diagrams are Feynman diagrams representing the flow equations. Diagram (1) is a circle with a square vertex at the top, labeled (1) and (2), with external lines  $\sigma_1$  and  $-\sigma_1$ . Diagram (2) is a circle with a square vertex at the top, labeled (3) and (4), with external lines  $\sigma_1$  and  $-\sigma_1$ . Diagram (3) is a circle with a square vertex at the top, labeled (6) and (7), with external lines  $\sigma_1$  and  $-\sigma_1$ . Diagram (4) is a circle with a square vertex at the top, labeled (9) and (10), with external lines  $\sigma_1$  and  $-\sigma_1$ . The diagrams are labeled with frequencies  $\omega$  and  $\sigma_1 + \omega$ .

where the vertex functions are given by

- (1)  $\Gamma_\lambda^{(3)}(\sigma_1, \omega, -\sigma_1 - \omega)$ , (2)  $\Gamma_\lambda^{(3)}(-\sigma_1, -\omega, \sigma_1 + \omega)$ ,
- (3)  $\Gamma_\lambda^{(3)}(\sigma_1, 0, -\sigma_1)$ , (4)  $\Gamma_\lambda^{(3)}(-\sigma_1, 0, \sigma_1)$ ,
- (5)  $\Gamma_\lambda^{(3)}(\omega, -\omega, 0)$ , (6)  $\Gamma_\lambda^{(3)}(\sigma_1, 0, -\sigma_1)$ ,
- (7)  $\Gamma_\lambda^{(3)}(-\sigma_1, 0, \sigma_1)$ , (8)  $\Gamma_\lambda^{(3)}(\sigma_1 + \omega, -\sigma_1 - \omega, 0)$ ,
- (9)  $\Gamma_\lambda^{(4)}(\sigma_1, 0, -\sigma_1, 0)$ , (10)  $\Gamma_\lambda^{(3)}(-\sigma_1, 0, \sigma_1)$ .

The crucial point to notice is that all vertices that appear in the diagrams have only two nonzero frequencies. The set of differential equations is therefore closed; the last diagram

However, within the vertex expansion scheme it remains unclear how to compute the derivatives of  $\Gamma^{(2)}$  numerically. This is because at each given  $\lambda$  we know the value of  $\Gamma^{(2)}$  only for the true mean value  $\tilde{X}_\lambda(0)$ , but not in a vicinity around it; we therefore cannot approximate the derivative by a ratio of finite differences.

We can circumvent this problem by deriving an additional flow equation for  $\Gamma_\lambda^{(3)}(\sigma_1, \sigma_2, 0)$  (illustrated in Fig. 3; the more complex situation with  $x$  and  $\tilde{x}$  fields will be addressed below) and in principle also for  $\Gamma_\lambda^{(4)}(\sigma_1, \sigma_2, 0, 0)$ , which we neglect in our model because the largest contribution of  $\Gamma^{(4)}$  is suppressed by a factor  $\beta$  due to an additional interaction vertex. We obtain this flow equation by differentiating the one for  $\Gamma_\lambda^{(2)}$  with respect to  $X^*(0)$ , i.e.,  $\frac{\delta}{\delta X^*(0)} \partial_\lambda \Gamma_\lambda^{(2)} = \partial_\lambda \Gamma_\lambda^{(3)}$  and then setting the frequencies of the original three-point vertices at those legs to zero that are connected to the single scale propagator, in line with the BMW scheme. But we need to keep the dependence on  $\omega$  of the vertices that emerge when we differentiate a propagator by the background field, so that we treat the frequency dependence of this additional vertex like that of the regulator in the original diagram. Otherwise we would make an additional approximation on top of BMW. Thus, drawing only the first argument of the propagators, in diagrammatic language we obtain

requires a four-point vertex for which we could obtain a flow equation analogously. So we have found an explicit flow equation for  $\Gamma_\lambda^{(3)}(\sigma_1, \sigma_2 = -\sigma_1, 0)$ , indicated by the dashed line in Fig. 3. As a consequence we have to solve a coupled set of ODEs instead of a single PDE.

If we do not want to neglect the flow of the four-point vertex completely, we can differentiate the diagrams once again, which leads to a flow equation of  $\Gamma_\lambda^{(4)}(\sigma_1, \sigma_2, 0, 0)$ . This flow equation then depends on  $\Gamma_\lambda^{(3)}(\sigma_1, \sigma_2, 0)$ ,  $\Gamma_\lambda^{(4)}(\sigma_1, \sigma_2, 0, 0)$ , and  $\Gamma_\lambda^{(5)}(\sigma_1, \sigma_2, 0, 0, 0)$ . Due to the emergence of the latter, the set of equations can be closed only if we truncate the series at some order (unlike the original BMW scheme).

The scheme described above also generalizes to the case where we have two fields components  $x$ ,  $\tilde{x}$  and the

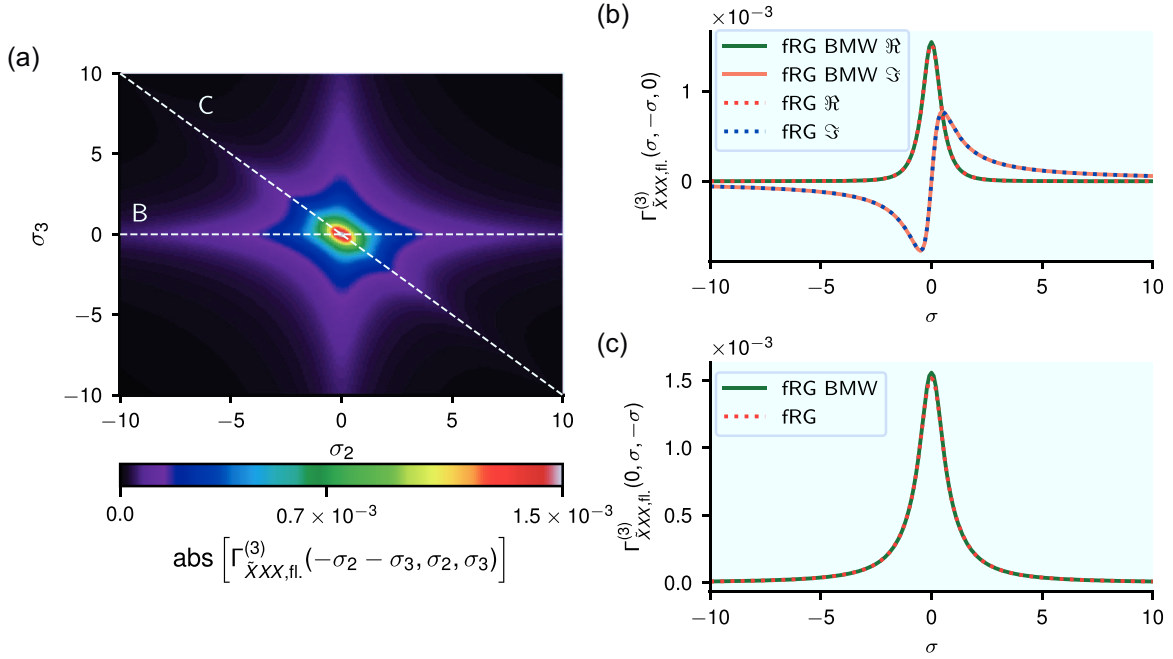


FIG. 4.  $\Gamma_{\bar{x}x,\text{fl.}}^{(3)}$  computed by fRG schemes. (a) Full frequency dependence as a result of the calculation that takes into account the flow of the mean value,  $\Gamma_{\text{fl.}}^{(2)}$ , and  $\Gamma_{\bar{x}x,\text{fl.}}^{(3)}$ . (b) and (c)  $\Gamma_{\bar{x}x,\lambda,\text{fl.}}^{(3)}(-\sigma_2 - \sigma_3, \sigma_2, \sigma_3)$  along the sections  $\sigma_3 = 0$  (b) and  $\sigma_2 = -\sigma_3$  (c), as indicated by the white dashed lines in (a); comparison to the respective types of vertices that appear in the BMW approximation.  $\Gamma_{\bar{x}x,\lambda,\text{fl.}}^{(3)}(-\sigma_2, \sigma_2, 0)$  in panel (b) quantifies the change of the linear response function due to an altered constant mean activity (indicated by the derivative with respect to the zero mode  $\sigma_3 = 0$ ); in more neuroscientific terms: it shows the dependence of the susceptibility (the neuron's linear response strength to an input) on the baseline activity to linear order.  $\Gamma_{\bar{x}x,\lambda,\text{fl.}}^{(3)}(0, \sigma_2, -\sigma_2)$  in panel (c) is somewhat complementary: It is the lowest order term describing the fluctuation-mediated effect of time-dependent deviations on the constant part of the mean activity. This term, for example, quantifies the change of the constant baseline activity due to a small sinusoidal stimulus with frequency  $\sigma_2$ ; the linear order of this response averages out over time, but the quadratic response does not. Note that  $\Gamma_{\bar{x}x,\lambda,\text{fl.}}^{(3)}(0, \sigma_2, -\sigma_2) \in \mathbb{R}$  because its Fourier transform  $\Gamma_{\bar{x}x,\lambda,\text{fl.}}^{(3)}(0, t_2, -t_2)$  is real by definition and symmetric because the last two arguments are those of two  $x$  at different time points, which are interchangeable.

corresponding propagators  $\Delta_{\bar{x}x}$ ,  $\Delta_{xx}$ . We then get two sets of 12 diagrams each (compare Appendix A 10) the first of which describing the flow of the two one-dimensional sections  $\Gamma_{\bar{x}x,\text{fl.}}^{(3)}(0, \sigma_1, -\sigma_1)$  (type 1) and the second one that of  $\Gamma_{\bar{x}x,\text{fl.}}^{(3)}(\sigma_1, -\sigma_1, 0)$  (type 2). Every diagram consists of three three-point interaction vertices that are either of type 1 or of type 2. Thus, the common flow of the two sections is computed consistently within this approximation.

Figure 4 compares the three point vertices obtained from the truncated flow equation to the result from the BMW approximation. The latter of course only yields the three-point vertex  $\Gamma_{\bar{x}x}^{(3)}(\sigma_1, \sigma_2, \sigma_3)$  along the one-dimensional sections  $-\sigma_1 = \sigma_2 + \sigma_3 = 0$  [type 1, Fig. 4(c)] and  $\sigma_3 = 0$  [type 2, Fig. 4(b)]. The agreement between the two approximations is high. This result is to be expected, since the fluctuation corrections *per se* are small in the regime considered, so that the bare vertices still constitute the largest contributions to any fluctuation correction.

#### L. Analyzing bifurcations by effective potentials

A fundamental question when considering neuronal dynamics is the stability of the system and the global network state that emerges if the system is left at rest. While in deter-

ministic systems such a consideration reduces to finding fixed points, typically of a set of differential equations, in stochastic systems the situation is more complicated due to the presence of fluctuations. To determine the fluctuation corrections on the stationary statistics of a stochastic system and to study the stability of the found solutions, it is convenient to introduce what is known as the effective potential.

In this section we introduce two different approaches and apply them to the example of a bistable system. Limiting the study to stationary solutions  $\bar{x}^* := x^*(t) = \text{const}$ , such that  $X(\omega) = 2\pi\delta(\omega)\bar{x}^*$ , we can use the OM effective action (7) to define the effective potential

$$U_{\text{OM}}(\bar{x}^*) := \frac{1}{T} \Gamma_{\text{OM}}(\bar{x}^*), \quad (48)$$

with  $T$  being the total time during which we observe the system. The effective potential inherits the property that stationary points correspond to the true mean value of the system from the effective action. The effective potential further plays the role of a rate function [111] that describes departures of the temporal average from the ensemble average in the limit of long observation times (see Ref. [112], Sec. III).

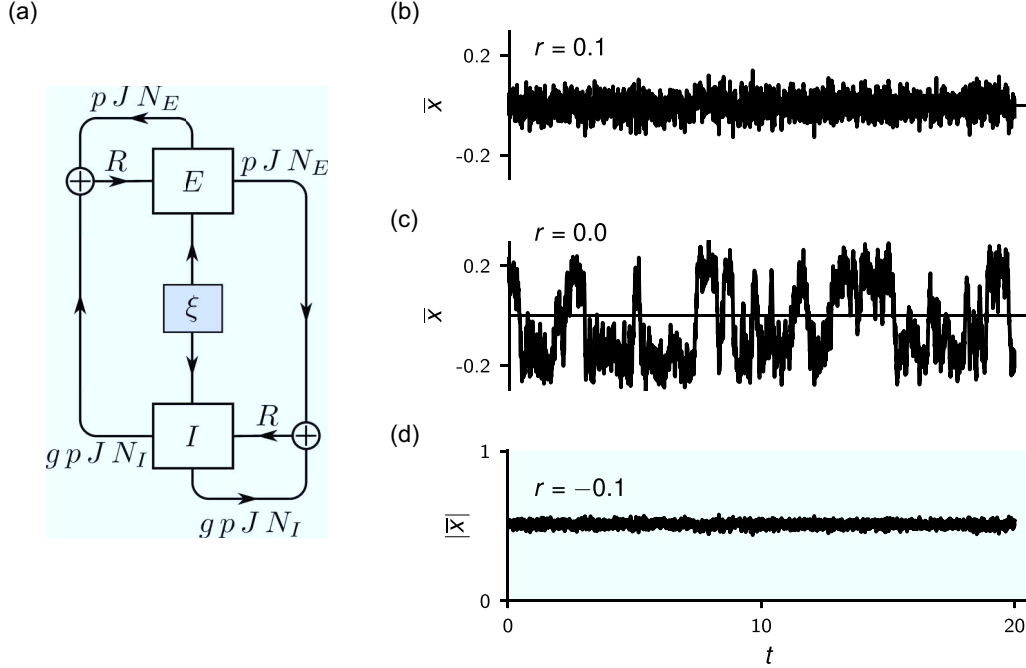


FIG. 5. *Diverging fluctuations in an excitatory-inhibitory network.* (a) Sketch of the network consisting of  $N = N_E + N_I$  neurons composed of an excitatory (E) and an inhibitory (I) population. The connection probability is given by  $p$  and the synaptic weight by  $J$  ( $gJ$ ) if the presynaptic neuron belongs to the excitatory (inhibitory) population. Each neuron has a fixed outdegree of  $pN$ . Thus, the average recurrent input weight to each neuron equals  $R = pJ(N_E + gN_I)$ . All neurons are driven by external white noise ( $\xi$ ) with zero mean and standard deviation  $\sigma$ . Panels (b) to (d) show the simulation results of the population-averaged firing rate  $\bar{x}(t) = N^{-1} \sum_i x_i(t)$  as a function of time for three different values of  $r = 1 - R$ . (b) Network in the balanced state ( $r > 0$ ) shows small fluctuations around a vanishing mean value. (c) Close to the critical point ( $r = 0$ ) the fluctuations increase considerably. (d) In the bistable regime ( $r < 0$ ) the fluctuations decrease again and are no longer centered around zero but around  $\pm c$ , where  $c > 0$ . For the simulation we used rate neurons with a nonlinearity of the form  $\phi(x) = \tanh(x)$ . The other parameters are:  $N_E = 800$ ,  $N_I = 200$ ,  $J = N^{-\frac{1}{2}}$ ,  $p = 0.1$ ,  $\sigma = 0.1$ . The simulations were performed with NEST [113].

In tree-level approximation (12) and with (7) we have

$$U_{\text{OM},0}(\bar{x}^*) = -\frac{1}{T} S_{\text{OM}}(\bar{x}^*) \\ = \frac{1}{2TD} \int_0^T dt [-f(\bar{x}^*)]^2 = \frac{1}{2D} [f(\bar{x}^*)]^2. \quad (49)$$

For  $D > 0$ , its curvature at the minimum  $\bar{x}^* = \bar{x}$  equals the inverse of the zero-frequency fluctuations  $\langle X(0)^2 \rangle - \langle X(0) \rangle^2$  around the mean, which we deduce by using  $f(\bar{x}) = 0$  from

$$U''_{\text{OM},0}(\bar{x}) = \frac{\partial^2}{\partial \bar{x}^2} U_0(\bar{x}^*)|_{\bar{x}} = \frac{[f'(\bar{x})]^2}{D}, \quad (50)$$

compared to the covariance (5) in linear response.

This relation holds beyond this lowest order approximation: The curvature of  $U_{\text{OM}}$  at a stationary point is the inverse of the zero frequency mode of the correlation, which follows from Eq. (A28) at the end of Appendix A 5.

### 1. Computing the effective potential in the MSRDJ formalism

For systems in thermodynamic equilibrium, the deterministic force appearing in (2) can be written as  $f(x) = -V'(x)$ . As a consequence, the stationary distribution obeys

$$p(x) \propto \exp \left[ -\frac{2}{D} V(x) \right]. \quad (51)$$

For such systems, de Dominicis has defined an effective potential [81]

$$U_{\text{DD}}[\bar{x}^*] = V(\bar{x}^*) + \dots \quad (52)$$

[see Appendix A 11 i.p. Eq. (A46)]; here “...” are fluctuation corrections. For a typical network dynamics in multiple dimensions, the deterministic force can usually not be written in such a form. For example, if one considers a coupling term  $\sum_j J_{ij} x_j$  between neurons as in Eq. (1); only for a symmetric matrix  $J_{ij} = J_{ji}$  it is the derivative of the potential  $V(x) = \frac{1}{2} \sum_{ij} x_i J_{ij} x_j$ .

To illustrate the usefulness of these two approaches, the de Dominicis equilibrium effective potential (52) and the OM form (48), we study the dynamics of an excitatory-inhibitory network of rate neurons [Fig. 5(a)], which is a generalization [114] of the classical model by Sompolinsky, Crisanti, and Sommers [68]. The model is given by an  $N$ -dimensional stochastic differential equation of the general form (1). It describes the activity of  $N_E$  excitatory and  $N_I$  inhibitory nonlinear neurons in a sparse random network with a fixed number of outgoing connections  $p \cdot N$  for each neuron. Here  $p$  denotes the connection probability and  $N$  the number of neurons. Nonzero connections  $J_{ij}$  take on the values  $J$  or  $gJ$  depending on whether neuron  $j$  is excitatory or inhibitory, with  $g < 0$ . We here choose  $\phi = \tanh$ , as in the original work [68]. Focusing on the population-averaged activity

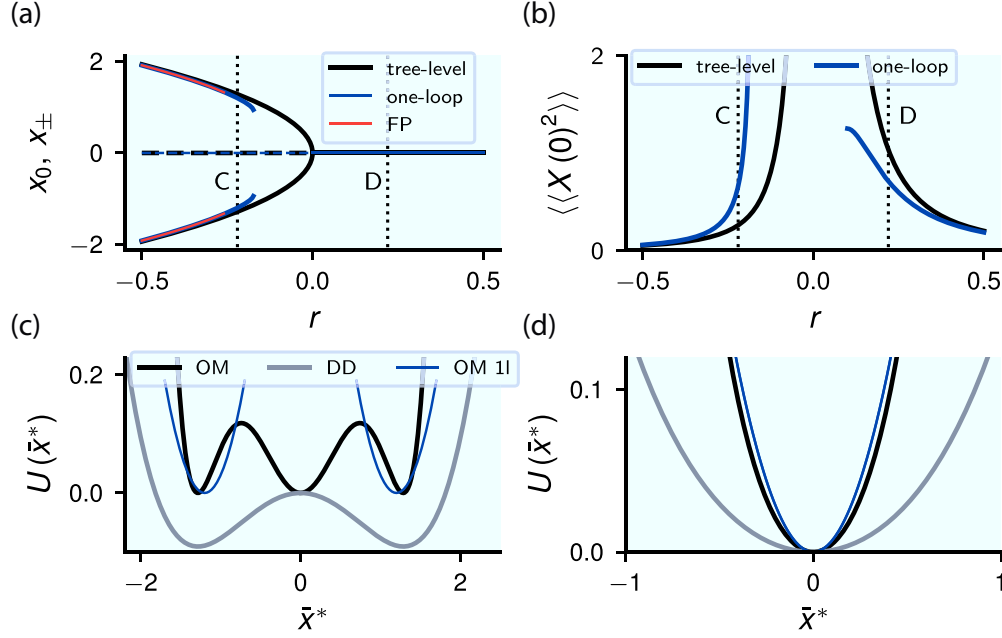


FIG. 6. *Critical point at the loss of balance.* Dynamical equation (54) as a model of the population activity. (a) Stationary points of the deterministic system (tree level, black) and the stochastic system (one-loop, blue) as a function of  $r = 1 - R$ . For  $r < 0$ , the fixed point  $x_0 = 0$  is unstable (dashed horizontal lines). Exact solution from Fokker-Planck equation (FP) in red. The dotted vertical lines denote the values of  $r$  that are used in panels (c) and (d). (b) Zero-frequency variance  $\langle X(0)^2 \rangle - \langle X(0) \rangle^2 = U_{OM}''(\bar{x}^*)^{-1}$  of the stochastic system as a function of  $r$  at the stable stationary points determined from the curvature of the tree-level approximation (black) and one loop approximation (blue) of  $U_{OM}$ . The one-loop result for  $r > 0$  is shown only for  $r > r_c$ , where  $r_c$  is the value of the leak term below which the one-loop corrections are greater than the tree-level contributions (Ginzburg criterion; see Ref. [13], chap. 6.4), i.e.,  $|\Gamma_{xx,fl}^{(2)}| > |r|$ . (c) Effective potentials  $U_{OM}$  (56) and  $U_{DD}$  (57) in the broken symmetry phase [ $r = -0.31$ , left black dotted vertical line in panels (a) and (b)]. Tree-level approximation ( $U_{OM}$ : black,  $U_{DD}$ : gray) and one-loop approximation of  $U_{OM}$  (A47) (blue); one-loop approximation is expanded up to second order in  $\delta x = x^* - x_{\pm}^1$ , where  $x_{\pm}^1 \neq 0$  is the one-loop stationary point of  $U_{OM}$  shown in A (blue curve). (d) Same as panel (c), but in the symmetric phase [ $r = 0.22$ , right black dotted vertical line in panels (a) and (b)]; one-loop result expanded in  $\delta x$  around  $x_0 = 0$ . For all panels  $u = 0.2$  and  $D = 0.05$ .

$x(t) = \frac{1}{N} \sum_i x_i(t)$  only, (1) can be rewritten as

$$\begin{aligned}
 dx(t) + x(t) dt &= \frac{1}{N} \sum_i \sum_j J_{ij} \phi[x_j(t)] dt + dW(t) \\
 &= pJ \left\{ \sum_{j \in E} \phi[x_j(t)] + g \sum_{j \in I} \phi[x_j(t)] \right\} dt + dW(t) \\
 &= pJ(N_E + gN_I) \phi[x(t)] dt + O[\delta x_i(t)] dt + dW(t),
 \end{aligned} \tag{53}$$

where  $dW(t) = \frac{1}{N} \sum_i dW_i(t)$  is the noise component projected in the population direction  $(1, \dots, 1)$ , and  $\delta x_i(t) = x_i(t) - x(t)$  is the deviation of each individual neuron activity from the population average  $x(t)$ . The terms  $O[\delta x_i(t)]$  arise from a Taylor expansion of the nonlinearity  $\phi$  around  $x(t)$ . We notice that the population-averaged activity is driven by fluctuations  $\delta x_i(t)$  of individual neurons and external fluctuations  $dW_i(t)$ . The former arise from the recurrent processing of uncorrelated external inputs  $dW_i(t)$  via random connections  $J_{ij}$ . Numerical simulations show that the variance of the population activity strongly depends on the ratio  $R := pJ(N_E + gN_I)$  between excitation and inhibition in the network [Figs. 5(b)–5(d)]. In particular,

the size and timescale of fluctuations strongly increase for  $R \rightarrow 1$  [Fig. 5(c)], the point where excitation and inhibition in the network exactly balance the neuronal leak term on the left side of (53). Moreover, for  $R > 1$  we observe a nonzero mean activity [Fig. 5(d)], even though the external input has zero mean and the nonlinearity is point-symmetric. These observations point towards a phase transition in the model.

A fully self-consistent treatment of the model including the colored-noise fluctuations  $\delta x_i$  of individual neurons is possible. To this end the MSRDJ formalism needs to be combined with a disorder average [43,68]. However, in order to expose the phase transition elicited from the interplay of general fluctuations on the right-hand side of (53) and the ratio  $R$  between excitation and inhibition, it is sufficient to only consider white noise fluctuations. Then the population dynamics reduces to

$$\begin{aligned}
 dx(t) + x(t) dt &= R \phi[x(t)] dt + dW(t) \\
 &\approx R \left[ x(t) - \frac{1}{3} x^3(t) \right] dt + dW(t),
 \end{aligned} \tag{54}$$

where we expanded the nonlinearity  $\phi(x) = \tanh(x) \approx x - \frac{1}{3} x^3$ , which can be done for small external noise amplitudes  $D$  defined as  $\langle dW(t) dW(s) \rangle = D \delta_{t,s} dt$ . Expression (54) describes the stereotypical setting of a bistable system (see “model A” in Ref. [5]) for which both the de Dominics equilibrium effective potential (52) and the OM form



(48) are applicable to study phase transitions (Fig. 6). The deterministic part can be written as the gradient of the potential  $V(x) = \frac{r}{2}x^2 + \frac{u}{12}x^4$ ; the system is hence identical to fluctuations around the equilibrium state of a Ginzburg-Landau model (model A in Ref. [5]). In this analogy, the parameter  $r = 1 - R$  plays the role of the reduced temperature—when it vanishes, the system is at a critical point—and  $u = R$  is the strength of the interaction. The fix points in the noiseless case ( $D = 0$ ) are

$$x_0 := 0, \quad x_{\pm} := \pm \sqrt{-\frac{3r}{u}}, \quad \text{for } r < 0; u > 0, \quad (55)$$

The trivial fix point  $x_0 = 0$  is stable as long as  $r > 0$ . As  $r$  becomes negative, the two stable fixed points  $x_{\pm}$  come into existence. They move out of zero in a continuous manner, the hallmark of a continuous phase transition, shown in Fig. 6(a). So the system becomes bistable if the level of recurrent positive feedback is high enough; namely, at  $R > 1$ , the deterministic system shows a pitchfork bifurcation. This is what happens in a network if excitation becomes dominant, so that the balanced state [9] is destabilized and a pair of stable states, one at high and another at low activity, appear [10]. Furthermore, one notices that the timescale of fluctuations diverges if  $R \rightarrow 1$ ,  $r \rightarrow 0$ , because the leak term in (54) vanishes.

This analysis shows that the network at the point of balance between excitatory and inhibitory coupling can be mapped to the prototypical model of a continuous dynamics phase transition, the time-dependent  $x^4$  theory (model A in Ref. [5]). A difference between the original model A and the network studied here is that the random connectivity leads to an effective, spatially homogeneous all-to-all coupling. As is known from the general theory of critical phenomena, the divergence of fluctuations often leads to considerable deviations from the above mean-field analysis, for example, the mismatch of critical exponents. In the following, we therefore illustrate how to assess fluctuation corrections on the example of the simplified dynamics (54).

In the stochastic system, the effective potential can be used to investigate this continuous phase transition. The corresponding effective potential in tree-level approximation (49) takes the form

$$\begin{aligned} U_{\text{OM},0}(\bar{x}^*) &= \frac{1}{2D} [V'(\bar{x}^*)]^2 \\ &= \frac{1}{2D} (\bar{x}^*)^2 \left[ r + \frac{u}{3} (\bar{x}^*)^2 \right]^2, \end{aligned} \quad (56)$$

shown in Fig. 6(b). This effective potential differs from the one constructed by de Dominicis. The latter with (A45) yields

$$U_{\text{DD},0}(\bar{x}^*) = V(\bar{x}^*) = \frac{1}{2} (\bar{x}^*)^2 \left[ r + \frac{u}{6} (\bar{x}^*)^2 \right], \quad (57)$$

shown in Figs. 6(c) and 6(d) for  $r < 0$  and  $r > 0$ , respectively. However, the fixed points (55) are the stationary points of  $V$  and thus of  $U_{\text{DD}}$ . These are also stationary points of  $U_{\text{OM}}$ . In addition,  $U_{\text{OM}}$  has the stationary solutions that are roots of  $0 = V''(\bar{x}^*) = r + u(\bar{x}^*)^2$ , namely,  $\bar{x}_{\pm}^* = \sqrt{-\frac{r}{u}}$  (as minima). These are the inflection points of  $V$ , which denote the points at which the static theory (51) has a diverging propagator (see also the discussion at the end of Sec. 6.4 in Ref. [13]).

The vicinity of the joint stationary points of  $U_{\text{DD}}$  and  $U_{\text{OM}}$  can also be seen in the light of equal-time versus frequency-zero fluctuations. The curvature of  $U_{\text{DD}}$  and hence, to leading order, of  $V$ —by (51)—is the inverse of the equal-time covariance  $[\frac{2}{D} U_{\text{DD}}''(\bar{x}^*)]^{-1} = \langle x(t)x(t) \rangle - \langle x(t) \rangle \langle x(t) \rangle$ . The curvature of  $U_{\text{OM}}$  at a stationary point yields—by (50) and (5)—the covariance of the zero frequency fluctuations  $[U_{\text{OM}}''(\bar{x}^*)]^{-1} = \langle X(0)^2 \rangle - \langle X(0) \rangle^2$ . These two relations show that points of vanishing curvature in both cases (56) and (57) signify the divergence of fluctuations, hence a critical point. In the current example, both effective potentials show that such a fluctuation infinity at the fixed point  $\bar{x}^* = 0$  appears if  $r = 0$ ; at the point where the network dynamics changes from inhibition dominance ( $r > 0$ ) to excitation dominance ( $r < 0$ ), shown in Fig. 6(b).

Computing the effective potential in one-loop approximation [see Appendix A 12, Eq. (A47)], the divergence of the fluctuations appears at smaller  $r < 0$ , whereas for positive  $r$  fluctuations are reduced compared to the tree-level approximation. In this example we see a considerable correction caused by the fluctuations. Thus, the point where balance is lost, the transition temperature  $r_c$ , is shifted towards smaller  $r$ , similar to the Ginzburg-Landau model where fluctuation corrections reduce the critical value  $r_c$ . There the one-loop corrections to the variance, shown in Fig. 6(b), also are considerable.

The one-loop corrections to the effective potential diverge as  $r \rightarrow 0$ , as expected at a continuous phase transition. The solution to the equation of state disappears already far above  $r = 0$ , as shown in Fig. 6(a). This shows that the behavior of the system close to  $r \simeq 0$  is indeed strongly fluctuation-driven and qualitatively different from the simple bifurcation in its deterministic counterpart, the tree-level approximation. This simple example illustrates that deterministic and stochastic models of neuronal activity may show qualitatively quite different behavior in particular at such critical points. The details of the calculations for this model are presented in Appendix A 12.

For  $r < 0$  the system thus possesses two degenerate solutions. If the external drive  $\tilde{j}$  to the system is varied, we observe a first-order phase transition: as  $\tilde{j}$  crosses zero, the mean jumps over from one local minimum of  $U$  to the other. The true  $U_{\text{OM}}$  inherits the convexity of  $\Gamma_{\text{OM}}$ , and should hence have a flat segment between the two local minima in Fig. 6(c). The nonconvexity of the approximations (56) and (57) is an artifact of the simple approximation used here; in particular whether there is a local minimum in  $U_{\text{DD}}$  or a local maximum in  $U_{\text{OM}}$  as  $\bar{x}^* = 0$  is inconsequential; both would be replaced by a straight line in the convex envelope of  $U$ ; the latter is obtained because  $W$ , computed as the Legendre transform of the (nonconvex) approximation of  $\Gamma_{\text{OM/DD}}$ , has different left- and right-sided derivatives. Transforming back one obtains a convex approximation of  $\Gamma$  and hence  $U$  (see Appendix A 3 for a detailed discussion of convexity and differentiability of  $W$ ).

Note also that on a global scale, the identification of  $U_{\text{OM}}$  with an energy landscape is not possible, because it assumes stationarity and is therefore only valid near a stable fixed point. As a consequence, the maxima of  $U_{\text{OM}}$  do not indicate borders of the basin of attraction of this stable fixpoint,

contrary to what would be expected for an energy. Moreover, unstable fixed points of the system will show up as minima of  $U_{\text{OM}}$ , as is obvious from the tree-level approximation (12) that is positive semidefinite and vanishes whenever  $f(x^*) = 0$ .

### III. DISCUSSION

This article surveys methods to obtain self-consistent approximations by functional and diagrammatic techniques for stochastic differential equations as they appear in models of neuronal networks. Besides a systematic introduction, going from simple to more complex methods, we present three main new findings.

First, we expose the fundamental relation between the Onsager-Machlup (OM) effective action, which has a direct physical and probabilistic interpretation, and the Martin-Siggia-Rose-de Dominicis-Janssen (MSRDJ) effective action, which is computationally favorable. The general exposition of this fundamental link, to our knowledge, has been missing in the literature; it has earlier surfaced in specific problems in certain approximations [89]. In particular, the derivation of the OM effective action from the corresponding MSRDJ effective action naturally extends the definition of the former beyond Gaussian noise. The OM effective action in addition allows the analysis of bifurcations in stochastic systems. These can be studied conveniently by help of the corresponding effective potential, which exposes whether the stochastic system makes a first-order phase transition or a continuous phase transition and which allows the assessment of fluctuations at the transition. We show for the neuroscientifically important example of the balanced state [9], that the loss of balance, which in the deterministic system causes a pitchfork bifurcation, in the stochastic system becomes a continuous phase transition dominated by fluctuations. We also expose the relation to the de Dominicis effective potential [81] in equilibrium systems.

Second, we derive two effective equations that are equivalent to the stochastic nonlinear system. The first is a deterministic integro-differential equation that captures the time evolution of the mean of the process. A related equation has previously been derived within the Doi-Peliti formalism of Markovian dynamics [45]. The second is a stochastic, but linear integro-differential equation that has identical second-order statistics as the full system. These effective equations serve us here to provide an intuitive interpretation of the meaning of various vertex functions and to show how to relate stochastic nonlinear models to effective deterministic or stochastic linear systems.

Third, we develop a truncation scheme for the hierarchy of flow equations that arises in the functional renormalization group, which is based on the BMW scheme [54]. We here transfer this method from the derivative expansion to the vertex expansion, and demonstrate that this scheme yields a closed set of flow equations for the vertex functions which accurately captures the statistics of the system. The presented scheme is generic and may therefore be employed beyond the application to neuronal dynamics.

The link between the OM and the MSRDJ formalism also allows us to comment on a set of more subtle points. We carefully consider the convexity of the cumulant-generating functional  $W$  and discuss physically relevant cases in which

$W$  becomes nondifferentiable as a result of degeneracy, for example, by spontaneous symmetry breaking as it appears in attractor networks or in networks that show bistability: the existence of a convex set of solutions to the equation of state. The relation to the OM effective action enables us to address the question whether the effective action in the MSRDJ formalism is well defined. To our knowledge, this is still an open question (see also Ref. [26]). The work by Andersen [82] presents a mathematically rigorous version of the MSR operator formalism [39] and concludes that there are cases where the Legendre transform cannot be applied. The problem in defining a Legendre transform for both sources  $j$  and  $\tilde{j}$  at once is their mutual dependence. This necessitates Andersen [82] to consider an ensemble of paths with an initial period of trivial dynamics (see i.p. his Sec. V and his Appendix D). In the path-integral formulation that we follow here, albeit not mathematically rigorous in a strict sense, we are able to address the problem from another view point. We separate the Legendre transform into two steps. The first, which can rigorously be done thanks to the convexity of  $W$  in  $j$ , and a second, which is in fact only needed formally: we show that the solutions of the equation of state obtained from the MSRDJ formalism fulfill the requirement  $\langle x \rangle = x^*$ , as requested by the well-defined OM effective action. What hence remains open is to show that all solutions of the OM equation of state also solve the MSRDJ equation of state.

The model systems studied in the current manuscript are intentionally left simple to illustrate the techniques in a minimal setting. In the following we therefore provide a slightly wider outlook for potential applications that are of relevance to the study of neuronal networks.

The initial part of this paper reformulates the problem of finding self-consistency equations by help of the effective action. We here apply the standard approach known from quantum field theory and statistical physics [79]. This technique yields self-consistent equations for the mean of the process that incorporate fluctuation corrections. Applications to neuronal networks include the study of bifurcations in the network dynamics, as we demonstrate here. Pitchfork bifurcations, for example, are responsible for the occurrence of multistability, the basis of classical attractor networks [12]. The effective action allows us to transfer the concept of a bifurcation in a deterministic differential equation [115] to a stochastic system: We need to investigate the bifurcations of the stationary points of the effective action, instead of studying the differential equation itself. A pitchfork bifurcation, the transition from a regime with a unique solution to one with multiple fixed points, corresponds in the stochastic system to a critical point; the effective action changes from having a single minimum to exhibiting a flat segment that, beyond the bifurcation point, admits a continuum of stationary states. Traversing the bifurcation point, the curvature vanishes and hence fluctuations diverge. We here showed that the OM effective action clearly exposes this fundamental property in the example of a network at the point where feedback changes from dominance of inhibition to dominance of excitation. Beyond the transition point, the system may be brought to jump from one end of the plateau to the other—showing a first-order phase transition as an external parameter is varied; the network is bistable.

The study of transitions to oscillatory states, as they are ubiquitously observed in neuronal systems [116], would require the computation of the effective action as a functional of a field with Fourier components at nonzero frequencies. If the stationary point of the functional is assumed at a constant field configuration at one side of the bifurcation and by an oscillatory state on the other side, we have the stochastic analog of a Hopf bifurcation. These bifurcations play a central role for the generation of oscillations [61] and for the appearance of spatiotemporal waves which are observed in cortical networks [117–119]. The formalism exposed here makes the influence of noise on such bifurcations accessible. For example, the recently found phase transition at the onset of an oscillatory state [49] could be analyzed within this framework. Bifurcations in neuronal networks in the presence of symmetries can be studied by means of the equivariant branching lemma [120]. So far these techniques neglect the influence of the noise altogether (i.e., employ the tree-level approximation), and therefore their applicability is limited to network states with weak noise. The formulation of bifurcations in terms of the effective action would allow an extension of this method to study how symmetries constrain bifurcations between fluctuation-dominated states.

A closely related point is the transition between multiple stable states, such as up- and downstates [121,122] or the different states of an attractor network [12]. The average noise-driven paths of transitions between such metastable states allows the assessment of the statistics of transitions between multiple states, for example to quantify the vulnerability to noise of information encoded in the activation of an attractor. Technically, one here seeks escape solutions to the equation of state which have nonvanishing values for the response field  $\tilde{x}$  [78,123] (see also Ref. [77], i.p. chap. 10 for a review). In the setting of given initial value and free endpoint (relaxation), however, we can use that  $\tilde{x} = 0$  and we can limit ourselves to small deviations  $\delta x$  of the physical variable. This enables the computation of the effective equation of motion for the mean value as a Taylor expansion of the equation of state. The theoretical prediction agrees with the simulation reasonably well. A related approach was here used to provide an approximation for the effective potential: if the approximation of the MSRDJ effective action is quadratic in the response field, extremizing  $\tilde{x}$  is equivalent to integrating out the response field to obtain the OM effective action. This technique has an advantage over the computation of  $\Gamma[x, \tilde{x}]$  for arbitrary values of  $\tilde{x} \neq 0$ , because in the latter case closed response loops do not vanish, neither do the propagators  $\Delta_{\tilde{x}\tilde{x}}$ , thus proliferating the number of diagrams to compute.

The loop expansion is shortly reviewed here, because it provides qualitative insights into the leading order of the fluctuation corrections. In the context of neuronal networks, the seminal work by Buice and Cowan [84] has introduced this technique to the study of neuronal networks. Since the structure of the one-loop diagrams is identical to those that appear in the functional renormalization group, one may use this method to check which additional vertices are produced along the RG flow, thus providing information for a good ansatz for the effective action. We here show that the loop expansion for the considered example is an expansion  $\propto \beta^2 D$ , where  $D$  is the amplitude of the noise and  $\beta$  the prefactor of

the nonlinearity. In our example, fluctuations are small so that the one-loop result is already quite accurate. The sign of the fluctuation corrections together with the form of the effective equations for the mean and for the second-order fluctuations, moreover expose qualitative mechanisms that arise from the fluctuation corrections: we show that a convex nonlinearity always causes a positive shift of the mean of the process and that the additional linear memory kernel that arises from the self-energy has a sign that diminishes the leak term, thus causing a slower relaxation of the system; the interplay of noise and nonlinearity thus prolongs the memory of a stimulus within the system. For small deflections from the steady state, this indirect contribution, moreover, typically dominates over the effect of the nonlinearity *per se*. Nevertheless, many studies of neuronal networks neglect this feedback, and keep the nonlinear terms at their mean-field level. This approach has been shown to yield good results [see Ref. [48], Eq. (6) and [124], Eq. (3.8)] if fluctuations are not too strong. This is in line with our results provided that the noise level is low, because the linear memory kernel scales with  $D\beta^2$ , as can be seen in (32). Therefore for  $D\beta^2 \ll 1$ , while  $\beta = O(1)$ , it might indeed be sufficient to consider the deterministic effect of the nonlinearity, but not the interaction with the noise. However, for  $D\beta^2 = O(1)$  while  $\beta \ll 1$ , the nonlinear effects by themselves are negligible, but their interaction with the noise induces a significant memory term. Setting  $\beta$  exactly to zero obviously makes both effects vanish, which for very noisy environments might lead to the erroneous conclusion that the nonlinearity without the noise is the reason for the deviation from the linear case. For large times especially, the linear noise-mediated component due to its “memory” wins over the deterministic nonlinear part. Correspondingly we show that the power spectrum at low frequencies is enhanced. Convex nonlinearities of the gain functions of neurons, that are required for these qualitative features to hold, are typical in regimes in which neurons are driven by fluctuations [125].

Networks with disordered connectivity, where connections are drawn randomly, are commonly treated in mean-field approximation [68,125,126]. The loop expansion is a principled way to go beyond this lowest order approximation. The approximation is typically performed with help of auxiliary fields, the physical meaning of which is the time-lagged autocorrelation function of the input to a neuron [see, e.g., Ref. [43], Appendix A, Eq. (A6)]. Constructing the effective action in these fields allows the systematic computation of fluctuation corrections to the mean-field solution [see, e.g., Ref. [43], Appendix A, Eq. (A8)].

The functional renormalization group (fRG) approach is presented here in the context of neuronal dynamics as a method that overcomes the limitations of the loop expansion with regard to self-consistency that is restricted to the mean. Instead, all vertex functions are potentially renormalized by fluctuation corrections, thus in principle allowing a fully self-consistent treatment also including corrections to the propagators and the interaction vertices. In the regime of weak fluctuations, we show that the results are slightly superior to the one-loop approximation, but here do not yield qualitatively new results. Computing higher order loop approximations is, moreover, inherently difficult, whereas all integrals in the fRG approach always have one-loop structure. The fRG

approach, however, leads to improved results over the one-loop approximation even though the frequency resolution of higher order vertices is limited by the adapted BMW approximation introduced here. Given in addition that similar ansätze have been successfully applied to spatially extended systems like the KPZ model [51], we believe that the insights gained by this work will prove useful in studying neuronal networks embedded in space. Here also more sophisticated approaches might become useful, for example, the decomposition of vertices in so-called channels, characterized by the way they can be separated into two pieces by cutting two lines (particle-particle, particle-hole, and crossed particle-hole in solid-state physics terms). For a momentum-independent bare interaction, the contribution of each channel has a characteristic momentum structure, which can be used to drastically reduce the numerical effort both in fRG [127,128] and parquet calculations [129].

From a conceptual point of view, the functional renormalization group is interesting, because the flow generates new interaction vertices that are not contained in the original model. Thus, this method shows how the description of a neuronal network changes as fluctuations are integrated out: It exposes which effective interactions are generated. A specific feature of a flat regulator in frequency domain is its direct physical interpretation as a leak term of the neuronal dynamics. It controls the relaxation rate. Each point along the renormalization group flow therefore corresponds to a physical system with a different neuronal timescale. This insight may be used to study the approach towards a critical point at which the leak term vanishes and the timescale of fluctuations diverges. A more general discussion of frequency-dependent regulators can be found in Duclut and Delamotte [106].

This view is complementary to the typical application of an RG analysis, where mostly a momentum-dependent regulator is used so that the short-ranged degrees of freedom are subsequently integrated out. A rescaling of the momenta then yields identical momentum ranges before and after this marginalization, so that fixed points may occur (see, e.g., Ref. [130], i.p. “The Scaling Form of the RG Equation of the Dimensionless Potential”). In this view, each point on the RG trajectory represents the same system, just described at a different level of coarse graining.

Despite its simplicity, the here-considered model exposes two fundamental properties: First, the fluctuation corrections to the self-energy  $\Gamma_{xx,fl}^{(2)}$  shift the point of transition with regard to mean-field theory. The latter predicts criticality at the point of vanishing leak term  $m = 0$ . The self-energy corrections reduce the leak term, thus promoting critical fluctuations. The critical point is therefore reached already at a nonzero negative value  $m_c < 0$  of the leak term. Qualitatively, the behavior of the self-energy corrections is therefore opposite to the best known text book model of criticality, the  $\phi^4$  theory, where the transition is delayed to a negative mass term [e.g., Ref. [13], Eq. (6.26)]. In addition, a second mechanism causes a shift of the transition point, which is absent in an even theory as the  $\phi^4$  model: Fluctuation corrections to the mean value increase the mean value  $\bar{x}$ . Thus, the effective leak term  $m(\bar{x})$  is weakened, further promoting the approach to the critical point.

These generic observations only depend on the assumption of an expansive nonlinear neuronal gain function, so that we

expect qualitatively similar results for example in a (fully or densely connected) network. The shift of the transition point obviously depends on the amplitude of the noise. It is known that fluctuations vary in neuronal networks in response to stimuli [131,132]. Thus, neuronal systems may dynamically change their distance to the critical point within short periods of time.

A particularly interesting feature of the approach to the critical point are trajectories that depart from the stationary mean towards the location of the second, unstable, fixed point. Their dynamics slows down not only due to the reduced leak term by the two mechanisms described above, but also due to passing the vicinity of the second, unstable fixed point. In neuronal systems this mechanism may be useful to generate transient behavior on slow timescales, beyond the slow down of fluctuations close to the stable fixed point. One may speculate if such mechanisms play a role in long transient behavior observed in delayed response tasks [133].

Recently a Ginzburg-Landau type theory of neuronal activity has been formulated by Di Santo *et al.* [49]. A bit earlier, Henningson and Illes [134] succeeded in fitting a simpler, linear model—a leaky heat equation with additional Gaussian noise—to the recordings of subthreshold fluctuations in acute hippocampal brain slices from rat. Such models, expressed as partial stochastic differential equations, naturally fall into the realm of the statistical field theoretical methods discussed here. In particular the study of second-order phase transitions has come into reach now, either by employing the established formalism of statistical field theory based on Wilson’s renormalization group for nonequilibrium stochastic dynamics (see Ref. [5] for an authoritative review) or by the functional renormalization group methods presented here. Whether or not nontrivial fixed points in neuronal networks are accessible by former methods that rely on the closeness of the fixed point to a Gaussian one is so far unclear. The closely related Kardar-Parisi-Zhang model [50], for example, exhibits fixed points in the strong coupling regime, which is therefore only accessible by nonperturbative methods, for example, the fRG approach presented here [135].

The currently employed theory of second-order phase transitions in neuronal networks follows two main themes. The first employs dynamic models like branching processes. It is determined by the branching parameter, the average number of downstream descendants produced by the current activity [136,137]. It relates second-order phase transitions to the transition originally studied in the sandpile model [138]. In a similar spirit, Buice and Cowan [84] have introduced a network of neurons, which can be either active, quiescent, or refractory and are described by a master equation. This model also shows a dynamic phase transition, so this is part of the first theme. In the second theme, experimentally measured activity is compared to equilibrium ensembles, such as pairwise maximum entropy models [88,139]; the discrepancy between the nonequilibrium dynamics of neuronal networks and this latter approach based on equilibrium thermodynamics has been identified as a pressing problem [33]. Following a field theoretical approach would in particular allow the study of critical exponents in models where neuronal activity unfolds in a spatially extended field, representing a coarse-grained view on the activity of mesoscopic numbers of neurons



at each space point. Thus it would enable experimental predictions, for example with regard to the spatial structure of correlated activity. For the Manna sandpile model [140] such a continuous theory has been formulated and it has been found to belong to the universality class of directed percolation with a conserved quantity (C-DP) [141–144]; the conservation of the number of sand grains here gives rise to the conserved quantity. Belonging to the C-DP universality class, the Manna sandpile model in particular features an absorbing state. Also the three-state neural dynamics by Buice and Cowan can be shown to belong to the C-DP universality class [84]. Therefore, this model has an absorbing state, too. In neuronal networks, though, we typically see ongoing activity; the absence of an absorbing state would therefore give rise to a different structure of the effective field theory, possibly also affecting the universality class. An alternative approach is therefore to start at the biophysics of neuronal networks on the microscopic level and to derive the structure of an effective long-range field theory. Investigating such models, the functional renormalization group has proven one of the few tools that make nonperturbative RG fixed points accessible [52].

So far field theoretical methods have been applied to neuronal networks with Markovian dynamics on discrete state spaces [46,84], employing the Doi-Peliti [85] formalism or the alternative approach by Biroli *et al.* [65,66], which is closer to the MSRDJ formulation used here. Also neuronal dynamics described by stochastic differential equations [7,8,37,43,145,146] and stochastically spiking models (nonlinear Hawkes processes [147,148]) have recently been formulated by field theoretical methods [11]. For quadratic integrate-and-fire models in the mean driven regime, a mapping to a coupled set of phase oscillators, moreover, allows the application of the MSRDJ formalism [47,149]. The renormalization group methods that we presented here can directly be applied to these systems.

Networks of leaky integrate-and-fire models [150] in the fluctuation driven, asynchronous irregular state [10,125] are, however, inherently complicated to treat by field theoretical methods; the reason is that an action for such models is cumbersome to define due to the hard threshold and reset of the membrane potential. This model and its biophysically more realistic extensions [96], however, form a kind of gold standard. It would therefore be a major step to treat networks of such models by systematic approaches as they are offered by field theory. So far methods for this central model are constrained to *ad hoc* mean-field approximations, typically resting on the annealed approximation of the connectivity [10,151]; in particular this mean-field based approach prohibits a systematic study of critical phenomena.

In summary, the current work imports methods from established fields of physics into the field of theoretical neuroscience that we think have a high potential to solve some of the technical difficulties that arise in the study of neuronal networks in the presence of fluctuations, nonlinearities, phase transitions, and critical phenomena.

#### ACKNOWLEDGMENTS

We thank PierGianLuca Porta Mana for fruitful discussions. We also express our gratitude towards the three anonymous

reviewers, who provided highly valuable feedback on the contents and the presentation, in particular, for raising the question of convexity and well-definedness of the MSRDJ effective action. Their comments and advice substantially improved our manuscript. We are grateful to our colleagues in the NEST developer community for continuous collaboration. All network simulations carried out with NEST [152]. This work was partly supported by the Exploratory Research Space seed funds MSCALE and G:(DE-82)ZUK2-SF-CLS002 (partly financed by Hans Herrmann Voss Stiftung) of the RWTH university; the Jülich-Aachen Research Alliance Center for Simulation and Data Science (JARA-CSD) School for Simulation and Data Science (SSD); the Helmholtz Association: Young Investigator's grant VH-NG-1028; European Union's Horizon 2020 Framework Programme for Research and Innovation under the Specific Grant Agreement No. 785907 (Human Brain Project SGA2); Jülich Aachen Research Alliance (JARA); and the German Federal Ministry for Education and Research (BMBF Grant No. 01IS19077A).

#### APPENDIX

##### 1. Normalization and escape

It is often stated that in stationary settings all moments of the response field vanish (Refs. [[83], p. 38] and [153]). This statement follows from the normalization of the probability functional  $p[x|\tilde{j}]$  for all paths,  $\int \mathcal{D}x p[x|\tilde{j}] = 1$ . The latter is given by

$$p[x|\tilde{j}] = \int \mathcal{D}\tilde{x} \exp(S[x, \tilde{x}] + \tilde{j}^T \tilde{x}). \quad (\text{A1})$$

The normalization can therefore also be written as  $Z[0, \tilde{j}] \equiv 1$ , which, upon  $n$ -fold differentiation by  $\tilde{j}$ , yields

$$\langle \tilde{x}(t_1) \cdots \tilde{x}(t_n) \rangle \equiv 0 \quad \forall t_1, \dots, t_n, n. \quad (\text{A2})$$

Note, however, that this holds only for paths for which either the endpoint or the starting point is given. Fixing both, as is done for escape problems (see, e.g., Ref. [77], chap. 10), effectively leads to an additional term in the action and therefore to nonzero moments of powers of the response field: specifying the end point of the path, we implicitly restrict the ensemble of paths in the integral appearing in  $Z$ . In the path-integral formulation, we include the initial point  $x_0$  and the final point  $x_T$  as

$$\begin{aligned} \mathcal{Z}[j, \tilde{j}] &= \int \mathcal{D}x \int \mathcal{D}\tilde{x} \exp(S[x, \tilde{x}] - \tilde{x}^T \delta(\circ) x_0 \\ &\quad + j^T x + \tilde{j}^T \tilde{x}) \delta(x(T) - x_T). \end{aligned}$$

The presence of the initial condition  $x_0$  obviously does not affect the normalization; it can as well be absorbed into a shift of  $\tilde{j} \rightarrow \tilde{j} - \delta(\circ)x_0$ . Fixing the final condition  $x_T$ , however, leads to the relation

$$\mathcal{Z}[0, \tilde{j}] = p(x(T) = x_T | x_0, \tilde{j}),$$

which is the conditional probability to reach the final point  $x_T$  from the initial point  $x_0$  given the inhomogeneity  $\tilde{j}$ . This probability is not necessarily independent of  $\tilde{j}$ , so that in general nonzero moments (A2) appear.

## 2. General properties of the effective action in the MSRDJ formalism

Multiple derivatives of  $\Gamma$  with respect to  $x$  *only* are always zero, as we will demonstrate in this section. We have just seen that if we do not specify an endpoint for  $x$ , the expectation value of all powers of  $\tilde{x}$  vanish. As a consequence, we see from (23) that  $\Gamma_{xx}^{(2)}[x^*, 0] = 0$ . Extending our analysis to higher order derivatives of  $\Gamma$  not involving  $\tilde{x}$ , we observe that

$$\Gamma_{x_1 x_2 x_3}^{(3)} = \sum_{y \in \{x, \tilde{x}\}} \sum_{y_1, y_2, y_3} \Gamma_{x_1 y_1}^{(2)} \Gamma_{x_2 y_2}^{(2)} \Gamma_{x_3 y_3}^{(2)} W_{y_1, y_2, y_3} \\ \stackrel{\Gamma_{xx}^{(2)}=0}{=} - \sum_{\tilde{x}_1, \tilde{x}_2, \tilde{x}_3} \Gamma_{x_1 \tilde{x}_1}^{(2)} \Gamma_{x_2 \tilde{x}_2}^{(2)} \Gamma_{x_3 \tilde{x}_3}^{(2)} \underbrace{W_{\tilde{x}_1, \tilde{x}_2, \tilde{x}_3}^{(3)}}_{=0} = 0. \quad (\text{A3})$$

Similarly, we can argue for all higher order vertices: they can be decomposed into “tree diagrams” with derivatives of  $W$  as nodes and  $\Gamma^{(2)}$  as connecting elements. A tree diagram is defined by having the property to not include loops, and especially, that means that two nodes are connected by at most one element  $\Gamma^{(2)}$ . Because we have only  $x$  at the external legs and  $\Gamma_{xx}^{(2)} = 0$ , we have all  $W^{(n)}$  connected to external legs to be with respect to  $\tilde{j}$ . Therefore, the only possibility to “justify”  $j$  derivatives are  $\Gamma_{xx}^{(2)}$ -components acting as internal connecting elements providing one  $j$  derivative each. Since the graphs are treelike, we have exactly one  $W^{(n)}$  node more than connecting elements. However, we need at least one  $j$  derivative at every node to prevent that it vanishes. We deduce that the contribution of at least one of the nodes is zero. This demonstrates that

$$\underbrace{\Gamma_{x, \dots, x}^{(n)}}_{n \text{ times}} = 0 \quad \forall n.$$

## 3. Convexity and spontaneous symmetry breaking

Cumulant-generating functions are convex. This can be seen from the Hoelder inequality that holds for two non-negative sequences  $g_k, h_k \geq 0$  with  $\alpha + \beta = 1$  and  $0 \leq \alpha, \beta \leq 1$

$$\sum_k (g_k)^\alpha (h_k)^\beta \leq \left( \sum_k g_k \right)^\alpha \left( \sum_k h_k \right)^\beta \quad (\text{A4})$$

and from the fact that probabilities are positive, so that one can always define an “action” as the log probability  $p(x) =: e^{S(x)}$  (we here omit the normalization by the partition function for brevity that would read  $p(x) = e^{S(x) - \ln Z}$ ). We here follow a modified version of the argument in Ref. [154]; a similar proof can be found in Ref. [112]. Applied to the moment-generating function  $Z(j) = \langle e^{j^T x} \rangle$  one gets with a generalization of Hoelder’s inequality for infinite-dimensional spaces

$$Z(\alpha j_1 + \beta j_2) = \langle e^{(\alpha j_1 + \beta j_2)^T x} \rangle = \int_x e^{(\alpha j_1 + \beta j_2)^T x + S(x)} \\ \stackrel{\alpha + \beta = 1}{=} \int_x e^{\alpha(S(x) + j_1^T x)} e^{\beta(S(x) + j_2^T x)} \\ = \int_x (e^{S(x) + j_1^T x})^\alpha (e^{S(x) + j_2^T x})^\beta$$

$$\stackrel{\text{Hoelder}}{\leq} \left( \int_x e^{S(x) + j_1^T x} \right)^\alpha \left( \int_x e^{S(x) + j_2^T x} \right)^\beta \\ = Z(j_1)^\alpha Z(j_2)^\beta. \quad (\text{A5})$$

So consequently the cumulant-generating function  $W = \ln Z$

$$W(\alpha j_1 + \beta j_2) \leq \alpha W(j_1) + \beta W(j_2) \quad (\text{A6})$$

has a graph that is always below its chord; it is convex down.

In the case that  $W(j)$  is differentiable, this means that its Hessian is positive definite (a corresponding short proof can be found in Ref. [[4], p. 166]). The definition of the effective action by the Legendre-Fenchel transform instead of the ordinary Legendre transform is only required if  $W$  is nonanalytic; if it has a cusp at a certain value  $j^*$ . Such a cusp corresponds to the situation of spontaneous symmetry breaking: the mean value that is conjugate to  $j$  is different if  $j^*$  is approached from above or below:

$$\langle x^+ \rangle := \lim_{j \searrow j^*} W^{(1)}(j) \\ \neq \lim_{j \nearrow j^*} W^{(1)}(j) \\ =: \langle x^- \rangle.$$

The authoritative book by Vasiliev contains a more detailed discussion of the role of Legendre transforms in the study of phase transitions (see Ref. [79], i.p. Sec. 6).

The Legendre transform  $\mathcal{L}$  of any function  $f(j)$  is convex down. This is because for

$$g(x) := \sup_j j^T x - f(j)$$

we find with  $\alpha + \beta = 1$  that

$$g(\alpha x_a + \beta x_b) = \sup_j j^T (\alpha x_a + \beta x_b) - (\alpha + \beta) f(j) \\ \leq \sup_{j_a} \alpha [j_a^T x_a - f(j_a)] + \sup_{j_b} \beta [j_b^T x_b - f(j_b)] \\ = \alpha g(x_a) + \beta g(x_b), \quad (\text{A7})$$

which shows that  $g$  is convex down. Convexity of  $f$  is not required here. This general result holds in particular for the effective action defined as

$$\Gamma(x^*) := \sup_j j^T x^* - W(j), \quad (\text{A8})$$

which therefore is convex down, too.

Furthermore, the Legendre transform is an involution on convex functions; applied twice we come back to the original function. However, in the case that the original function was not convex, the result would be the convex envelope of the original function (see, e.g., Ref. [111] i.p. Fig. 9 and surrounding text). So far, this issue cannot arise if we were able to compute  $\Gamma$  or  $W$  exactly; both functions are convex and therefore are the Legendre transforms of one another. Moreover,  $\Gamma(x^*)$  for a typical physical system is in addition differentiable everywhere. For if it had a cusp, this would mean that  $W(j)$  has a flat segment; the value of the source  $j$  would not affect the mean  $\langle x \rangle$  for values within this segment and all fluctuations would vanish, an untypical behavior (thinking of  $j$  being the external magnetic field and  $\langle x \rangle$  the

magnetization): so even if  $W$  is nonanalytic in some point  $j_c$ , its Legendre transform is analytic.

An issue arises when approximations are made. We will illustrate the point with help of the simplest tree-level approximation, the loopwise approximation to lowest order. The approximation of the effective action then is

$$\Gamma_0(x^*) = -S(x^*),$$

which is not necessarily convex; let us think of the action  $S(x) = -\frac{1}{2}x^2 + \frac{1}{4}x^4$ , for example, which has two minima at  $x_{\pm}^* = \pm 1$  and an intermediate local maximum at  $x = 0$ , clearly a nonconvex function, which is meant to approximate the convex function  $\Gamma$ . Legendre-transforming this approximation to  $W_0(j) = \mathcal{L}\{\Gamma_0\}(j) = \mathcal{L}\{-S\}(j)$  yields a function in  $j$  with a cusp at  $j^* = 0$ , because the supremum operation in  $W(j) = \sup_x jx + S(x)$  for  $j < 0$  finds the supremum at  $x \leq -1$ , and for  $j > 0$  finds the supremum at  $x \geq 1$ . As  $j$  moves through zero from below, the point of the supremum thus jumps from  $x = -1$  to  $x = +1$ . Since the position of the supremum is the left-sided (for  $j < 0$ ) or the right-sided (for  $j > 0$ ) slope of  $W(j)$ , the latter function has a cusp at zero

$$\langle x^{\pm} \rangle \equiv W^{(1)}(0_{\pm}) = \pm 1. \quad (\text{A9})$$

We may perform the Legendre transform explicitly by finding the supremum as the solution to  $\partial_x(S(x) + jx) = 0$  for  $x \in (-\infty, -1]$  for  $j < 0$  and within  $x \in [1, \infty)$  for  $j > 0$ . Transforming back to  $\Gamma_0^* := \mathcal{L}\{W_0\}$ , we obtain the convex envelope of the original  $\Gamma_0$ : The two minima at  $x_{\pm}^* = \pm 1$  are joined by a straight line. This follows directly from the cusp of  $W$  in (A9), because computing  $\Gamma_0^*(x^*) = \sup_j jx - W(j)$  for  $x^* \in (-1, 1)$  always assumes the supremum for  $j$  at  $j = 0$ ; so the resulting function  $\Gamma^*$  is flat on this segment, the value of which is  $W(0)$ . These relations are easiest appreciated graphically. A detailed explanation including graphical illustrations can for example be found in Ref. [[111], i.p. Fig 9].

The FRG, in particular in its implementation with the derivative expansion, has the interesting property that the resulting partial differential equation for the effective action (or effective potential, the effective action at vanishing Fourier mode  $k$ ) becomes convex as the flow parameter evolves (see, e.g., Ref. [130], i.p. Fig. 2.15 and related discussion). This is in contrast to simpler approximation schemes, such as the loop expansion, as we have illustrated above on its lowest order approximation. Still, as more loop corrections are incorporated, the plateau becomes successively flatter.

#### 4. Convexity of the MSRDJ cumulant-generating functional

In the form (10),  $W[j]$  is a cumulant generating functional of the field  $x$  and thus, by Eq. (A6), a convex functional in  $j$ . We can therefore perform the Legendre transform with regard to  $j$  to obtain the effective action

$$\Gamma_1[x^*, \tilde{j}] := \sup_j j^T x^* - W_{\text{MSRDJ}}[j, \tilde{j}] \quad (\text{A10})$$

as in Eq. (A8) only that we left  $\tilde{j}$  as a parameter indicating some additional input. By the convexity of  $W$  in  $j$  it is assured that the mapping between  $x^*$  and  $j$  is one-to-one and the Legendre transform with regard to  $j$  is involutive.

#### a. Necessity of the Legendre-Fenchel transform

Let us first show that the cumulant-generating functional  $W[j, \tilde{j}]$  indeed may have nonanalytical behavior that requires the use of the Legendre-Fenchel transform rather than the ordinary Legendre transform; this happens, for example, in a bistable system. For concreteness, let us assume the stochastic differential equation of the form

$$dx(t) = -V'(x)dt + dW(t) \quad (\text{A11})$$

with  $V(x) = -\frac{1}{2}x^2 + \frac{1}{4}x^4$  and initial condition  $x(0) = 0$  on the local maximum of  $V$ . For  $\tilde{j} = 0$  depending on the realization of the noise  $dW$ , the system will move close to either of the two minima  $x_{\pm} = \pm 1$  of the potential  $V$ ; for sufficiently small noise, the system will stay close to the spontaneously chosen minimum for prolonged times.

We first consider the analytical properties of  $W$  in  $j$  at  $\tilde{j} = 0$ . The presence of the source term  $\int_0^T j(t)x(t)dt$  for  $j = \epsilon$  assigns a different probability to the paths  $x(t) = x_{\pm}$ , namely,

$$p[x(t) = x_+ = 1]/p[x(t) = x_- = -1] = e^{2\epsilon T}. \quad (\text{A12})$$

So in the  $T \rightarrow \infty$  limit, a nonzero source  $j$  suppresses either of these symmetric solutions in the integration measure. Here time  $T$  plays a similar role as system size for spontaneous symmetry breaking in static thermodynamics (see, e.g., Ref. [154], i.p. Sec. 2.9). Therefore,

$$\begin{aligned} \lim_{T \rightarrow \infty} \frac{1}{T} \int_0^T \langle x(t) \rangle_{\pm} dt \\ = \frac{1}{T} \lim_{\epsilon \searrow 0} \frac{1}{\pm \epsilon} \{W[j(t) = \pm \epsilon, 0] - W[0, 0]\} \simeq \pm 1 \end{aligned}$$

yields a different left and right-sided derivative and hence mean value. So indeed one needs a Legendre-Fenchel transform to define  $\Gamma_1$  as in (A10).

#### b. Differentiability of $\Gamma_1$ in $\tilde{j}$

We now consider the dependence of  $\Gamma_1$  on the source  $\tilde{j} \neq 0$ . Such a nonzero source term corresponds to an inhomogeneity on the right-hand side of Eq. (A11)

$$\begin{aligned} dx(t) &= -V'(x)dt + dW(t) - \tilde{j} \\ &= -[V(x) + \tilde{j}x]'dt + dW(t). \end{aligned} \quad (\text{A13})$$

In a system in thermodynamic equilibrium, we may write the stationary probability distribution of Eq. (A11) as

$$p(x(t)) \propto \exp \left\{ -\frac{2}{D} V[x(t)] - \frac{2}{D} \tilde{j} x(t) \right\}. \quad (\text{A14})$$

The additional inhomogeneity  $-\tilde{j}$  in (A13) can therefore be regarded as a modified source term  $(j(t) - \frac{2}{D}\tilde{j})x(t)$ . We therefore have

$$W[j, \tilde{j}] = \ln \int \mathcal{D}x \exp \left\{ \dots + \int \left[ j(t) - \frac{2}{D}\tilde{j} \right] x(t) dt \right\}.$$

The Legendre transform with regard to  $j$  eliminates the non-differentiability in  $\tilde{j}$ . This is because the left- and right-sided

derivatives are identical, as both limits

$$\begin{aligned}
 \frac{\partial \Gamma_1[x^*; \pm\epsilon]}{\partial \epsilon} &= \lim_{\epsilon \searrow 0} \frac{1}{\pm\epsilon} \left\{ \sup_j j^T x^* - W[j, \pm\epsilon] - \left( \sup_k k^T x^* - W[k, 0] \right) \right\} \\
 &= \lim_{\epsilon \searrow 0} \frac{1}{\pm\epsilon} \left\{ \sup_j j^T x^* - W \left[ \underbrace{j \mp \frac{2}{D}\epsilon}_j, 0 \right] - \left( \sup_k k^T x^* - W[k, 0] \right) \right\} \\
 &= \lim_{\epsilon \searrow 0} \frac{1}{\pm\epsilon} \left\{ \sup_j \left( \hat{j} \pm \frac{2}{D}\epsilon \right)^T x^* - W[\hat{j}, 0] - \left( \sup_k k^T x^* - W[k, 0] \right) \right\} \\
 &= \lim_{\epsilon \searrow 0} \frac{1}{\pm\epsilon} \left( \pm\epsilon^T \frac{2}{D} x^* \right) = \frac{2}{D} x^*
 \end{aligned}$$

exist for nonzero  $D$  and are identical. We here used that a one-dimensional dynamics can always be considered as following an equilibrium distribution of the form (A14). For systems for which the right-hand side is not given by the gradient of a potential [in contrast to Eq. (A13)], it is less clear that the Legendre transform with respect to  $j$  is differentiable with respect to  $\tilde{j}$ . However, it is plausible that the effective action depends smoothly on the input  $-\tilde{j}$ .

In the case of a nonequilibrium system, we assume that we have a cumulant-generating functional with potentially a nonanalytical cusp at  $j_c$ ; since left- and right-sided derivatives are equal almost everywhere (the set of points where  $W$  is nonanalytic has measure zero; see, e.g., Ref. [155], Sec. 25), it is sufficient to assume a single such point as  $j = j_c$  where  $W^{(1)}[j_c+, \tilde{j}] \neq W^{(1)}[j_c-, \tilde{j}]$ . To study the derivative in  $\tilde{j}$  we assume that the presence of a nonzero  $\tilde{j} = \pm\epsilon$  has an infinitesimal effect on potentially all cumulants; that is to say, we assume that we can expand the cumulant-generating functional of the perturbed system

$$W[j, \pm\epsilon] = W[j, 0] \pm \epsilon \left\{ \sum_{n=0}^{\infty} \frac{G_n^+ j^n}{n!}, \quad j > j_c \right\} + O(\epsilon^2).$$

This assumption is equivalent to stating that we assume all linear response Green's functions  $G_n$  for cumulants of arbitrary order  $n$  to exist. For a given physical system this assumption has to be checked; however, it is quite reasonable to assume to hold for typical systems. The zeroth-order terms  $G_0$  must be chosen such that  $W[0, \pm\epsilon] = 0$  (due to normalization) and that  $W[j, \pm\epsilon]$  is continuous at  $j_c$ ; for otherwise  $W$  would be nonconvex, thus in contradiction to being a cumulant-generating functional. Here the notation  $\epsilon G_n^\pm j^n$  is to read  $\int ds \epsilon(s) \prod_{i=1}^n \{ \int dt_i j(t_i) \} G^\pm(s, t_1, \dots, t_n)$ .

Considering the left- and right-sided derivative by  $\tilde{j}$

$$\frac{\partial \Gamma_1[x^*; \pm\epsilon]}{\partial(\pm\epsilon)} = \lim_{\epsilon \searrow 0} \frac{1}{\pm\epsilon} \left\{ \sup_j \left( j^T x^* - W[j, 0] \pm \sum_{n=0}^{\infty} \frac{\epsilon G_n^\pm j^n}{n!} \right) - \sup_k (k^T x^* - W[k, 0]) + O(\epsilon^2) \right\}, \quad (\text{A15})$$

we need to distinguish three cases: (1) If  $x^*$  is such that the supremum in (A10) is assumed at a point  $j \neq j_c$ ,  $W$  is differentiable in  $j$ . So  $j^*(x^*)$  is a local maximum of  $j^T x^* - W[j]$ , hence the first variation by  $j$  vanishes, so that we get, w.l.o.g. assuming  $j > j_c$ ,

$$\begin{aligned}
 \frac{d}{d(\pm\epsilon)} \left( j^T x^* - W[j, 0] \pm \sum_{n=1}^{\infty} \frac{\epsilon G_n^\pm j^n}{n!} \right) \Big|_{\epsilon=0} &= \underbrace{\frac{\partial j^T}{\partial(\pm\epsilon)} x^* - \frac{\partial W^T}{\partial j} \frac{\partial j}{\partial(\pm\epsilon)}}_{\substack{x^* \\ \equiv 0 \text{ vanishing variation}}} + \sum_{n=1}^{\infty} \frac{G_n^+ j^n}{n!} = \sum_{n=1}^{\infty} \frac{G_n^+}{n!} j^n.
 \end{aligned} \quad (\text{A16})$$

So the left- and right-sided derivatives by  $\epsilon$  are identical;  $\Gamma_1[x^*; \tilde{j}]$  is differentiable in  $\tilde{j}$  for such  $x^*$ .

(2) If the supremum in (A10) is assumed at a point  $j = j_c$ , we have (in the unperturbed system with  $\epsilon = 0$ )

$$W^{(1)}[j_c-, 0] \leq x^* \leq W^{(1)}[j_c+, 0].$$

In the case that the unequal signs hold strictly as “<” the  $x^*$  form an open set; to it is clear that one can find an  $\epsilon$  small enough so that it also holds that

$$W^{(1)}[j_c-, 0] \pm \sum_{n=1}^{\infty} \frac{\epsilon G_n^- j_c^{n-1}}{n-1!} < x^* < W^{(1)}[j_c+, 0] \pm \sum_{n=1}^{\infty} \frac{\epsilon G_n^+ j_c^{n-1}}{n-1!}. \quad (\text{A17})$$



Hence for all such  $\epsilon$  one has the supremum at  $j = j_c$ . Therefore the first term in the derivative (A15) evaluates to

$$j_c^T x^* - W[j_c, 0] \pm \sum_{n=0}^{\infty} \frac{\epsilon G_n^- j_c^n}{n!} = j_c^T x^* - W[j_c, 0] \pm \sum_{n=0}^{\infty} \frac{\epsilon G_n^+ j_c^n}{n!},$$

where equality in the latter condition holds due to continuity of the convex functions  $W[j, \pm\epsilon]$  in  $j$ , as stated above. The second term correspondingly assumes the supremum at  $k = j_c$ , so that the result of the limit in (A15) is

$$\frac{\partial \Gamma_1[x^*; \pm\epsilon]}{\partial(\pm\epsilon)} = \sum_{n=0}^{\infty} \frac{G_n^- j_c^n}{n!} = \sum_{n=0}^{\infty} \frac{G_n^+ j_c^n}{n!}, \quad (\text{A18})$$

independent of whether we take the left- or the right-sided derivative.

(2) The last case to be checked is if  $x^* = W^{(1)}[j_c^-, 0]$  or  $x^* = W^{(1)}[j_c^+, 0]$ . It is sufficient to consider one case, say, “+.” If  $\epsilon$  is such that  $x^*$  moves into the inner region so that (A17) holds, the derivation under point (2) shows that the derivative evaluates to (A18). In the other case  $x^* > W^{(1)}[j_c^+, 0] \pm \sum_{n=1}^{\infty} \frac{\epsilon G_n^+ j_c^{n-1}}{n-1!}$  and hence we have a local maximum  $j(x^*)$ , as in case (1); the derivative is hence (A16) with  $j = j_c$  in the limit; so the left- and right-sided derivatives both yield the same result.

In summary, under the assumption of the existence of linear response Green’s functions for all cumulants follows that  $\Gamma_1[x^*; \tilde{j}]$  is everywhere differentiable in  $\tilde{j}$ ; a Legendre transform with regard to  $\tilde{j}$  is thus sufficient. The Legendre-Fenchel transform from  $j$  to  $x^*$  is, however, required in systems that show spontaneous symmetry breaking.

### c. Consistency of Legendre transform in $\tilde{j}$

It is left to be checked that the additional transform from  $\tilde{j}$  to  $\tilde{x}^*$

$$\Gamma[x^*, \tilde{x}^*] = \Gamma_1[x^*; \tilde{j}] - \tilde{j}^T \tilde{x}^*$$

is also such that a one-to-one relationship exists. Here a proof of the convexity of  $\Gamma_1[x^*; \tilde{j}]$  seems not to be possible; to the contrary, it can be shown rigorously that for certain systems that the Legendre transform with regard to both,  $j$  and  $\tilde{j}$ , is not well defined [82]. For the special case of an Ornstein-Uhlenbeck process it is simple to check that  $\Gamma_1$  is convex down in  $\tilde{j}$ . In general this is, however, not true. We therefore here instead demonstrate a weaker condition: We show that the equation of state that follows from a formal definition of the MSRDJ effective action is indeed identical to that of the OM effective action. The latter, as stated above, can be defined rigorously. This is done by deriving the nontrivial part of the equation of state of the MSRDJ formalism (22) directly from the well-defined effective action  $\Gamma_1$ .

We start by rewriting the definition of the Legendre-Fenchel transform as

$$\Gamma_1[x^*; \tilde{j}] = -\sup_j \ln \int_x \exp(S_{\text{OM}}[x; \tilde{j}] + j(x - x^*)).$$

The supremum assumed at the physical value  $j = 0$  implies that  $x^* = \langle x \rangle$  equals the mean of the process. This condition, with  $\delta x = x - x^*$ , is equivalently given by

$$0 \stackrel{!}{=} \langle \delta x \rangle \equiv \int_{\delta x} \delta x \exp(S_{\text{OM}}[x^* + \delta x; \tilde{j}]), \quad (\text{A19})$$

where we assumed the OM form of the action, but kept the dependence on the source  $\tilde{j}$  [as in (16)]

$$S_{\text{OM}}[x; \tilde{j}] = -\frac{1}{2D} [\partial_t x - f(x) + \tilde{j}]^T [\partial_t x - f(x) + \tilde{j}].$$

We have seen in (13) that we may express this action as the Legendre transform with respect to the auxiliary field  $\tilde{x}$ ; this is so because  $S_{\text{OM}}$  is convex in  $\partial_t x - f(x) + \tilde{j}$  and every convex function can be written as a Legendre transform of a suitably chosen function (namely, its Legendre transform)

$$S_{\text{OM}}[x; \tilde{j}] = \text{extremize}_{\tilde{x}} \tilde{x}^T [\partial_t x - f(x) + \tilde{j}] + \frac{D}{2} \tilde{x}^T \tilde{x}. \quad (\text{A20})$$

The extremum is hence attained at  $\tilde{x} = -D^{-1}[\partial_t x - f(x) + \tilde{j}]$ . This allows us to rewrite the OM action, expanded in  $\delta x = x - x^*$ , as

$$\begin{aligned} S_{\text{OM}}[x^* + \delta x] &= \frac{1}{2} \underbrace{\frac{-1}{D} [\partial_t x - f(x) + \tilde{j}]^T}_{\tilde{x}^T} \left[ \partial_t x^* - f(x^*) + \tilde{j} + \partial_t \delta x - f^{(1)}(x^*) \delta x + \sum_{n=2}^{\infty} \frac{f^{(n)}(x^*)}{n!} \delta x^n \right] \\ &= \text{extremize}_{\tilde{x}} \tilde{x}^T [\partial_t \delta x - f^{(1)}(x^*) \delta x] + \frac{D}{2} \tilde{x}^T \tilde{x} + \tilde{x}^T [\partial_t x^* - f(x^*) + \tilde{j}] + \tilde{x}^T \sum_{n=2}^{\infty} \frac{f^{(n)}(x^*)}{n!} \delta x^n. \end{aligned}$$

The first two terms in the second line contain all terms bilinear in  $\delta x$  and  $\tilde{x}$ , so they define the propagator. The third term can be regarded as a shift of the mean of the noise; a term that is linear in  $\tilde{x}$ . The last term contains the non-Gaussian terms that produce corrections. If we neglected these corrections, the remaining terms would correspond to an Ornstein-Uhlenbeck process  $\delta x$  that is driven by a noise  $\xi$  with mean  $\langle \xi \rangle = \partial_t x^* - f(x^*) + \tilde{j}$  and variance  $D$ . Because the noise is chosen to be Gaussian, we can rewrite the extremum condition (A20) as an integral over  $\tilde{x}$ :

$$0 \stackrel{!}{=} \langle \delta x \rangle \equiv \int_{\delta x, \tilde{x}} \delta x \exp \left( \tilde{x}^T (\partial_t - f^{(1)}(x^*)) \delta x + \frac{D}{2} \tilde{x}^T \tilde{x} + \tilde{x}^T (\partial_t x^* - f(x^*) + \tilde{j}) + \tilde{x}^T \sum_{n=2}^{\infty} \frac{f^{(n)}}{n!} \delta x^n \right). \quad (\text{A21})$$

In the following we will show that this equation is fulfilled if the term  $\partial_t x^* - f(x^*) + \tilde{j}$  is represented by the negative of all one-line irreducible diagrams with one uncontracted  $\tilde{x}$ -leg; we denote the sum of these diagrams by  $\Xi$ . If we assume (as we normally do) that the representation by diagrams is convergent, this can be seen as the defining property of  $\Gamma_{\text{MSRDJ}, \tilde{x}, \text{fl.}}^{(1)}$  that we formally obtain from a Legendre transform with respect to both,  $j$  and  $\tilde{j}$ . We can then conclude that  $\partial_t x^* - f(x^*) + \tilde{j} = -\Xi = \Gamma_{\text{MSRDJ}, \tilde{x}, \text{fl.}}^{(1)}$ . We will first demonstrate how to obtain this result from a formal Legendre transform also with regard to  $\tilde{j}$ . Afterwards, we will demonstrate that indeed the identification of  $\partial_t x^* - f(x^*) + \tilde{j} = -\Xi$  solves Eq. (A21).

The equations of state derived from the formally performed Legendre transform of  $W[j, \tilde{j}]$  with regard to  $j$  and  $\tilde{j}$  to  $\Gamma_{\text{MSRDJ}}[x^*, \tilde{x}^*]$  are

$$\begin{aligned} \tilde{j}(t) &= \frac{\delta \Gamma_{\text{MSRDJ}}}{\delta \tilde{x}^*(t)} \rightarrow \partial_t x^* - f(x^*) + D \tilde{x}^* + \tilde{j} = \Gamma_{\text{MSRDJ}, \tilde{x}, \text{fl.}}^{(1)}[x^*, \tilde{x}^*], \\ j(t) &= \frac{\delta \Gamma_{\text{MSRDJ}}}{\delta x^*(t)} \rightarrow -\partial_t \tilde{x}^* - f'(x^*) \tilde{x}^* + j = \Gamma_{\text{MSRDJ}, x, \text{fl.}}^{(1)}[x^*, \tilde{x}^*]. \end{aligned} \quad (\text{A22})$$

The second equation for the physically relevant value  $j \equiv 0$  admits the solution  $\tilde{x}^* \equiv 0$ . This is so because the left-hand side is linear in  $\tilde{x}^*$  and the right-hand side vanishes for  $\tilde{x}^* = 0$ , because one cannot produce any nonvanishing diagrams with one amputated  $x$ -leg. One can therefore insert  $\tilde{x}^* \equiv 0$  into the first equation of state to obtain a single nontrivial equation

$$\partial_t x^* - f(x^*) + \tilde{j} = \Gamma_{\text{MSRDJ}, \tilde{x}, \text{fl.}}^{(1)}[x^*, 0], \quad (\text{A23})$$

which shows the first part of our assertion by the usual proof that  $\Gamma_{\text{fl.}}$  is composed of one-line irreducible diagrams alone (see, e.g., Kleinert [72], Sec. 3.23.6, or Helias and Dahmen [80] Sec. XIV).

We hence are left to show the diagrammatic statement, namely, that

$$\begin{aligned} 0 &= \int_{\delta x, \tilde{x}} \delta x \exp \left( \tilde{x}^T [\partial_t - f^{(1)}(x^*)] \delta x + \frac{D}{2} \tilde{x}^T \tilde{x} \right. \\ &\quad \left. - \tilde{x}^T \Xi(x^*) + \tilde{x}^T \sum_{n=2}^{\infty} \frac{f^{(n)}}{n!} \delta x^n \right). \end{aligned} \quad (\text{A24})$$

The Gaussian part in the first line defines the usual propagators  $\Delta_{xx} = \langle xx \rangle$  and  $\Delta_{\tilde{x}x} = \langle \tilde{x}x \rangle$ , whereas  $\Delta_{\tilde{x}\tilde{x}} \equiv 0$ . A non-vanishing contribution requires the explicitly present term  $\delta x$  in the integrand to be contracted. It cannot be contracted by the propagator  $\Delta_{xx}$ , because the other leg of the propagator would need to connect to a  $\delta x$  from an interaction vertex of the form  $\tilde{x} \delta x^n$ ; contracting the remaining  $\tilde{x}$  would hence require at least one closed response loop formed by  $\Delta_{\tilde{x}x}$ , so the contribution vanishes. For the same reason there cannot appear any tadpole subdiagrams that are attached by a  $\delta x$ . The only possibility is hence to contract the explicitly present  $\delta x$  with an  $\tilde{x}$  of an interaction vertex by the propagator  $\Delta_{\tilde{x}x}$ . Thus the produced diagrammatic corrections to the mean are of the form of tadpole diagrams

$\Delta_{\tilde{x}\tilde{x}}$  graph with single uncontracted  $\tilde{x}$ .

We defined  $-\Xi$  to contain all one-line irreducible diagrams with one amputated  $\tilde{x}$ -leg and negative sign. The presence of the term  $-\tilde{x} \Xi(x^*)$  hence cancels all irreducible tadpole diagrams with a single amputated  $\tilde{x}$ -leg. Likewise, reducible contributions cannot appear, because any reducible diagram would contain at least one tadpole subdiagram; but these subdiagrams are canceled by the presence of  $-\tilde{x} \Xi(x^*)$  as well. As a result, we conclude that no diagrams remain, and hence Eq. (A24) holds. This proves that the solution to the equations of state (A23), obtained from the formal joint Legendre transform with regard to both,  $j$  and  $\tilde{j}$ , solves condition Eq. (A21) (even if it is not clear that this is the only solution).

In summary, the specific feature of the MSRDJ formalism that the expectation value of  $\tilde{x}$  vanishes cures the fact that the Legendre transform with respect to  $\tilde{j}$  is not necessarily well defined, because it allows the reduction from the pair of equations of state (A22) to a single one (A23). The latter can be derived in the well-defined OM formalism, as shown above. The Legendre transform from  $\Gamma_1[x^*, \tilde{j}]$  to  $\Gamma[x^*, \tilde{x}^*]$  can therefore be considered a formal step, merely used to simplify the diagrammatic derivation of the equation of state.

## 5. The effective action in the MSRDJ and the Onsager-Machlup formalism

Considering  $\Gamma$  as a potential whose extremal points are the solutions of a differential equation and that  $\tilde{x} = 0$  is the extremizing solution, we might conclude from  $\Gamma_{x, \tilde{x}}^{(n)} = 0$  [shown in Eq. (A3)] that  $\Gamma$  is constant [or at least nonanalytic in  $(\tilde{x}, 0)$ ]. However,  $\Gamma$  is clearly nonconstant. It turns out that setting  $\tilde{x} = 0$  is correct for the stationary point  $\tilde{x}$ , but does not give us the true shape of the “energy landscape” for a different  $x$  in a neighborhood of  $\tilde{x}$ . This is so because it is forbidden to set  $\tilde{x}$  to a constant value prior to the calculation of the statistics of  $x$ ; instead we must integrate it out, since it is just a Hubbard-Stratonovich auxiliary field used to formulate

a constraint. Only for Gaussian noise, this leads to the OM action (7). For arbitrary noise distributions, we can define the cumulant-generating function without the need to first define the OM action by writing

$$W_{\text{OM}}[j] = \ln \int \mathcal{D}x \int \mathcal{D}\tilde{x} \exp(S[x, \tilde{x}] + j^T x). \quad (\text{A25})$$

This makes sense because we introduced  $\tilde{x}$  as an auxiliary variable to represent the delta-distribution and  $\tilde{j}$  to measure the response function. If we are not interested in the latter, but just in the statistics of  $x$ , we can drop  $\tilde{j}$  in (15) to obtain (A25). The OM-type effective action then takes the form

$$\begin{aligned} \Gamma_{\text{OM}}[x^*] &= \sup_j j^T x^* - W_{\text{OM}}[j] \\ &= [j^T x^* - W_{\text{OM}}[j]]_{j \text{ such that } x^* = \frac{\partial}{\partial j} W_{\text{OM}}[j]}. \end{aligned} \quad (\text{A26})$$

Let us expose the connection to the MSRDJ formalism more clearly by performing the Legendre transform with respect to  $j$  and  $\tilde{j}$  gradually instead of simultaneously:

$$\Gamma_1[x^*, \tilde{j}] := \sup_j j^T x^* - W[j, \tilde{j}],$$

$$\Gamma_2[x^*, \tilde{x}^*] := \tilde{j} \tilde{x}^* + \Gamma_1[x^*, \tilde{j}]|_{\tilde{j} \text{ such that } \tilde{x}^* = -\partial_{\tilde{j}} \Gamma_1[x^*, \tilde{j}]}$$

In order to define  $\Gamma_2$ , we had to assume that the relation  $\tilde{j} \rightarrow \partial_{\tilde{j}} \Gamma_1[x^*, \tilde{j}]$  is invertible. This is given if  $\Gamma_1$  is convex in  $\tilde{j}$ . So this is a sufficient condition, but not a necessary one.<sup>8</sup> We easily see that  $\Gamma_{\text{OM}}[x^*] = \Gamma_1[x^*, 0]$ . For the identification of  $\Gamma_2$ , observe that for the elimination of  $j$  obtaining  $\Gamma_1$ , we choose  $j[x^*, \tilde{j}]$  such that

$$x^* = \frac{\partial W}{\partial j}[j[x^*, \tilde{j}], \tilde{j}].$$

Note that by this notation, we have also lifted possible ambiguities due to a multivalued derivative of  $W$  with respect to  $j$ , because we have fixed  $W^{(1)}$  to  $x^*$  (see also Sec. A2). In the second step, yielding  $\Gamma_2$ , we determine  $\tilde{j}$  in the following way:

$$\begin{aligned} \tilde{x}^* &= -\frac{d}{d\tilde{j}} \Gamma_1[x^*, \tilde{j}] = -\frac{d}{d\tilde{j}} \{j[x^*, \tilde{j}]x^* - W[j[x^*, \tilde{j}], \tilde{j}]\} \\ &= -\frac{\partial j}{\partial \tilde{j}} x^* + \underbrace{\frac{\partial W}{\partial j}[j[x^*, \tilde{j}], \tilde{j}]}_{=x^*} \frac{\partial j}{\partial \tilde{j}} + \frac{\partial W}{\partial \tilde{j}}[j[x^*, \tilde{j}], \tilde{j}] \\ &= \frac{\partial W}{\partial \tilde{j}}[j[x^*, \tilde{j}], \tilde{j}], \end{aligned}$$

which leads to the identification  $\Gamma_{\text{MSRDJ}}[x^*, \tilde{x}^*] = \Gamma_2[x^*, \tilde{x}^*]$ . Therefore, we obtain  $\Gamma_{\text{OM}}$  by performing the Legendre transform of  $\Gamma_{\text{MSRDJ}}$  with respect to  $\tilde{x}^*$  and setting  $\tilde{j} = 0$  afterwards, which is equivalent to finding the  $\tilde{x}^*$  extremizing  $\Gamma_{\text{MSRDJ}}[x^*, \tilde{x}^*]$  for given  $x^*$ , or, in other words,

$$\Gamma_{\text{OM}}[x^*] = \underset{\tilde{x}}{\text{extremize}} \Gamma_{\text{MSRDJ}}[x^*, \tilde{x}] =: \underset{\tilde{x}}{\text{extremize}} \Gamma[x^*, \tilde{x}].$$

<sup>8</sup>Consider, for example, the function  $f: \mathbb{R}^2 \rightarrow \mathbb{R}: (x, y)^T \rightarrow \frac{1}{2}(x^2 - y^2)$ , which is not convex, but Legendre-transformable (namely, on itself).

The Legendre transform (A26) implies

$$\frac{\delta^2}{\delta x(t) \delta x(t')} \Gamma_{\text{OM}}[x] = \left\{ \frac{\delta^2}{\delta j(t) \delta j(t')} W[j, \tilde{j}] \right\}^{-1}. \quad (\text{A27})$$

So, expressed in words, the second derivative of  $\Gamma_{\text{OM}}$  at  $x^*$  equals the inverse of  $\langle \delta x \delta x \rangle$ . Note that all  $[\cdot]^{-1}$  are meant as the inverse of operators acting on functions. For our model, in frequency domain these inversions are simple (matrix) inversions, whereas in time domain this amounts to finding the Green's function of the operator or, in other words, solving a differential equation. Therefore, we can relate the integrated covariances, given by the zero mode of the covariances in Fourier space by Fourier-transforming (A27) and inverting it:

$$\frac{\delta^2}{\delta J(\omega) \delta J(\omega')} W[J, \tilde{J}] = \left\{ \frac{\delta^2}{\delta X(\omega) \delta X(\omega')} \Gamma_{\text{OM}}[X] \right\}^{-1}. \quad (\text{A28})$$

## 6. Relation between $S_{\text{OM}}$ and $S_{\text{MSRDJ}}$ in case of non-Gaussian noise

In this section, we demonstrate that approximations of  $\Gamma_{\text{OM}}$  and  $\Gamma_{\text{MSRDJ}}$  are not as simply related as their exact counterparts. For non-Gaussian noise, even the comparison of the tree-level approximations of the effective actions in both formalisms yield counterintuitive result,

$$-S_{\text{OM}}[x] \neq \underset{\tilde{x}}{\text{extremize}} -S_{\text{MSRDJ}}[x, \tilde{x}] \text{ in general.} \quad (\text{A29})$$

To see this as an example, consider the SDE:

$$\frac{d}{dt} x = f(x) + \xi,$$

with the cumulant-generating function of the noise  $\xi$  including a nonvanishing third-order cumulant of strength  $\alpha$  as defined in (25). Then, the MSRDJ-action is given by

$$S_{\text{MSRDJ}}[x, \tilde{x}] = \tilde{x}[\dot{x} - f(x)] + W_{\xi}(\tilde{x}).$$

We want to calculate

$$S_{\text{OM}}[x] := \ln \left\{ \int d\tilde{x} \exp(S_{\text{MSRDJ}}[x, \tilde{x}]) \right\}$$

to linear order in  $\alpha$ . We expand  $S_{\text{MSRDJ}}$  around the saddle point  $\tilde{x}_0[x]$ , defined by

$$\frac{\partial S_{\text{MSRDJ}}}{\partial \tilde{x}}[x, \tilde{x}_0[x]] = 0,$$

which leads to

$$\tilde{x}_0[x] = \frac{f(x) - \dot{x}}{D} - \frac{\alpha}{2} \frac{[f(x) - \dot{x}]^2}{D^2} + O(\alpha^2).$$

By expanding  $\tilde{x}_0[x]$  in  $\alpha$  and inserting it into  $S$  and  $\frac{\partial^2 S}{\partial \tilde{x}^2}$ , we observe that

$$\begin{aligned} S_{\text{MSRDJ}}[x, \tilde{x}_0[x]] &= -\frac{[\dot{x} - f(x)]^2}{2D} + \frac{\alpha}{3!} \frac{[f(x) - \dot{x}]^3}{D^3} \\ &\quad + O(\alpha^2), \end{aligned}$$

$$\frac{\partial^2 S_{\text{MSRDJ}}}{\partial \tilde{x}^2}[x, \tilde{x}_0[x]] = D \left\{ 1 - \frac{\alpha}{D^2} [\dot{x} - f(x)] \right\} + O(\alpha^2).$$

$$(\text{A30})$$

Computing the contribution from the fluctuations around the stationary point with respect to  $\tilde{x}$  yields

$$\begin{aligned}
 \int d\tilde{x} \exp(S_{\text{MSRDJ}}[x, \tilde{x}]) &= \int d\tilde{x} \exp \left( S_{\text{MSRDJ}}[x, \tilde{x}_0] + \frac{\partial^2 S_{\text{MSRDJ}}}{\partial \tilde{x}^2}[x, \tilde{x}_0] \frac{(\tilde{x} - \tilde{x}_0[x])^2}{2} + \underbrace{\frac{\partial^3 S_{\text{MSRDJ}}}{\partial \tilde{x}^3}[x, \tilde{x}_0]}_{=\alpha} \frac{(\tilde{x} - \tilde{x}_0[x])^3}{3!} \right) \\
 &\stackrel{y:=\tilde{x}-\tilde{x}_0[x]}{=} \exp(S_{\text{MSRDJ}}[x, \tilde{x}_0[x]]) \int dy \exp \left( \frac{1}{2} \frac{\partial^2 S_{\text{MSRDJ}}}{\partial \tilde{x}^2}[x, \tilde{x}_0] y^2 \right) \left( 1 + \frac{1}{3!} \alpha y^3 \right) + O(\alpha^2) \\
 &= \exp(S_{\text{MSRDJ}}[x, \tilde{x}_0[x]]) \sqrt{\frac{2\pi}{\frac{\partial^2 S_{\text{MSRDJ}}}{\partial \tilde{x}^2}[x, \tilde{x}_0]}} + O(\alpha^2) \\
 &= \exp(S_{\text{MSRDJ}}[x, \tilde{x}_0[x]]) \sqrt{\frac{2\pi}{D\{1 - \frac{\alpha}{D^2}[\dot{x} - f(x)]\}}} + O(\alpha^2) \\
 &= \exp \left( -\frac{[\dot{x} - f(x)]^2}{2D} + \frac{\alpha}{3!} \frac{[f(x) - \dot{x}]^3}{D^3} \right) \sqrt{\frac{2\pi}{D}} \left( 1 + \frac{\alpha}{2D^2} [\dot{x} - f(x)] \right) + O(\alpha^2).
 \end{aligned}$$

So, in total, we have

$$S_{\text{OM}}[x] = \frac{1}{2} \ln \left( \frac{2\pi}{D} \right) - \underbrace{\frac{[\dot{x} - f(x)]^2}{2D} - \frac{\alpha}{3!} \frac{[\dot{x} - f(x)]^3}{D^3}}_{=\sup_{\tilde{x}} S_{\text{MSRDJ}}[x, \tilde{x}] + O(\alpha^2)} + \frac{\alpha}{2D^2} [\dot{x} - f(x)] + O(\alpha^2).$$

This is the announced result (26). We see that the fluctuations around the saddle-point value of the action lead to additional terms contributing to  $S_{\text{OM}}$ , not only constant, but also  $x$ -dependent ones. We can reformulate this to (A29), so the relation we obtained for the respective effective actions does not hold for the actions, i.e., the tree-level approximations of the effective actions.

## 7. The loop expansion for vertices up to order three, the propagator, and its small parameter

In this section, we explain in more detail how to translate the Feynman diagrams into algebraic expressions and which diagrams contribute to the first order of the loop expansion. This is of course textbook knowledge [4,72,80]. However, we find it useful to recapitulate the calculation in our notation preparing the introduction of the functional renormalization group, and furthermore, it gives us the opportunity to show what is the small parameter in our model. This is unclear *a priori* because its action is not multiplied by a small constant, as usually assumed in the context of a loop expansion.

### a. General structure of diagrams contributing to $\Gamma_{\text{fl}}$ .

To obtain all diagrams that contribute to the  $l$ -loop correction to  $\frac{\delta^n}{\delta X^n} \frac{\delta^m}{\delta \tilde{X}^m} \Gamma_{\text{fl}}$ , we draw all possible connected, one-particle irreducible (1PI) diagrams with  $l$  loops and  $n$  ingoing and  $m$  outgoing external legs. One-particle irreducible diagrams are those that cannot be separated into two unconnected pieces by cutting a single propagator. This is an advantage in terms of practical computations of the Legendre transform  $\Gamma_{\text{fl}}$  over the cumulant-generating function  $W$  where one has to account for all connected diagrams, leading to a larger number of terms to evaluate (a self-contained proof as an induction over the number of loops can be found in Ref. [80]).

In our case the number of diagrams reduces further, because in the Itô discretization of the stochastic differential equation, loops that are constructed out of only directed propagators ( $\Delta_{\tilde{X}X}$ ) pointing all in the same direction evaluate to zero [8]. Therefore, all diagrams that contain such a response loop vanish. This is the reason why the diagram shown in Eq. (29) is indeed the only one to be considered for the one-loop contribution to the one-point vertex. Usually there are several ways of connecting propagators and interaction vertices that lead to the same diagram. We account for this fact by multiplying each diagram with a prefactor that equals the number of equivalent diagrammatic representations. We will demonstrate how to determine the multiplicity and how to translate diagrams into algebraic expressions by means of the example of the one-loop contributions to the propagator.

*Example: one-loop fluctuation corrections to  $\Gamma_{\text{fl.}}^{(2)}$ .* The first fluctuation corrections to  $\Gamma_{\text{fl.}}^{(2)}$  consist of those diagrams that have two interaction vertices and two amputated legs. The latter property defines what is known as “self-energy corrections,”

$$\Gamma_{\tilde{X}\tilde{X},\text{fl.}}^{(2)}(\sigma_1, \sigma_2) = (-8) \text{ (diagram)} = \left[ \Gamma_{\tilde{X}\tilde{X},\text{fl.}}^{(2)}(\sigma_1, \sigma_2) \right]^*$$

$$\frac{1}{2!} \Gamma_{\tilde{X}\tilde{X},\text{fl.}}^{(2)}(\sigma_1, \sigma_2) = (-2) \text{ (diagram)}.$$

In principle, we could also draw a diagram of this shape with two ingoing external legs which, however, would contain a response loop and therefore vanishes. Thus, there is no contribution to  $\Gamma_{\tilde{X}\tilde{X},\text{fl.}}^{(2)}$ . The prefactors are determined as follows. For the first diagram we have two interaction vertices to choose from to get the external outgoing leg. Moreover, we have to select one of the two ingoing legs from the remaining vertex to be the external ingoing leg. Finally, there are two possibilities to connect the internal legs of the two vertices: either as shown above or cross-connected. In total this gives a multiplicity of  $2^3 = 8$ . The minus sign is due to the sign in our definition of the effective action and hence is present in all diagrams. The prefactor of the second diagram stems from the two possibilities to connect the internal legs. Using this counting scheme, we have to include the factors of the Taylor expansion on the left-hand side ( $\frac{1}{2!}$  for two times the derivative with respect to  $\tilde{X}$ ).

Now we use Table I to obtain the algebraic expression for the diagrams where we have to integrate over all internal frequencies. Taking into account all frequency conservations at the propagators and the interaction vertices we get for the first diagram

$$\Gamma_{\tilde{x}\tilde{x},\text{fl.}}^{(2)} = -8 \int d\omega \frac{\beta^2}{(2\pi)^4} \frac{2\pi D}{\omega^2 + m^2} \frac{2\pi}{-i(\omega + \sigma_2) + m} \delta(\sigma_1 + \sigma_2) = 4 \frac{\beta^2 D}{2\pi m} \frac{1}{i\sigma_1 + 2m} \delta(\sigma_1 + \sigma_2),$$

where we used the residue theorem to solve the integral. With the second diagram we proceed in the same way and obtain

$$\Gamma_{\tilde{x}\tilde{x},\text{fl.}}^{(2)} = 2 \frac{D^2}{2\pi m} \frac{1}{\sigma_1^2 + (2m)^2} \delta(\sigma_1 + \sigma_2).$$

Distributing the result for the mixed derivative evenly between the two off-diagonal entries we can write the one-loop corrections to the second derivative of the effective action as

$$\Gamma_{\text{fl.}}^{(2)}(\sigma_1, \sigma_2) = \begin{pmatrix} 0 & \frac{1}{-i\sigma_1 + 2m} \\ \frac{1}{i\sigma_1 + 2m} & \frac{D}{\sigma_1^2 + (2m)^2} \end{pmatrix} \frac{2\beta^2 D}{2\pi m} \delta(\sigma_1 + \sigma_2).$$

### b. The propagator in one-loop approximation

Making use of the property of the Legendre transform  $\Gamma^{(2)}\Delta = 1$  [see (23)], we obtain the one-loop approximation of the propagator and hence, the variance and the response functions by solving the former identity for  $\Delta$ . In frequency domain this yields

$$1 = \begin{pmatrix} \Gamma_{\tilde{X}\tilde{X}}^{(2)}(\omega)\Delta_{\tilde{X}\tilde{X}}(-\omega) & \Gamma_{\tilde{X}\tilde{X}}^{(2)}(\omega)\Delta_{\tilde{X}\tilde{X}}(-\omega) \\ \Gamma_{\tilde{X}\tilde{X}}^{(2)}(\omega)\Delta_{\tilde{X}\tilde{X}}(-\omega) - \Gamma_{\tilde{X}\tilde{X}}^{(2)}(\omega)\Delta_{\tilde{X}\tilde{X}}(-\omega) & \Gamma_{\tilde{X}\tilde{X}}^{(2)}(\omega)\Delta_{\tilde{X}\tilde{X}}(-\omega) - \Gamma_{\tilde{X}\tilde{X}}^{(2)}(\omega)\Delta_{\tilde{X}\tilde{X}}(-\omega) \end{pmatrix}. \quad (\text{A31})$$

For  $\Gamma^{(2)}$  we use the one-loop result that we derived in the previous section

$$\Gamma^{(2)}(\omega) = -S^{(2)} + \Gamma_{\text{fl.}}^{(2)} = \begin{pmatrix} 0 & (-i\omega + m + \frac{A}{-i\omega + 2m}) \\ (i\omega + m + \frac{A}{i\omega + 2m}) & D\left(1 - \frac{A}{\omega^2 + (2m)^2}\right) \end{pmatrix}.$$

The variables  $m$  and  $A$  are expressed in terms of the model parameters as  $m = -l + 2\beta x^*$  and  $A = 2\beta^2 D/m$ . Equation (A31) is solved by

$$\begin{aligned} \Delta_{\tilde{X}\tilde{X}}(\omega) &= 0, \\ \Delta_{\tilde{X}\tilde{X}}(\omega) &= [\Delta_{\tilde{X}\tilde{X}}(\omega)]^* = \frac{i\omega + 2m}{(i\omega + m)(i\omega + 2m) + A}, \\ \Delta_{\tilde{X}\tilde{X}}(\omega) &= \Delta_{\tilde{X}\tilde{X}}(\omega)D\Delta_{\tilde{X}\tilde{X}}(\omega) - \Delta_{\tilde{X}\tilde{X}}(\omega)\Gamma_{\tilde{X}\tilde{X},\text{fl.}}^{(2)}(\omega)D\Delta_{\tilde{X}\tilde{X}}(\omega)\Gamma_{\tilde{X}\tilde{X},\text{fl.}}^{(2)}(\omega)\Delta_{\tilde{X}\tilde{X}}(\omega), \end{aligned}$$



where, we introduced the notation  $\Delta(\omega, \omega') = \Delta(\omega)2\pi\delta(\omega + \omega')$ . In time domain these equations read

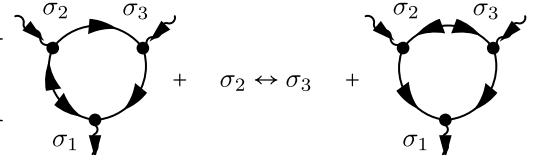
$$\Delta_{\tilde{x}\tilde{x}}(t, t') = \Delta_{\tilde{x}\tilde{x}}(t', t) = -H(t' - t) \left[ \frac{m_1 - 2m}{m_1 - m_2} e^{m_1|t-t'|} + \frac{2m - m_2}{m_1 - m_2} e^{m_2|t-t'|} \right] \quad (\text{A32})$$

$$\Delta_{xx}(t', t) = - \left\{ \frac{D[m_1^2 - (2m)^2 + A]}{2(m_1^2 - m_2^2)m_1} e^{m_1|t-t'|} + \frac{D[(2m)^2 - m_2^2 - A]}{2(m_1^2 - m_2^2)m_2} e^{m_2|t-t'|} \right\}, \quad (\text{A33})$$

where  $m_{1/2} = 3m/2 \pm \sqrt{m^2/4 - A}$  for which the relation  $m_2 < 2m < m < m_1 < 0$  holds in case of a choice of parameters for which the classical fixed point  $x_0$  is stable.

### c. The three-point vertex in one-loop approximation

The corrections to the three-point interaction vertex read as

$$\begin{aligned} \Gamma_{\tilde{X}XX, \text{fl.}}^{(3)}(\sigma_1, \sigma_2, \sigma_3) &= -8 \left[ \text{Diagram 1} + \sigma_2 \leftrightarrow \sigma_3 + \text{Diagram 2} \right] \\ &= -\frac{8\beta^3 D}{(2\pi)^2 m} \frac{(4m + i\sigma_1)}{(2m + i\sigma_1)(2m - i\sigma_2)(2m - i\sigma_3)} \delta(\sigma_1 + \sigma_2 + \sigma_3). \end{aligned}$$


Often it is useful to go into the time domain, which yields

$$\Gamma_{\tilde{x}xx, \text{fl.}}^{(3)}(t_1, t_2, t_3) = \begin{cases} -8\beta^3 \frac{D}{m} e^{2m(t_1-t_3)}, & t_1 > t_2 > t_3 \\ -8\beta^3 \frac{D}{m} e^{2m(t_1-t_2)}, & t_1 > t_3 > t_2 \\ 0, & \text{else} \end{cases} \quad (\text{A34})$$

For the BMW approximation we will need the two quantities  $\Gamma_{\tilde{X}XX, \text{fl.}}^{(3)}(\sigma_1, -\sigma_1, 0)$  and  $\Gamma_{\tilde{X}XX, \text{fl.}}^{(3)}(0, \sigma_2, -\sigma_2)$  which in one-loop approximation read

$$\Gamma_{\tilde{X}XX, \text{fl.}}^{(3)}(\sigma_1, -\sigma_1, 0) = -\frac{4\beta^3 D}{(2\pi)^2} \frac{4m + i\sigma_1}{m^2(2m + i\sigma_1)^2}, \quad \Gamma_{\tilde{X}XX, \text{fl.}}^{(3)}(0, \sigma_2, -\sigma_2) = -\frac{16\beta^3 D}{(2\pi)^2 m} \frac{1}{\sigma_2^2 + 4m^2},$$

which in a time domain yields

$$\Gamma_{\tilde{x}xx, \text{fl.}, 1}^{(3)}(t_1, t_2) = -\frac{8\beta^3 D}{2\pi m} H(t_1 - t_2) \left( t_1 - t_2 - \frac{1}{2m} \right) e^{2m(t_1-t_2)}, \quad \Gamma_{\tilde{x}xx, \text{fl.}, 2}^{(3)}(t_1, t_2) = \frac{8\beta^3 D}{2\pi m} \frac{1}{2m} e^{2m|t_1-t_2|}.$$

A comparison between the fluctuation corrections  $\Gamma_{\text{fl.}}$  and the corresponding terms in the action  $S$  reveals that  $\Gamma_{\tilde{x}\tilde{x}, \text{fl.}}^{(2)}$  counteracts the tree-level contribution  $m$ , whereas the  $\tilde{x}\tilde{x}$ - and the  $\tilde{x}xx$ -contributions are enhanced. Therefore, the linear term  $m$  of the differential equation gets weakened such that for large noise it could even effectively vanish. This would correspond to a second-order phase transition signaled by the divergence of fluctuations (given by the Ginzburg criterion; see, e.g., Ref. [13], i.p., Sec. 6.4). However, we are unable to explore this regime because the destabilization of the trivial fix point is always accompanied by a breakdown of the loop expansion, as we will demonstrate in the following.

### d. Reduction from three to one parameter

Obviously, we increase the escape probability by decreasing the leak term, which amounts to approaching the critical point. These two effects cannot be decoupled by appropriately redefining the noise level  $D$ . We see this by rescaling the time as  $s = l t$  and accordingly the fields  $\tilde{y}(s) = \sqrt{D/l} \tilde{x}(t)$  and  $y(s) = \sqrt{l/D} x(t)$ , which leads to

$$S[\tilde{y}, y] = \int ds \left[ \tilde{y}^T (\partial_s + 1) y - \beta' \tilde{y}^T y^2 + \tilde{y}^T \frac{1}{2} \tilde{y} \right], \quad \text{where } \beta' = \sqrt{\frac{D}{l^3}}.$$

The unstable fixed point is then given by  $x_0 = 1/\beta'$  in the noiseless case. Therefore,  $\beta'$  is the only free parameter of the model and the strength of the nonlinearity determines also the distance between the stable and the unstable fixed point. So it is impossible to find a set of parameters for which on the one hand the system operates far from the unstable fixed point so that the expansion around the stable fixed point is accurate and for which on the other hand and concurrently the effect of the nonlinearity is stronger than the linear part.

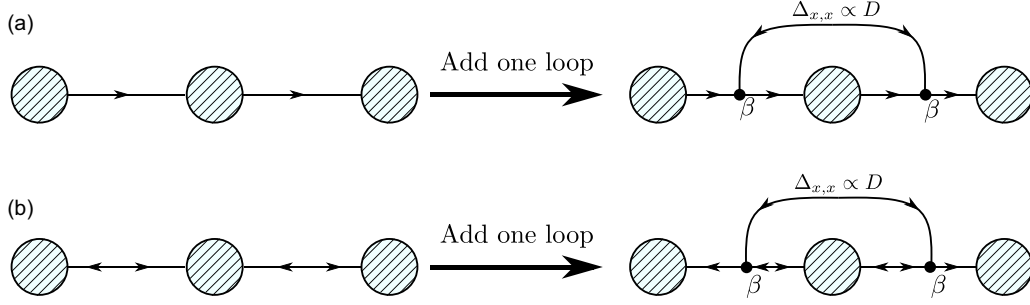


FIG. 7. Adding an additional loop to an arbitrary diagram: In panel (a) we attach the concerning line to two  $\Delta_{xx}$  lines, in panel (b) to two  $\Delta_{xx}$  lines. The mixed case is analogous and therefore omitted. Shaded circles denote arbitrary parts of a diagram.

### e. The small parameter of the loop expansion

In this section we will argue that the expansion of the effective action in diagrams with an increasing number of loops is effectively an expansion in terms of powers of  $\beta^2 D$ . Therefore, diagrams with higher number of loops contribute less important corrections as long as the product of strength of the nonlinearity and the noise variance is small.

We note that every additional loop requires exactly one  $\Delta_{xx}$ -propagator and two interaction vertices. We see this as follows: Adding a loop means attaching a propagator line to two points in the original diagram. This requires points at which exactly three lines meet; if we had interactions higher than three, there could also be more. The interaction bears the strength  $\beta$  which leads to the part  $\beta^2$  in the loop expansion parameter. It is not clear *a priori*, however, that the line connecting these two interactions cannot be a  $\Delta_{xx}$ -line. But Fig. 7 demonstrates that the form of the interaction with two ingoing lines and one outgoing line always forces us to plug in a  $\Delta_{xx}$  propagator, which introduces the factor  $D$ . So, the loop expansion in our case is an expansion in the parameter  $\beta^2 D$ . This consideration compares only different loop orders and not the first loop order to the tree level, and therefore, this is not in contradiction to (30).

## 8. Equation of motion for $\delta x$ from Fokker-Plank equation

We start by multiplying the Fokker-Plank equation [92] for a time-dependent density

$$\tau \partial_t \rho(x, t) = -\partial_x \left[ f(x) - \frac{D}{2} \partial_x \right] \rho(x, t)$$

by  $x$  and integrating over  $x$ :

$$\partial_t \langle x \rangle(t) = - \int dx x \left\{ \partial_x [f(x) \rho(x, t)] - \frac{D}{2} \partial_x^2 \rho(x, t) \right\} = \int dx f(x) \rho(x, t) = -l \langle x(t) \rangle + \beta \langle x(t)^2 \rangle,$$

where in the second step we used partial integration. From the second term only a derivative under an integral remains, which vanishes because we assume that  $\rho$  vanishes at the borders of the integral—a property that we will use repeatedly in the following. In the last equality, furthermore, we inserted  $f(x) = -lx + \beta x^2$ . Now, we need an ODE for the second moment, which we obtain analogously:

$$\begin{aligned} \partial_t \langle x^2 \rangle(t) &= - \int dx x^2 \left\{ \partial_x [f(x) \rho(x, t)] - \frac{D}{2} \partial_x^2 \rho(x, t) \right\} = \int dx [2x f(x) \rho(x, t) - D x \partial_x \rho(x, t)] \\ &= \int dx [2x f(x) \rho(x, t) + D \rho(x, t)] = -2l \langle x^2 \rangle(t) + 2\beta \langle x^3 \rangle(t) + D. \end{aligned}$$

Truncating the hierarchy of moments by a Gaussian closure, that is approximating

$$\langle x^3 \rangle = \langle x^3 \rangle + 3 \langle x^2 \rangle \langle x \rangle + \langle x \rangle^3 = \langle x^3 \rangle + 3 \langle x^2 \rangle \langle x \rangle - 2 \langle x \rangle^3 \approx 3 \langle x^2 \rangle \langle x \rangle - 2 \langle x \rangle^3$$

leads to

$$\partial_t \langle x^2 \rangle(t) \approx -2l \langle x^2 \rangle(t) + 6\beta \langle x^2 \rangle(t) \langle x \rangle(t) - 4\beta \langle x \rangle(t)^3 + D.$$

Using  $\langle x^2 \rangle = \langle x^2 \rangle - \langle x \rangle^2$ , the equations for the first two cumulants read

$$\partial_t \langle x \rangle(t) = -l \langle x \rangle(t) + \beta \{ \langle x^2 \rangle(t) + [\langle x \rangle(t)]^2 \}, \quad (\text{A35})$$

$$\partial_t \langle x^2 \rangle(t) = -2l \langle x^2 \rangle(t) + 4\beta \langle x^2 \rangle(t) \langle x \rangle(t) + D. \quad (\text{A36})$$

We can interpret the one-loop equation of motion as an approximation of the solution of the Fokker-Planck equations of motion (A35) and (A36). To see this, we formally solve (A36) and insert the result into (A35). It is convenient to express the time dependence of  $x$  and  $\Delta$  as a deviation from the stationary solution, defining

$$\langle x \rangle(t) = \bar{x} + \delta x(t), \quad (\text{A37})$$

$$\langle x^2 \rangle(t) = \bar{\Delta} + \delta \Delta(t), \quad \bar{m} = -l + 2\beta \bar{x}, \quad m(t) = -l + 2\beta \langle x \rangle(t) = \bar{m} + 2\beta \delta x(t). \quad (\text{A38})$$

Using these definitions, we obtain for the stationary case

$$0 = -l\bar{x} + \beta \bar{x}^2 + \beta \bar{\Delta} \quad \text{and} \quad \bar{\Delta} = -\frac{D}{2\bar{m}},$$

which follows from (A35) and (A36), respectively. Expressing these equations in the new variables (A37) and (A38) yields

$$\begin{aligned} \partial_t \delta x(t) &= \partial_t \langle x \rangle(t) = -(l - 2\beta \bar{x})\delta x(t) + \beta \delta x(t)^2 \underbrace{-l\bar{x} + \beta \bar{x}^2 + \beta \bar{\Delta}}_{=0} + \beta \delta \Delta(t) \\ &= \bar{m}\delta x(t) + \beta \delta x(t)^2 + \beta \delta \Delta(t) \end{aligned} \quad (\text{A39})$$

and

$$\partial_t \delta \Delta(t) = \underbrace{2\bar{m}\bar{\Delta} + D}_{=0} + 2[\bar{m} + 2\beta \delta x(t)]\delta \Delta(t) + 4\beta \bar{\Delta} \delta x(t) = 2m(t)\delta \Delta(t) + 4\beta \bar{\Delta} \delta x(t).$$

The latter equation turns out to be more convenient for our purpose compared to (A36). Solving it by variation of constants, we obtain

$$\delta \Delta(t) = 4\beta \bar{\Delta} \int_{t_0}^t dt'' \delta x(t'') e^{\int_{t''}^t dt' 2m(t')} = 4\beta \bar{\Delta} \int_{t_0}^t dt'' \delta x(t'') e^{2\bar{m}(t-t'')} e^{4\beta \int_{t''}^t dt' \delta x(t')}, \quad (\text{A40})$$

where we introduced the initial time  $t_0$ . We notice that  $\langle x^2 \rangle(t = t_0) = \Delta^*$ , since  $\delta \Delta(t = t_0) = 0$ . This corresponds to  $x$  being distributed according to the stationary distribution with mean value shifted by the initial deflection  $\delta x(t_0)$ . If we assume that  $\delta x(t)$  is small for all  $t$ , we can expand the second exponential function in (A40) and neglect terms of  $O(\delta x^3)$ . Thus

$$\begin{aligned} \delta \Delta(t) &= 4\beta \bar{\Delta} \int_{t_0}^t dt'' \delta x(t'') e^{2\bar{m}(t-t'')} + 16\beta \bar{\Delta}^2 \int_{t_0}^t dt'' \delta x(t'') e^{2\bar{m}(t-t'')} \int_{t''}^t dt' \delta x(t') + O(\delta x^3) \\ &= 4\beta \bar{\Delta} \int_{t_0}^t dt' \delta x(t') e^{2\bar{m}(t-t')} + 16\beta \bar{\Delta}^2 \int_{t_0}^t dt' \delta x(t') \int_{t_0}^{t'} dt'' \delta x(t'') e^{2\bar{m}(t-t'')} + O(\delta x^3). \end{aligned}$$

If we insert this result into (A39) we obtain up to second order

$$\partial_t \delta x(t) = \bar{m}\delta x(t) + \beta \delta x(t)^2 + 4\beta^2 \bar{\Delta} \int_{t_0}^t dt' \delta x(t') e^{2\bar{m}(t-t')} + 16\beta \bar{\Delta}^3 \int_{t_0}^t dt' \delta x(t') \int_{t_0}^{t'} dt'' \delta x(t'') e^{2\bar{m}(t-t'')},$$

which equals exactly the one-loop result (32).

## 9. Derivation of fRG-flow equations

For completeness, the derivation of the Wetterich equation [35] as presented in Ref. [36] is repeated in the following. The difference of the current presentation is the additional presence of the response field. We will use the property  $\partial_\lambda \Gamma_\lambda = -\partial_\lambda W_\lambda$ , which holds generally for Legendre transforms of quantities depending on a parameter, here  $\lambda$  [[4], Eq. (1.93)]. This yields, using the regulator for the form introduced in (36),

$$\begin{aligned} \frac{\partial \tilde{\Gamma}_\lambda[X^*, \tilde{X}^*]}{\partial \lambda} &= -\frac{\partial W_\lambda[J, \tilde{J}]}{\partial \lambda} = -\frac{1}{\mathcal{Z}[J, \tilde{J}]} \int \mathcal{D}X \int \mathcal{D}\tilde{X} \frac{\partial}{\partial \lambda} \Delta S_\lambda[X, \tilde{X}] \exp(S_\lambda[X, \tilde{X}]) \exp(J^T X + \tilde{J}^T \tilde{X}) \\ &= \frac{1}{2} \int d\omega \int d\omega' \left\langle X(\omega) \frac{\partial R_\lambda(\omega, \omega')}{\partial \lambda} \tilde{X}(\omega') \right\rangle \\ &= \frac{1}{2} \int d\omega \int d\omega' \left\{ \Delta_{\tilde{X}X, \lambda}(\omega', \omega) \frac{\partial R_\lambda(\omega, \omega')}{\partial \lambda} + X^*(\omega) \frac{\partial R_\lambda(\omega, \omega')}{\partial \lambda} \tilde{X}^*(\omega') \right\} \\ &= \frac{1}{2} \text{Tr} \left\{ \Delta_{\tilde{X}X, \lambda} \frac{\partial R_\lambda}{\partial \lambda} \right\} + \frac{\partial}{\partial \lambda} \Delta S_\lambda[X^*, \tilde{X}^*]. \end{aligned} \quad (\text{A41})$$

In the third line we used  $\langle \tilde{X}(\omega') X(\omega) \rangle = \langle \tilde{X}(\omega') X(\omega') \rangle + \langle \tilde{X}(\omega') \rangle \langle X(\omega) \rangle = \Delta_{\tilde{X}X, \lambda}(\omega', \omega) + X^*(\omega) \tilde{X}^*(\omega')$ . From the relation (37) between  $\tilde{\Gamma}_\lambda$  and  $\Gamma_\lambda$  we arrive directly at the final form of the Wetterich equation as presented in Eq. (38).

### 10. Flow equations for the self-energy and the interaction vertex

The nonvanishing diagrams for the self-energy translate to

$$\begin{aligned}
 \frac{\partial \Gamma_{\tilde{X}X,\lambda}^{(2)}(\sigma_1, -\sigma_1)}{\partial \lambda} &= \frac{1}{2} \int \frac{d\omega}{(2\pi)} \Gamma_{\tilde{X}XX,\lambda}^{(3)}(\sigma_1, -\sigma_1 - \omega, \omega) \Delta_{XX,\lambda}(\omega) \frac{\partial R_\lambda}{\partial \lambda} \Delta_{\tilde{X}X,\lambda}(\omega) \Gamma_{XX\tilde{X},\lambda}^{(3)}(-\sigma_1, -\omega, \sigma_1 + \omega) \Delta_{\tilde{X}X,\lambda}(\sigma_1 + \omega) \\
 &+ \frac{1}{2} \int \frac{d\omega}{(2\pi)} \Gamma_{\tilde{X}XX,\lambda}^{(3)}(\sigma_1, -\sigma_1 - \omega, \omega) \Delta_{XX,\lambda}(\omega) \Gamma_{XX\tilde{X},\lambda}^{(3)}(-\sigma_1, -\omega, \sigma_1 + \omega) \\
 &\times \Delta_{\tilde{X}X,\lambda}(\sigma_1 + \omega) \frac{\partial R_\lambda}{\partial \lambda} \Delta_{\tilde{X}X,\lambda}(\sigma_1 + \omega) \\
 &+ \frac{1}{2} \int \frac{d\omega}{(2\pi)} \Gamma_{\tilde{X}XX,\lambda}^{(3)}(\sigma_1, -\sigma_1 - \omega, \omega) \Delta_{X\tilde{X},\lambda}(\omega) \Gamma_{X\tilde{X}X,\lambda}^{(3)}(-\sigma_1, -\omega, \sigma_1 + \omega) \\
 &\times \Delta_{XX,\lambda}(\sigma_1 + \omega) \frac{\partial R_\lambda}{\partial \lambda} \Delta_{\tilde{X}X,\lambda}(\sigma_1 + \omega), \\
 \frac{\partial \Gamma_{\tilde{X}\tilde{X},\lambda}^{(2)}(\sigma_1, -\sigma_1)}{\partial \lambda} &= \frac{1}{2} \int \frac{d\omega}{(2\pi)} \Gamma_{\tilde{X}XX,\lambda}^{(3)}(\sigma_1, -\sigma_1 - \omega, \omega) \Delta_{XX,\lambda}(\omega) \frac{\partial R_\lambda}{\partial \lambda} \Delta_{\tilde{X}X,\lambda}(\omega) \\
 &\times \Gamma_{\tilde{X}XX,\lambda}^{(3)}(-\sigma_1, -\omega, \sigma_1 + \omega) \Delta_{XX,\lambda}(\sigma_1 + \omega) + \sigma_1 \rightarrow -\sigma_1.
 \end{aligned}$$

The diagrams for the flow of the interaction vertex are given by

$$\begin{aligned}
 &\frac{\partial \Gamma_{\tilde{X}XX,\lambda}^{(3)}(\sigma_1, \sigma_2, \sigma_3)}{\partial \lambda} \\
 &= -\frac{1}{2} \left[ \begin{array}{c} \text{Diagram 1: Circle with vertices } \sigma_1, \sigma_2, \sigma_3. \text{ Square on } \sigma_2 \rightarrow \sigma_3 \text{ arc.} \\ \text{Diagram 2: Circle with vertices } \sigma_1, \sigma_2, \sigma_3. \text{ Square on } \sigma_1 \rightarrow \sigma_2 \text{ arc.} \\ \text{Diagram 3: Circle with vertices } \sigma_1, \sigma_2, \sigma_3. \text{ Square on } \sigma_3 \rightarrow \sigma_1 \text{ arc.} \\ \text{Diagram 4: Circle with vertices } \sigma_1, \sigma_2, \sigma_3. \text{ Square on } \sigma_2 \rightarrow \sigma_1 \text{ arc.} \\ \text{Diagram 5: Circle with vertices } \sigma_1, \sigma_2, \sigma_3. \text{ Square on } \sigma_1 \rightarrow \sigma_3 \text{ arc.} \\ \text{Diagram 6: Circle with vertices } \sigma_1, \sigma_2, \sigma_3. \text{ Square on } \sigma_3 \rightarrow \sigma_2 \text{ arc.} \end{array} \right] \\
 &+ \sigma_2 \leftrightarrow \sigma_3.
 \end{aligned}$$

### 11. Effective potential from MSRDJ formalism: Equilibrium systems

For systems in thermodynamic equilibrium, where the statistical weight for each configuration  $x(t)$  is of Boltzmann form (setting the inverse temperature  $\beta = \frac{2}{D}$ )

$$p(x) \propto \exp \left[ -\frac{2}{D} V(x) \right], \quad (\text{A42})$$

a construction of such an effective action has been given in the seminal work of de Dominicis [81] (see his Appendix). In this particular case, the Langevin equation

$$dx(t) = -V'(x)dt + dW(t) \quad (\text{A43})$$

has an equilibrium distribution of the form (A42), given that the variance  $D$  of the noise is  $\langle dW(s)dW(t) \rangle = D\delta_{ts}dt$ ; a condition that follows from demanding vanishing probability flux in the associated Fokker-Planck equation (see, e.g., Ref. [154]); it is one expression of the fluctuation-dissipation theorem that holds in equilibrium systems.

Moreover, a linear term  $\frac{D}{2}hx(t)$  in addition to the potential  $V$  leads to a source term  $h^T\tilde{x}$  in the MSRDJ action  $S[x, \tilde{x}] = \tilde{x}^T[\partial_t x + V'(x)] + \frac{D}{2}\tilde{x}^T\tilde{x} + h^T\tilde{x}$  which corresponds to (A43). The equation of state (18) for  $\tilde{x}$  admits a solution  $\tilde{x} \equiv 0$ , for which the equation of state for  $x$  takes the form

$$h[x^*] = \frac{\delta\Gamma}{\delta\tilde{x}^*(t)} = -\frac{\delta S}{\delta\tilde{x}^*(t)} + \dots = \partial_t x^* + V'(x^*) + \dots, \quad (\text{A44})$$

where  $\dots$  denote all fluctuation corrections. The construction of the effective action by de Dominicis proceeds by functionally integrating the equation of state [see Ref. [81], Eq. (A4)]

$$\Gamma_{\text{DD}}[x^*] := \int_0^{x^*} \delta x h[x] = \Gamma_{\text{DD}}[0] + \frac{1}{2}x^{*\text{T}}\partial_t x^* + V(x^*) + \dots. \quad (\text{A45})$$

The last step requires that the equation of state (A44) be the derivative of a functional; otherwise the functional integration would not yield a unique result, independent of the integration path. This is where the equilibrium properties, the existence of a Boltzmann weight (A42), enter. The latter implies further that the problem can be treated with statics alone. For a constant solution  $x^*(t) = \bar{x}^*$ , the effective potential is thus

$$U_{\text{DD}}[\bar{x}^*] := \Gamma[\bar{x}^*] = V(\bar{x}^*) + \dots. \quad (\text{A46})$$

## 12. Effective potential in a bistable network model

We here compute the one-loop corrections to the OM effective potential for the bistable system (54). The MSRDJ action is

$$S[x, \tilde{x}] = \tilde{x}^T \left[ (\partial_t + r)x + \frac{u}{3}x^3 \right] + \frac{D}{2}\tilde{x}^T\tilde{x}.$$

To lowest order in the fluctuations we have  $\Gamma_0[x^*, \tilde{x}^*] = -S[x^*, \tilde{x}^*]$  for the MSRDJ effective action and the OM effective action (24) is  $S_{\text{OM}}[x^*] = \frac{1}{2D}[(\partial_t + r)x + \frac{u}{3}x^3]^2$ . Next, we assume a stationary solution  $\bar{x}^*$  and compute all corrections around vanishing response fields  $\tilde{x} = 0$ .

### a. Corrections to the mean

The only one-loop contribution to  $\Gamma_{\tilde{x},\text{fl.}}^{(1)}$  is given by the tadpole diagram

$$\begin{aligned} \Gamma_{\tilde{x},\text{fl.}}^{(1)} &= (-1) \text{ (tadpole diagram) } \\ &= -\frac{uDx^*}{2|m|}, \end{aligned}$$

where  $m$  is a function of the mean value and given by  $m(x) = -r - ux^2$ . Including this into the equation of state, its physically relevant solutions read

$$x_0 = 0, \quad x_{\pm} = \pm \sqrt{-2\frac{r}{u} + \sqrt{\left(\frac{r}{u}\right)^2 - \frac{3D}{2u}}}.$$



### b. Self-energy

The one-loop corrections to  $\Gamma^{(2)}$  are given by the following diagrams:

$$\Gamma_{\tilde{X}X,\text{fl.}}^{(2)}(\sigma_1, \sigma_2) = (-1) \text{ (diagram 1)} + (-1) \text{ (diagram 2)}$$

$$\Gamma_{\tilde{X}\tilde{X},\text{fl.}}^{(2)}(\sigma_1, \sigma_2) = -\frac{1}{2} \text{ (diagram 3)}$$

The zero frequency components of the self-energy read

$$\int d\sigma_2 \Gamma_{\tilde{X}X,\text{fl.}}^{(2)}(0, \sigma_2) = \frac{1}{2\pi} \left[ \frac{(ux^*)^2 D}{m^2} + \frac{uD}{2m} \right], \quad \int d\sigma_2 \Gamma_{\tilde{X}\tilde{X},\text{fl.}}^{(2)}(0, \sigma_2) = \frac{1}{4\pi} \frac{(ux^*)^2 D^2}{m^3}.$$

### c. Construction of corrections to the effective potential

We have now expanded the effective action around the reference point  $\tilde{x}^* = 0$  and  $\bar{x}^*$ , which takes the form

$$\Gamma[x^*, \tilde{x}^*] = \tilde{x}^* \left[ \overbrace{-rx^* - \frac{u}{3}x^{*3} + \Gamma_{\tilde{X},\text{fl.}}^{(1)}}^{\text{eq. of state } 0} + (-\partial_t - r - ux^{*2} + \Gamma_{\tilde{X}X,\text{fl.}}^{(2)})(\bar{x}^* - x^*) \right] + \frac{1}{2}\tilde{x}^*(-D + \Gamma_{\tilde{X}\tilde{X},\text{fl.}}^{(2)})\tilde{x}^* + O[(\bar{x}^* - x^*)^2].$$

We compute only terms up to linear order in  $\bar{x}^* - x^*$  because this generates all terms up to quadratic order in the effective potential. This is enough to calculate its curvature, which equals the integrated covariance at the stationary points. The response field still appears quadratically in  $\Gamma[x^*, \tilde{x}^*]$ , so that we can extremize  $\tilde{x}^*$  by writing the OM effective action with corrected vertices as

$$\Gamma_{\text{OM}}[x^*] = \text{extremize}_{\tilde{x}^*} \Gamma[x^*, \tilde{x}^*] = [(-\partial_t - r - ux^{*2} + \Gamma_{\tilde{X}X,\text{fl.}}^{(2)})\delta x^*]_{\frac{1}{2}} [D - \Gamma_{\tilde{X}\tilde{X},\text{fl.}}^{(2)}]^{-1} [(-\partial_t - r - ux^{*2} + \Gamma_{\tilde{X}X,\text{fl.}}^{(2)})\delta x^*],$$

where  $\delta x^* = \bar{x}^* - x^*$ . Computing the effective potential we get

$$U(\bar{x}^*) = \Gamma_{\text{OM}}[\bar{x}^*]/T = \frac{1}{2} \frac{\left\{ \left[ r + ux^{*2} - D\left(\frac{ux^*}{m}\right)^2 - \frac{uD}{2m} \right] \delta x^* \right\}^2}{D - \frac{(ux^*D)^2}{2m^3}}, \quad (\text{A47})$$

where  $m = m(x^*) = -r - ux^{*2}$ .

### 13. Definition of the Fourier transform

By choosing the Fourier transform of the fields and the sources as the inverse of each other, we arrive at a representation of our formulas that look similar in time and frequency domain. Therefore we define

$$x(t) = \int \frac{d\omega}{2\pi} e^{i\omega t} X(\omega), \quad j(t) = \int d\omega e^{-i\omega t} J(\omega), \quad X(\omega) = \int dt e^{-i\omega t} x(t), \quad J(\omega) = \int \frac{dt}{2\pi} e^{i\omega t} j(t).$$

Thus, we obtain  $x^T j = \int dt x(t) j(t) = \int d\omega X(\omega) J(\omega)$ . Moreover, we get with  $y := (x, \tilde{x})^T$  for the matrix  $A$  of the quadratic part of the action  $S_0[x, \tilde{x}] = \int dt \int dt' y(t) A(t, t') y(t')$

$$A(t, t') = \int d\omega \int d\omega' e^{-i(\omega t + \omega' t')} A(\omega, \omega'), \quad A^{-1}(t, t') = \int \frac{d\omega}{2\pi} \int \frac{d\omega'}{2\pi} e^{i(\omega t + \omega' t')} A^{-1}(\omega, \omega'),$$

$$A(\omega, \omega') = \int \frac{dt}{2\pi} \int \frac{dt'}{2\pi} e^{i(\omega t + \omega' t')} A(t, t'), \quad A^{-1}(\omega, \omega') = \int dt \int dt' e^{-i(\omega t + \omega' t')} A^{-1}(t, t'),$$

due to the chain rule for functional derivatives. From this we can derive the following useful identities:

$$\begin{aligned}\int dt \int dt' y(t) A(t, t') y(t') &= \int d\omega \int d\omega' Y(\omega) A(\omega, \omega') Y(\omega'), \\ \int dt \int dt' \bar{j}(t) A^{-1}(t, t') \bar{j}(t') &= \int d\omega \int d\omega' \bar{J}(\omega) A^{-1}(\omega, \omega') \bar{J}(\omega'), \\ \int ds A(t, s) A^{-1}(s, t') &= \delta(t - t') \Leftrightarrow \int d\sigma A(\omega, \sigma) A^{-1}(\sigma, \omega') = \delta(\omega - \omega').\end{aligned}$$

For the interaction part of the action we obtain

$$\int dt \tilde{x}(t) x^2(t) = \int \frac{d\omega}{2\pi} \int \frac{d\omega'}{2\pi} \tilde{X}(\omega) X(\omega') X(-\omega - \omega').$$

- 
- [1] D. Dahmen, H. Bos, and M. Helias, *Phys. Rev. X* **6**, 031024 (2016).
  - [2] H. Sompolinsky, *Phys. Today* **41**, 70 (1988).
  - [3] V. Braitenberg and A. Schüz, *Anatomy of the Cortex: Statistics and Geometry* (Springer-Verlag, Berlin, 1991).
  - [4] J. Zinn-Justin, *Quantum Field Theory and Critical Phenomena* (Clarendon Press, Oxford, 1996).
  - [5] P. C. Hohenberg and B. I. Halperin, *Rev. Mod. Phys.* **49**, 435 (1977).
  - [6] U. C. Täuber, *Critical Dynamics: A Field Theory Approach to Equilibrium and Non-equilibrium Scaling Behavior* (Cambridge University Press, Cambridge, 2014).
  - [7] C. Chow and M. Buice, *J. Math. Neurosci.* **5**, 8 (2015).
  - [8] J. A. Hertz, Y. Roudi, and P. Sollich, *J. Phys. A: Math. Theor.* **50**, 033001 (2017).
  - [9] C. van Vreeswijk and H. Sompolinsky, *Science* **274**, 1724 (1996).
  - [10] N. Brunel, *J. Comput. Neurosci.* **8**, 183 (2000).
  - [11] G. K. Ocker, K. Josić, E. Shea-Brown, and M. A. Buice, *PLoS Comput. Biol.* **13**, e1005583 (2017).
  - [12] J. J. Hopfield, *Proc. Natl. Acad. Sci. USA* **79**, 2554 (1982).
  - [13] D. J. Amit, *Field Theory, the Renormalization Group, and Critical Phenomena* (World Scientific, Singapore, 1984).
  - [14] B. Lindner and A. Longtin, *J. Theor. Biol.* **232**, 505 (2005).
  - [15] E. Shea-Brown, K. Josic, J. de la Rocha, and B. Doiron, *Phys. Rev. Lett.* **100**, 108102 (2008).
  - [16] S. El Boustani and A. Destexhe, *Neural Comput.* **21**, 46 (2009).
  - [17] V. Pernice, B. Staude, S. Cardanobile, and S. Rotter, *PLoS Comput. Biol.* **7**, e1002059 (2011).
  - [18] S. Ostojic and N. Brunel, *PLoS Comput. Biol.* **7**, e1001056 (2011).
  - [19] J. Trousdale, Y. Hu, E. Shea-Brown, and K. Josic, *PLoS Comput. Biol.* **8**, e1002408 (2012).
  - [20] T. Tetzlaff, M. Helias, G. T. Einevoll, and M. Diesmann, *PLoS Comput. Biol.* **8**, e1002596 (2012).
  - [21] M. Helias, T. Tetzlaff, and M. Diesmann, *New J. Phys.* **15**, 023002 (2013).
  - [22] A. Renart, J. De La Rocha, P. Bartho, L. Hollender, N. Parga, A. Reyes, and K. D. Harris, *Science* **327**, 587 (2010).
  - [23] A. Riehle, S. Grün, M. Diesmann, and A. Aertsen, *Science* **278**, 1950 (1997).
  - [24] M. R. Cohen and J. H. R. Maunsell, *Nat. Neurosci.* **12**, 1594 (2009).
  - [25] B. E. Kilavik, S. Roux, A. Ponce-Alvarez, J. Confais, S. Grün, and A. Riehle, *J. Neurosci.* **29**, 12653 (2009).
  - [26] C. Duclut, thesis, Université Pierre et Marie Curie-Paris VI (2017).
  - [27] J. M. Beggs and D. Plenz, *J. Neurosci.* **24**, 5216 (2004).
  - [28] G. Tkačik, O. Marre, D. Amodei, E. Schneidman, W. Bialek, and M. J. Berry II, *PLoS Comput. Biol.* **10**, e1003408 (2014).
  - [29] H. Jaeger, Tech. Rep. GMD Report 148, German National Research Center for Information Technology, St. Augustin, Germany (2001).
  - [30] W. Maass, T. Natschläger, and H. Markram, *Neural Comput.* **14**, 2531 (2002).
  - [31] R. Legenstein and W. Maass, *Neural Netw.* **20**, 323 (2007).
  - [32] K. G. Wilson, *Rev. Mod. Phys.* **47**, 773 (1975).
  - [33] T. Mora and W. Bialek, *J. Stat. Phys.* **144**, 268 (2011).
  - [34] F. J. Wegner and A. Houghton, *Phys. Rev. A* **8**, 401 (1973).
  - [35] C. Wetterich, *Phys. Lett. B* **301**, 90 (1993).
  - [36] J. Berges, N. Tetradis, and C. Wetterich, *Phys. Rep.* **363**, 223 (2002).
  - [37] D. Martí, N. Brunel, and S. Ostojic, *Phys. Rev. E* **97**, 062314 (2018).
  - [38] S. Song, P. Sjöström, M. Reigl, S. Nelson, and D. Chklovskii, *PLoS Biol.* **3**, e68 (2005).
  - [39] P. Martin, E. Siggia, and H. Rose, *Phys. Rev. A* **8**, 423 (1973).
  - [40] H.-K. Janssen, *Z. Phys. B: Condens. Matter* **23**, 377 (1976).
  - [41] C. De Dominicis, *J. Phys. Colloques* **37**, C1 (1976).
  - [42] A. Crisanti and H. Sompolinsky, *Phys. Rev. E* **98**, 062120 (2018).
  - [43] J. Schuecker, S. Goedeke, and M. Helias, *Phys. Rev. X* **8**, 041029 (2018).
  - [44] D. Dahmen, S. Grün, M. Diesmann, and M. Helias, *Proc. Natl. Acad. Sci. USA* **116**, 13051 (2019).
  - [45] M. A. Buice and C. C. Chow, *Phys. Rev. E* **76**, 031118 (2007).
  - [46] M. A. Buice, J. D. Cowan, and C. C. Chow, *Neural Comput.* **22**, 377 (2010).
  - [47] M. A. Buice and C. C. Chow, *PLoS Comput. Biol.* **9**, e1002872 (2013).
  - [48] B. A. W. Brinkman, F. Rieke, E. Shea-Brown, and M. A. Buice, *PLoS Comput. Biol.* **14**, e1006490 (2018).

- [49] S. DiSanto, P. Villegas, R. Burioni, and M. A. Munoz, *Proc. Natl. Acad. Sci. USA* **115**, E1356 (2018).
- [50] M. Kardar, G. Parisi, and Y.-C. Zhang, *Phys. Rev. Lett.* **56**, 889 (1986).
- [51] L. Canet, H. Chaté, B. Delamotte, and N. Wschebor, *Phys. Rev. Lett.* **104**, 150601 (2010).
- [52] L. Canet, H. Chaté, and B. Delamotte, *J. Phys. A* **44**, 495001 (2011).
- [53] E. Frey, U. C. Täuber, and T. Hwa, *Phys. Rev. E* **53**, 4424 (1996).
- [54] J.-P. Blaizot, R. Méndez-Galain, and N. Wschebor, *Phys. Lett. B* **632**, 571 (2006).
- [55] H. R. Wilson and J. D. Cowan, *Biophys. J.* **12**, 1 (1972).
- [56] S.-I. Amari, *IEEE Trans. Syst., Man, Cybernetics SMC-2*, 634 (1972).
- [57] W. R. Softky and C. Koch, *J. Neurosci.* **13**, 334 (1993).
- [58] I. Ginzburg and H. Sompolinsky, *Phys. Rev. E* **50**, 3171 (1994).
- [59] E. Frey and M. F. Weber, *Rep. Prog. Phys.* **80**, 046601 (2017).
- [60] N. Brunel and V. Hakim, *Neural Comput.* **11**, 1621 (1999).
- [61] N. Brunel and X.-J. Wang, *J. Neurophysiol.* **90**, 415 (2003).
- [62] S. Ostojic, N. Brunel, and V. Hakim, *J. Neurosci.* **29**, 10234 (2009).
- [63] E. Ledoux and N. Brunel, *Front. Comput. Neurosci.* **5**, 1 (2011).
- [64] D. Grynatsky, T. Tetzlaff, M. Diesmann, and M. Helias, *Front. Comput. Neurosci.* **7**, 131 (2013).
- [65] A. Andreanov, G. Biroli, J.-P. Bouchaud, and A. Lefevre, *Phys. Rev. E* **74**, 030101(R) (2006).
- [66] A. Lefevre and G. Biroli, *J. Stat. Mech.* (2007) P07024.
- [67] G. K. Ocker, Y. Hu, M. A. Buice, B. Doiron, K. Josić, R. Rosenbaum, and E. Shea-Brown, *Curr. Opin. Neurobiol.* **46**, 109 (2017).
- [68] H. Sompolinsky, A. Crisanti, and H. J. Sommers, *Phys. Rev. Lett.* **61**, 259 (1988).
- [69] P. C. Bressloff, *J. Phys. A: Math. Theor.* **45**, 033001 (2012).
- [70] C. W. Gardiner, *Handbook of Stochastic Methods for Physics, Chemistry and the Natural Sciences*, 2nd ed. (Springer-Verlag, Berlin, 1985).
- [71] N. G. Van Kampen, *Stochastic Processes in Physics and Chemistry*, 3rd ed., North-Holland Personal Library (North-Holland, Amsterdam, 2007).
- [72] H. Kleinert, *Path Integrals in Quantum Mechanics, Statistics, Polymer Physics, and Financial Markets*, 5th ed. (World Scientific, Singapore, 2009).
- [73] L. Onsager and S. Machlup, *Phys. Rev.* **91**, 1505 (1953).
- [74] R. L. Stratonovich, in *Proc. Sixth All-Union Conf. Theory Prob. and Math. Statist.*, Vilnius (1960), pp. 471–482, English translation by A. N. Rossolimo, in *Selected Translations in Mathematical Statistics and Probability*, Vol. 10 (1971), pp. 273–286.
- [75] R. Graham, *Z. Phys. B: Condens. Matter* **26**, 281 (1977).
- [76] K. L. C. Hunt and J. Ross, *J. Chem. Phys.* **75**, 976 (1981).
- [77] A. Altland and B. Simons, *Concepts of Theoretical Solid State Physics* (Cambridge University Press, Cambridge, 2010).
- [78] P. C. Bressloff, *SIAM J. Appl. Math.* **70**, 1488 (2009).
- [79] A. Vasiliev, *Functional Methods in Quantum Field Theory and Statistical Physics* (Gordon and Breach, New York, 1998).
- [80] M. Helias and D. Dahmen, [arXiv:1901.10416](https://arxiv.org/abs/1901.10416) [cond-mat.dis-nn].
- [81] C. De Dominicis, *Phys. Rev. B* **18**, 4913 (1978).
- [82] H. C. Andersen, *J. Math. Phys.* **41**, 1979 (2000).
- [83] A. C. C. Coolen, [arXiv:cond-mat/0006011](https://arxiv.org/abs/cond-mat/0006011).
- [84] M. A. Buice and J. D. Cowan, *Phys. Rev. E* **75**, 051919 (2007).
- [85] M. Doi, *J. Phys. A: Math. Gen.* **9**, 1465 (1976).
- [86] L. Peliti, *J. Phys. (France)* **46**, 1469 (1985).
- [87] J. W. Negele and H. Orland, *Quantum Many-Particle Systems* (Perseus Books, New York, 1998).
- [88] E. Schneidman, M. J. Berry, R. Segev, and W. Bialek, *Nature (London)* **440**, 1007 (2006).
- [89] F. Cooper and J. F. Dawson, *Ann. Phys.* **365**, 118 (2016).
- [90] J. E. Mayer and M. Goeppert-Mayer, *Statistical Mechanics*, 2nd ed. (John Wiley & Sons, New York, 1977).
- [91] A. Roxin, N. Brunel, D. Hansel, G. Mongillo, and C. van Vreeswijk, *J. Neurosci.* **31**, 16217 (2011).
- [92] H. Risken, *The Fokker-Planck Equation* (Springer-Verlag, Berlin, 1996).
- [93] L. Ornigotti, A. Ryabov, V. Holubec, and R. Filip, *Phys. Rev. E* **97**, 032127 (2018).
- [94] R. Filip and P. Zemánek, *J. Opt.* **18**, 065401 (2016).
- [95] P. E. Latham, B. J. Richmond, P. G. Nelson, and S. Nirenberg, *J. Neurophysiol.* **83**, 808 (2000).
- [96] R. Brette and W. Gerstner, *J. Neurophysiol.* **94**, 3637 (2005).
- [97] V. Elgart and A. Kamenev, *Phys. Rev. E* **70**, 041106 (2004).
- [98] R. Zwanzig, *Nonequilibrium Statistical Mechanics* (Oxford University Press, Oxford, 2001).
- [99] H. J. Sommers, A. Crisanti, H. Sompolinsky, and Y. Stein, *Phys. Rev. Lett.* **60**, 1895 (1988).
- [100] G. La Camera, A. Rauch, D. Thurbon, H.-R. Lüscher, W. Senn, and S. Fusi, *J. Neurophysiol.* **96**, 3448 (2006).
- [101] R. Chaudhuri, K. Knoblauch, M.-A. Gariel, H. Kennedy, and X.-J. Wang, *Neuron* **88**, 419 (2015).
- [102] B. Bravi, P. Sollich, and M. Oppen, *J. Phys. A: Math. Theor.* **49**, 194003 (2016).
- [103] C. De Dominicis and P. C. Martin, *J. Math. Phys.* **5**, 14 (1964).
- [104] T. R. Morris, *Int. J. Mod. Phys. A* **9**, 2411 (1994).
- [105] C. Bagnuls and C. Bervillier, *Phys. Rep.* **348**, 91 (2001).
- [106] C. Duclut and B. Delamotte, *Phys. Rev. E* **95**, 012107 (2017).
- [107] F. Schütz and P. Kopietz, *J. Phys. A: Math. Gen.* **39**, 8205 (2006).
- [108] P. Kopietz, L. Bartosch, and F. Schütz, *Introduction to the Functional Renormalization Group* (Springer, Berlin, 2010).
- [109] J.-P. Blaizot, R. Méndez-Galain, and N. Wschebor, *Phys. Rev. E* **74**, 051116 (2006).
- [110] F. Benítez, J.-P. Blaizot, H. Chaté, B. Delamotte, R. Méndez-Galain, and N. Wschebor, *Phys. Rev. E* **85**, 026707 (2012).
- [111] H. Touchette, *Phys. Rep.* **478**, 1 (2009).
- [112] G. L. Eyink, *Phys. Rev. E* **54**, 3419 (1996).
- [113] J. Jordan, H. Mørk, S. B. Vennemo, D. Terhorst, A. Peyser, T. Ippen, R. Deepu, J. M. Eppler, A. van Meegen, S. Kunkel et al., Nest 2.18.0 (2019), URL <https://doi.org/10.5281/zenodo.2605422>.
- [114] J. Kadmon and H. Sompolinsky, *Phys. Rev. X* **5**, 041030 (2015).
- [115] S. H. Strogatz, *Nonlinear Dynamics and Chaos: With Applications to Physics, Biology, Chemistry, and Engineering* (Perseus Books, Reading, MA, 1994).
- [116] G. Buzsáki and A. Draguhn, *Science* **304**, 1926 (2004).

- [117] K. Takahashi, S. Kim, T. P. Coleman, K. A. Brown, A. J. Suminski, M. D. Best, and N. G. Hatsopoulos, *Nat. Commun.* **6**, 7169 (2015).
- [118] M. Denker, L. Zehl, B. E. Kilavik, M. Diesmann, T. Brochier, A. Riehle, and S. Grün, *Sci. Rep.* **8**, 5200 (2018).
- [119] J. Senk, K. Korvasová, J. Schuecker, E. Hagen, T. Tetzlaff, M. Diesmann, and M. Helias, [arXiv:1801.06046](https://arxiv.org/abs/1801.06046).
- [120] A. K. Barreiro, J. N. Kutz, and E. Shlizerman, *J. Math. Neurosci.* **7**, 10 (2017).
- [121] M. Steriade, A. Nuñez, and F. Amzica, *J. Neurosci.* **13**, 3252 (1993).
- [122] A. Destexhe, S. W. Hughes, M. Rudolph, and V. Crunelli, *Trends Neurosci.* **30**, 334 (2007).
- [123] P. C. Bressloff and O. Faugeras, *J. Stat. Mech.* (2017) 033206.
- [124] B. Bravi and P. Sollich, *Phys. Biol.* **14**, 045010 (2017).
- [125] D. J. Amit and N. Brunel, *Network: Comput. Neural Syst.* **8**, 373 (1997).
- [126] C. van Vreeswijk and H. Sompolinsky, *Neural Comput.* **10**, 1321 (1998).
- [127] C. Husemann and M. Salmhofer, *Phys. Rev. B* **79**, 195125 (2009).
- [128] N. Wentzell, G. Li, A. Tagliavini, C. Taranto, G. Rohringer, K. Held, A. Toschi, and S. Andergassen, [arXiv:1610.06520](https://arxiv.org/abs/1610.06520) (2016).
- [129] C. J. Eckhardt, G. A. H. Schober, J. Ehrlich, and C. Honerkamp, *Phys. Rev. B* **98**, 075143 (2018).
- [130] B. Delamotte, in *Renormalization Groups and Effective Field Theory Approaches to Many-Body Systems*, edited by J. S. Janos Polonyi (Springer, Berlin, 2012), pp. 49–130.
- [131] M. M. Churchland, B. M. Yu, J. P. Cunningham, L. P. Sugrue, M. R. Cohen, G. S. Corrado, W. T. Newsome, A. M. Clark, P. Hosseini, B. B. Scott, D. C. Bradley, M. A. Smith, A. Kohn, J. A. Movshon, K. M. Armstrong, T. Moore, S. W. Chang, L. H. Snyder, S. G. Lisberger, N. J. Priebe, I. M. Finn, D. Ferster, S. I. Ryu, G. Santhanam, M. Sahani and K. V. Shenoy, *Nat. Neurosci.* **13**, 369 (2010).
- [132] A. Litwin-Kumar, M. J. Chacron, and B. Doiron, *PLoS Comput. Biol.* **8**, e1002667 (2012).
- [133] M. Ohbayashi, K. Ohki, and Y. Miyashita, *Science* **301**, 233 (2003).
- [134] M. Henningson and S. Illes, *Front. Comput. Neurosci.* **11** (2017).
- [135] K. J. Wiese, *J. Stat. Phys.* **93**, 143 (1998).
- [136] V. Priesemann, M. Wibral, M. Valderrama, R. Pröpper, M. Le Van Quyen, T. Geisel, J. Triesch, D. Nikolic, and M. H. J. Munk, *Front. Syst. Neurosci.* **8**, 108 (2014).
- [137] J. Witting and V. Priesemann, *Nat. Commun.* **9**, 2325 (2018).
- [138] P. Bak, C. Tang, and K. Wiesenfeld, *Phys. Rev. Lett.* **59**, 381 (1987).
- [139] L. Martignon, H. von Hasseln, S. Grün, A. Aertsen, and G. Palm, *Biol. Cybern.* **73**, 69 (1995).
- [140] S. S. Manna, *J. Phys. A: Math. Gen.* **24**, L363 (1991).
- [141] A. Vespignani, R. Dickman, M. A. Muñoz, and S. Zapperi, *Phys. Rev. Lett.* **81**, 5676 (1998).
- [142] R. Dickman, A. Vespignani, and S. Zapperi, *Phys. Rev. E* **57**, 5095 (1998).
- [143] P. Le Doussal and K. J. Wiese, *Phys. Rev. Lett.* **114**, 110601 (2015).
- [144] K. J. Wiese, *Phys. Rev. E* **93**, 042117 (2016).
- [145] O. Harish and D. Hansel, *PLoS Comput. Biol.* **11**, e1004266 (2015).
- [146] S. K. Esser *et al.*, *Proc. Natl. Acad. Sci. USA* **113**, 11441 (2016).
- [147] A. G. Hawkes, *J. R. Statist. Soc. Ser. B* **33**, 438 (1971).
- [148] A. Hawkes, *Biometrika* **58**, 83 (1971).
- [149] S. Qiu and C. Chow, *Phys. Rev. E* **98**, 062414 (2018).
- [150] R. B. Stein, *Biophys. J.* **7**, 37 (1967).
- [151] D. J. Amit and N. Brunel, *Cereb. Cortex* **7**, 237 (1997).
- [152] <http://www.nest-simulator.org>.
- [153] H. Sompolinsky and A. Zippelius, *Phys. Rev. B* **25**, 6860 (1982).
- [154] N. Goldenfeld, *Lectures on Phase Transitions and the Renormalization Group* (Perseus Books, Reading, MA, 1992).
- [155] R. T. Rockafellar, *Convex Analysis*, Princeton Landmarks in Mathematics and Physics (Princeton University Press, 1970).